

**Reclamation of Unconventional Oil Processed Water through the Adsorption  
of Naphthenic Acids by Carbon Xerogel**

By

Yara Abdelaziz Rashed

A thesis submitted in partial fulfillment of the requirements for the degree of

Master of Science

In

Environmental Engineering

Department of Civil and Environmental Engineering  
University of Alberta

© Yara Abdelaziz Rashed, 2017

## Abstract

This study examines the use of carbon xerogel (CX) material for the adsorption of naphthenic acids (NAs). The adsorption of NAs is crucial for the reclamation of unconventional oil processed water, more specifically Alberta's oil sands process-affected water (OSPW). CX material is synthesized at specific operating pH conditions to result in a material that exhibits an extensive mesoporous character. Therefore, the employment of CX as an adsorbent can not only promote the adsorption of a wider range of complex NAs present in OSPW, but can also be synthesized to provide textural characteristics that adhere to contaminants present in all forms of unconventional oil processed water.

This thesis begins with a review of the fundamentals of the adsorption phenomena, then provides a comprehensive analysis of Alberta's OSPW with an elaborate description of the characteristics of NAs present in OSPW. Furthermore, the various treatment technologies that have been studied to treat OSPW from NAs is discussed with special focus on adsorption processes. The evaluation of the adsorbents discussed in this section reveals that their performance is restricted given that they are derived from raw materials, which accordingly limits their textural properties. As a result, the utilization of synthesized CX is necessary to enhance the removal of NAs from OSPW through adsorption.

As a preliminary investigation of CX to treat OSPW, identifying the adsorption mechanisms responsible for the removal of NAs is initially required to further enhance the performance of CX in actual OSPW. Therefore, this study focusses on examining the efficacy of CX in terms of adsorbing model NA compounds; more specifically, heptanoic acid (HPA), 5-cyclohexanepentanoic acid (CHPA), and 5-Phenylvaleric acid (PVA). All three model NAs contain a carboxylic acid and long chain structure, with exception to CHPA which contains an

additional cyclic ring, and PVA contains an aromatic ring. Therefore, by exploring the adsorption of these three model compounds, at pH 8, onto CX, the structure-activity relations responsible for adsorption are deduced. Furthermore, HPA, the simplest compound among the three, is examined in focus at three pH conditions, pH 8, 6.5, and 5, which are above, near, and below the pH of point zero charge for CX, 6.8. Therefore, the electrostatic interactions responsible for the adsorption of NAs onto CX can be identified. Note that at all conditions, similar investigations were conducted with granular activated carbon (GAC) to evaluate the effectiveness of CX relative to the conventional adsorbent used for the removal of NAs from OSPW.

Moreover, the results were analyzed per adsorbent capacity, the internal diffusion model, and adsorption rate models; pseudo-first order and pseudo-second order, to demonstrate that CX performs exceptionally well relative to GAC due to its mesoporous structure. More specifically, the results have revealed that PVA, the more complex NA is adsorbed more easily by CX due to  $\pi$ - $\pi$  interactions, followed by HPA due to its surfactant-like structure, and finally CHPA is adsorbed least due to its high molecular weight which delays its kinetics. The role of hydrophobic-hydrophobic forces has been noted during the diffusion of the three model NAs into the stagnant film surrounding the CX surface, and the hydrophobic bonding may be recognized as negatively charged assisted hydrogen bonding (-CAHB). In terms of HPA, van der Waals attractive forces, in the form of dipole-dipole attractions, have been recognized as the probable electrostatic mechanism responsible for the stronger attraction of HPA onto CX.

## Preface

This thesis is the original work of Yara Rashed. No part of this thesis has been previously published. A poster that summarizes the results of this thesis has been presented in the Canadian Society of Civil Engineers – Edmonton Section Annual Poster Competition on March 16, 2017. Under the supervision of Dr. Mohamed Gamal El-Din and Dr. Hongbo Zeng, Yara Rashed conducted all research, designed and performed all laboratory experiments, analyzed the data, and prepared this manuscript. In addition to supervising the project, Dr. Mohamed Gamal El-Din and Dr. Hongbo Zeng provided all instructions and reviewed all material prepared. The experiments were conducted in Dr. Mohamed Gamal El-Din's laboratories and all materials and equipment were used from his laboratories. Dr. Selamawit Messele and Dr. Pamela Chelme-Ayala also contributed by assisting Yara Rashed, through revisions of the data analysis and content prepared. In addition, Dr. Selamawit Messele conducted the all liquid chromatography – mass spectrometry analyses, the textural characterization mentioned in sectioned 3.1.1, and directly oversaw Yara Rashed's work.

## Acknowledgements

First and foremost, I would like to extend my deep gratitude to Dr. Mohamed Gamal El Din not only for giving me this worthwhile opportunity, but for his academic guidance and transfer of his prestigious knowledge. Likewise, I would like to thank Dr. Hongbo Zeng for his humbleness in accepting to co-supervise my research and providing me with guidance from the Chemical Engineering point of view.

In addition, I highly appreciate Dr. Selamawit Messele continuous efforts and her endless assistance, direction, answering all my questions, and making this thesis possible. Likewise, I would like to thank Dr. Pamela Chelme-Ayala for her support and providing me with all resources necessary. Of note, I would like to thank my colleague Somaye Nasr for her advice at all times, particularly with regards to my experimental results, and most importantly for teaching me how to conduct the experiments that were performed for this study.

I would like to acknowledge the financial support provided by a research grant from Natural Sciences and Engineering Research Council of Canada (NSERC) Senior Industrial Research Chair (IRC) in Oil Sands Tailings Water Treatment through the support by Syncrude Canada Ltd., Suncor Energy Inc., Shell Canada, Canadian Natural Resources Ltd., Total E&P Canada Ltd., EPCOR Water Services, Alberta Innovates - Energy and Environment Solution, and Alberta Environment and Parks. An NSERC Discovery grant is also acknowledged. A special thanks goes to Student Aid Alberta for granting me the Graduate Student Scholarship.

*To my family, notably my parents;  
Thank you for your patience, love, and support.*

## Table of Contents

Chapter 1 Introduction .....	1
1.1 Background & Motivation .....	1
1.2 Problem Statement .....	2
1.3 Research Objective.....	3
1.4 Hypothesis.....	3
1.5 Research Impact .....	3
1.6 Thesis Outline .....	4
Chapter 2 Background .....	5
2.1 Theory: Review of the Fundamentals of Adsorption.....	5
2.1.1 Adsorption Types .....	5
2.1.2 Steps of the Adsorption Process .....	5
2.1.3 Adsorption Kinetics and Models .....	6
2.1.3.1 Diffusion Models .....	7
2.1.3.2 Adsorption Rate Models .....	8
2.1.4 Forces of Adsorption .....	10
2.1.5 Factors that Affect Adsorption Performance.....	12
2.2 Literature Review: A Review of Oil Sands Process-Affected Water Treatment.....	17
2.2.1 Naphthenic Acids .....	18
2.2.1.1 Naphthenic Acids in OSPW.....	18
2.2.1.2 Toxicity of NAs .....	19
2.2.2 Comprehensive Analysis of OSPW .....	19
2.2.3 Removal of NAs from OSPW .....	23
2.2.3.1 Adsorption Process used for the Treatment of OSPW.....	23
2.2.4 An Evaluation of Current Adsorption Treatments .....	31
2.3 Use of Carbon Xerogel Material as an Adsorbent .....	34
2.3.1 Carbon Xerogel as an Adsorbent.....	34
Chapter 3 Experimental Setup .....	37
3.1 Materials.....	37
3.1.1 Adsorbent Preparation .....	37
3.1.2 NAs Stock Solution .....	38
3.2 Methods.....	41

3.2.1 Batch Adsorption Experiments.....	41
3.2.2 Liquid Chromatography – Mass Spectrometry (LC-MS) Analysis.....	42
Chapter 4 Results & Discussion .....	43
4.1 Data .....	43
4.2 Results.....	43
4.2.1 NAs Removal .....	44
4.2.2 NA Adsorption onto CX or GAC .....	47
4.2.3 Adsorption Kinetics Modeling of Data .....	50
4.2.3.1 Rate of Diffusion.....	50
4.2.3.2 Rate of Adsorption.....	60
4.3 Discussion of Results .....	70
4.3.1 The Effect of NA Structure on its Adsorption by CX and GAC .....	70
4.3.2 The Effect of pH on HPA Adsorption by CX and GAC .....	73
Chapter 5 Conclusions & Recommendations .....	75
References.....	77
Appendices.....	85
A.1 Kow Coefficients of Model NA Compounds .....	85
A.2 Experimental Data.....	85
A.3 Normalized Adsorption Capacity Results .....	90
A.3.1 pH 8 Data.....	90
A.3.2 HPA Data.....	91
A.4 Adsorption Kinetics Data .....	92
A.4.1 pH 8 Data.....	92
A.4.2 HPA Data.....	92

## List of Tables

<b>Table 3.1</b> Textural properties of GAC and CX .....	38
<b>Table 3.2</b> Properties of model NAs used in this study .....	40
<b>Table 4.1</b> Percent removal of model NAs due to the adsorption by GAC or CX at pH 8 .....	45
<b>Table 4.2</b> Percent removal of HPA due to the adsorption by GAC or CX at pH 8.....	47
<b>Table 4.3</b> Internal diffusion parameters that model the diffusion of HPA, CHPA, or PVA onto GAC or CX at pH 8 .....	52
<b>Table 4.4</b> Rates of film and pore diffusion of HPA, CHPA, or PVA onto GAC or CX at pH 8. 54	
<b>Table 4.5</b> Internal diffusion parameters that model the diffusion of HPA onto GAC or CX at pH 8, 6.5, and 5.....	58
<b>Table 4.6</b> Rates of film and pore diffusion of HPA onto GAC or CX at pH 8, 6.5, and 5 .....	60
<b>Table 4.7</b> PFO rate constants of HPA, CHPA, and PVA onto GAC and CX at pH 8 .....	62
<b>Table 4.8</b> PSO rate constants of HPA, CHPA, and PVA onto GAC and CX at pH 8 .....	64
<b>Table 4.9</b> PFO rate constants of HPA onto GAC and CX at pH 8, 6.5, and 5.....	67
<b>Table 4.10</b> PSO rate constants of HPA onto GAC and CX at pH 8, 6.5, and 5.....	69
<b>Table A.1</b> $K_{OW}$ Coefficients of Model NAs at Different pHs .....	85
<b>Table A.2</b> pH 8 Experiment Results: Concentration 'C' of the HPA, CHPA, & PVA solutions with I. Control, II. GAC, & III. CX .....	86
<b>Table A.3</b> pH 6.5 Experiment Results: Concentration of HPA, CHPA, & PVA solutions with I. Control, II. GAC, & III. CX.....	87
<b>Table A.4</b> pH 5 Experiment Results: Concentration of the HPA, CHPA, & PVA solutions with I. Control, II. GAC, & III. CX.....	89
<b>Table A.5</b> Normalized adsorption capacity of GAC or CX at pH 8 for HPA, CHPA, or PVA... 90	
<b>Table A.6</b> Normalized adsorption capacity of GAC or CX at pH 8, 6.5, or 5 for HPA .....	91
<b>Table A.7</b> PFO and PSO model parameters for the adsorption of HPA, CHPA, and PVA onto GAC or CX at pH 8 .....	92
<b>Table A.8</b> PFO and PSO model parameters for the adsorption of HPA onto GAC or CX at pH 8, 6.5, or 5 .....	92

## List of Figures

<b>Figure 4.1</b> Residual concentration of HPA, CHPA, or PVA due to adsorption by GAC or CX at pH 8.....	45
<b>Figure 4.2</b> Residual concentration of HPA due to adsorption by GAC or CX at different experimental pHs .....	46
<b>Figure 4.3</b> Normalized adsorption capacity of GAC or CX at pH 8 for HPA, CHPA, or PVA ..	48
<b>Figure 4.4</b> Normalized adsorption capacity of GAC or CX at pH 8, 6.5, and 5 for HPA .....	49
<b>Figure 4.5</b> Effect of pH on the normalized adsorption capacity of GAC or CX by HPA .....	50
<b>Figure 4.6</b> Internal diffusion model of HPA, CHPA, or PVA onto GAC or CX at pH 8.....	51
<b>Figure 4.7</b> Internal diffusion model of the adsorption of (a) HPA onto GAC, (b) HPA onto CX, (c) CHPA onto GAC, (d) CHPA onto CX, (e) PVA onto GAC, and (f) PVA onto CX at pH 8..	55
<b>Figure 4.8</b> Internal diffusion model of HPA onto GAC or CX at pH 8, 6.5, and 5 .....	57
<b>Figure 4.9</b> Internal diffusion model of normalized adsorption of HPA (a) onto GAC at pH 8, (b) onto CX pH at 8, (c) onto GAC at pH 6.5, (d) onto CX at pH 6.5, (e) onto GAC at pH 5, and (f) onto CX at pH 5 .....	59
<b>Figure 4.10</b> Linear PFO model of the adsorption of HPA, CHPA, & PVA onto GAC or CX at pH 8.....	61
<b>Figure 4.11</b> Linear PFO model of (a) HPA onto GAC, (b) HPA onto CX, (c) CHPA onto GAC, (d) CHPA onto CX, (e) PVA onto GAC, and (f) PVA onto CX at pH 8 .....	62
<b>Figure 4.12</b> Linear PSO model of the adsorption of HPA, CHPA, and PVA onto GAC or CX at pH 8.....	63
<b>Figure 4.13</b> Linear PSO Model of (a) HPA onto GAC, (b) HPA onto CX, (c) CHPA onto GAC, (d) CHPA onto CX, (e) PVA onto GAC, and (f) PVA onto CX at pH 8 .....	64
<b>Figure 4.14</b> Linear PFO model of the adsorption of HPA onto GAC or CX at pH 8, 6.5, or 5 ..	66
<b>Figure 4.15</b> Linear PFO model of HPA (a) onto GAC at pH 8, (b) onto CX pH at 8, (c) onto GAC at pH 6.5, (d) onto CX at pH 6.5, (e) onto GAC at pH 5, and (f) onto CX at pH 5 .....	67
<b>Figure 4.16</b> Linear PSO model of the adsorption of HPA onto GAC or CX at pH 8, 6.5, or 5 ..	68
<b>Figure 4.17</b> Linear PSO model of HPA (a) onto GAC at pH 8, (b) onto CX pH at 8, (c) onto GAC at pH 6.5, (d) onto CX at pH 6.5, (e) onto GAC at pH 5, and (f) onto CX at pH 5 .....	69

# Chapter 1 Introduction

## 1.1 Background & Motivation

The oil and gas sector is known to be one of the dominating industries in the world due to its profound impact not only on universal economics but on the environment in various ways. As oil and gas industries continue to seek innovative technologies to expand their production, it is worth noting that the demand on fresh water supplies continues to substantially rise. Likewise, advanced production inevitably generates large volumes of wastewater that must be processed not only for environmentally acceptable disposal, but also for potential reuse. Over the past decade oil and gas developments have appealed to the extraction of unconventional hydrocarbon resources. An unconventional resource that is known to be one of the most challenging to extract yet continues to be of worldwide interest is shale oil and gas. Shale reserves contain what seem to be an inexhaustible amount of hydrocarbons that are trapped within impermeable rocks and are most commonly extracted by horizontal drilling methods followed by hydraulic fracturing (fracking) (Hughes 2013). Hydraulic fracturing involves the high-pressure injection of fluid to crack the impermeable rocks allowing for accessibility to the hydrocarbons. A typical shale extraction process can require approximately 400,000 to 4 million liters of water for drilling and an additional 7 to 18 million liters for fracking, with up to 40% of fracking water discharging out of the well as flowback wastewater (Gregory et al. 2011).

Of local focus, unconventional oil reserves are present as oil sands in the form of crude oil deposits. Alberta's oil sands are known to be one of the largest oil accumulations in the world, attributing to more than 170 billion barrels of oil (Headley et al. 2013). The isolation of bitumen from sand and clay is completed through the Clarke caustic hot water extraction process which requires three to six barrels of water to produce one barrel of crude oil (Schramm et al. 2000; Schindler et al. 2006). Water used for the extraction process is in the form of alkaline hot water or high pressure steam, which forms a large amount of what is known to be oil sands process-affected water (OSPW) (Anderson et al. 2012). Due to Alberta's zero discharge policy; OSPW is stored in cement-lined tailing ponds which constitute to over 170 km<sup>2</sup> in the Athabasca Oil Sands region (Scott et al. 2008). In addition to OSPW, tailing ponds also consist of sand, clay, silt, and unrecovered bitumen, and thus have become a concern due to their potential of leaching into groundwater and the Athabasca River, posing several toxic effects (Ahad et al. 2013; Allen 2008). Plenty of aquatic organisms have been affected by the toxicity of OSPW including; fish, mammals,

plants, birds, bacteria, benthic invertebrates, zooplankton, phytoplankton, and overall, OSPW has created an ecological imbalance in Northern Alberta (Hagen et al. 2014; Pereira et al. 2013; Whitby et al. 2010).

The toxicity of OPSW is chiefly due to naphthenic acids (NAs), polycyclic aromatic hydrocarbons (PAHs), and salts (Allen 2008). Notably, the removal of NAs has been given much attention due to their toxic effect in addition to harming process equipment used in the bitumen recovery process (Quinlan et al. 2015). Concentration of NAs in natural waters of northern Alberta are typically below 1 mg/L, whereas in OSPW concentrations can reach up to 120 mg/L which is enough to pose toxic effects on aquatic life (Allen 2008). Methods that have been investigated for the comprehensive removal of NAs include, but are not limited to; advanced oxidation, biodegradation, coagulation/flocculation, membrane filtration, catalytic reactions, microbial reaction, and of particular interest, adsorption (Quinlan et al. 2015).

## 1.2 Problem Statement

Ongoing research is being conducted regarding the possibility of using various adsorbents to treat OSPW. Adsorbents of different types are being investigated, in addition to employing the modification of adsorbent surfaces to enhance their performance, or adding adsorbents to other treatments to take advantage of synergistic effects. A majority of adsorbents currently being explored are carbon materials as they are considered universal adsorbent due to the many advantages they pose. However, in most cases the performance of carbonaceous materials to adsorb NAs is considered limited due to their fixed textural properties as a result of being derived from raw materials. Therefore, novel approaches have begun to examine carbonaceous materials that can be synthesized to prepare an adsorbent with desired characteristics. In particular, carbon xerogel (CX) materials are currently being studied due to its mesoporous carbonaceous material with a unique advantage of having high adsorption capacity, low production cost, easy disposal, and comparable surface characteristics (Carabineiro et al. 2012).

The main virtue of an adsorbent is its surface characteristics as these characteristics determine the efficacy of adsorption and can enhance adsorption technologies. In order to determine the viability of an adsorbent, its surface should be analyzed and visualized to determine whether or not it contains characteristics that qualify it to be an effective adsorbent. Since research is being

conducted around CX material, surface characterization and visualization of CX is carried out to discern the interfacial forces occurring on the surface that are responsible for adsorption.

### 1.3 Research Objective

In this project, carbon xerogel material is evaluated for its ability of being a viable adsorbent for the removal of naphthenic acids. In particular, the feasibility of carbon xerogel will be assessed by addressing the following objectives:

- (1) To determine the adsorption capacity of CX material by examining the removal of model NA compounds at different operating conditions to explore the kinetics of removal.
- (2) Consequently, the adsorption mechanisms responsible for the removal of NAs by CX are identified based on the structure-activity relationships between the model compounds and the surface of the adsorbent.
- (3) To compare the adsorption performance and surface characteristics of CX to conventional granular activated carbon (GAC), a well-established adsorbent for the treatment of OSPW. In this way, the viability of CX to perform effectively as an adsorbent for OSPW treatment is verified.

### 1.4 Hypothesis

Given the complexity of NAs present in OSPW, their reclamation by means of adsorption mechanisms require an adsorbent with textural properties that can be tailored to suit the properties of NAs. Provided that CX material exhibit comparable surface characteristics, notably a mesoporous character, a wide range of NAs can be removed from OSPW by CX through a variety of adsorption mechanisms such as structure-activity relationships.

### 1.5 Research Impact

As mentioned earlier in section 1.1, the development of wastewater treatment technologies is of vital importance to enhance water management and control in the oil and gas industry, particularly in industries resorting to prominent unconventional reserves such as shale oil and gas, and oil sands. To address the environmental issues associated with the toxic compounds and pollutants of emerging concern present in Alberta's OSPW, several studies have been conducted to develop new technologies that can treat OSPW. Among the many treatment technologies currently being investigated, adsorption systems using a variety of adsorbents under a range of

conditions are being investigated. In order to develop an effective and efficient adsorption system for OSPW treatment, adsorbent materials to be employed for the treatment of OSPW should be not only tailored to the characteristics of NAs, but should also exhibit textural properties that enhance adsorption interactions to allow for effective removal. The results of this project will assist other studies in developing effective adsorption systems which will further support ongoing efforts to promote the sustainable development of Alberta by enhancing water quality in the Athabasca Oil Sands region and protect the environmental and public health.

## 1.6 Thesis Outline

This thesis consists of five chapters. The thesis begins with a general chapter that discusses the importance of wastewater treatment in the unconventional oil and gas industry, more distinctively pertaining to the Alberta oil sands industry. Moreover, the study of CX material as a feasible adsorbent for the treatment of OSPW is proposed. Afterwards, the second chapter presents an overview of the adsorption phenomena and adsorption treatments under study or currently established in the treatment of OSPW. In addition, recent studies exploring the use of CX are explored to propose the use of CX as an adsorbent for the reclamation of OSPW. Furthermore, the third chapter describes the investigations made to distinguish the adsorption mechanisms responsible for the removal of model NAs by CX material. Finally, the results of the adsorption kinetics investigations are discussed to deduce the mechanisms by which model NAs are adsorbed onto CX. Likewise, the performance of CX is compared to GAC to determine whether CX is considered a viable adsorbent. Finally, the thesis concludes by recommending further types of studies that would assist in confirming the feasibility of CX in OSPW treatment.

## Chapter 2 Background

### 2.1 Theory: Review of the Fundamentals of Adsorption

Adsorption is a mass transfer operation that involves the accumulation of adsorbate molecules (liquid or gaseous phase) at the surface or interface of an adsorbent (porous solid) (Thomas and Crittenden, B. 1998; Faust and Aly 1987; Crittenden, J. 2012).

#### 2.1.1 Adsorption Types

The means by which the adsorbate is transferred to the adsorbent determines the type of adsorption taking place. The most common adsorption mechanism in water treatment is physical adsorption, also known as physisorption. As its name implies, physical adsorption occurs through a physical attraction between the adsorbate and adsorbent as a result of relatively weak intermolecular forces, such as van der Waals forces. The binding mechanisms responsible for physical adsorption require less energy with low heat of adsorption, approximately 4 to 40 kJ/mol, and the process is considered exothermic. This low heat of adsorption consequently allows for a rapid process which is in fact reversible. Physical adsorption is considered more efficient as the adsorbate molecules cover the entire adsorbent surface without restrictions and the mechanism is not considered site specific. For this reason, an extensive adsorbent surface area plays an important role in physisorption. A notable feature of physisorption is that the weak interactions that result in physical attraction uphold the individuality of the interacting adsorbate-adsorbent species, unlike the other type of adsorption. (Faust and Aly 1987; Crittenden, J. 2012)

Conversely, adsorption which occurs by means of chemical reactions is known as chemical adsorption, i.e. chemisorption, and is less common in water treatment. Chemisorption occurs through the formation of chemical bonds between adsorbate molecules and the adsorbent surface resulting in a transfer of electrons. This more specific mechanism requires a much higher heat of adsorption, greater than 200 kJ/mol in comparison, and typically results in an irreversible yet also exothermic process. (Faust and Aly 1987; Crittenden, J. 2012)

#### 2.1.2 Steps of the Adsorption Process

The process of adsorption can be divided into stages based on the dominating mass transport mechanisms that take place. The four general steps of adsorption are as follows (Metcalf and Eddy 2014):

- (1) *Bulk Solution Transport*: is the movement of adsorbate molecules from the bulk solution to the fixed liquid film that surrounds the surface of the adsorbent as a boundary layer. In terms of mass transfer, this form of transport occurs by means of advection and diffusion in the form of dispersion.
- (2) *Film Diffusion Transport*: involves the transport of the adsorbate molecules from the stagnant liquid film to the access of the pores on the adsorbent surface. As entailed by the title of this step, the transport of the adsorbate molecules in this step requires diffusion.
- (3) *Pore Transport*: is the movement of the adsorbate molecules from the entrance of the adsorbent pores to within the pores. The adsorbates are transported along with the liquid through the pores by means of molecular diffusion or along the surface of the adsorbent by a gradient, thus by diffusion also. As mass transport through the pores may occur through either molecular diffusion or diffusion due to a gradient, it may also take place through a combination of the two.
- (4) *Adsorption*: happens when the adsorbate molecules have travelled through the pores of the adsorbent and affix themselves to available sites on the surface of the adsorbent. Attachment of adsorbate molecules occurs in the micropores (less than 2 nm), mesopores (2 to 50 nm), macropores (greater than 50 nm), and the outer surface until the adsorbent becomes saturated or the adsorbate is completely removed. Typically, the micropores adsorb more material due to their higher surface area relative to the meso- and the macropores which in some cases may observe negligible adsorption.

### 2.1.3 Adsorption Kinetics and Models

Each phase that takes place in the adsorption process can be quantified per specific models that further demonstrate the steps in a more measurable manner. To begin with, the initial step of bulk solution transport can be considered a form of external mass transfer since the adsorbate molecule is being transferred from the bulk liquid solution to the solid surface (Largitte and Pasquier 2016). Essentially external mass transfer can be modeled through Fick's laws of diffusion, however; given that the batch adsorption experiments conducted involve rapid and constant mechanical stirring, this step is essentially rushed enough that this form of transport may be assumed negligible in terms of modeling (Largitte and Pasquier 2016).

### 2.1.3.1 Diffusion Models

The most significant steps of the physical adsorption process are the film diffusion and pore transport phases since they are responsible for transporting the adsorbate molecules from the stagnant film surrounding the adsorbent to and within the pores by means of diffusion to finally access the surface and be adsorbed within (Metcalf and Eddy 2014). The rate at which the entire adsorption process takes place is determined by the step that is more time consuming, i.e. the rate limiting step. Therefore, as essential as the diffusion steps are, they are typically the most prolonged, compelling them to be the rate limiting steps. Thus, in physisorption the rate of diffusion determines the speed of the entire adsorption process. The diffusion phases can be modeled through the internal diffusion model which has been developed by Weber and Morris (1963) upon studying batch adsorption and generalized by the Bangham model to equation (1), which is the less complicated and relatively easier to use among all diffusion models (Largitte and Pasquier 2016; Nethaji 2012; Cheung et al. 2007):

$$q_t = k_i t^{1/2} + c \quad (1)$$

Where:

$k_i$ : Internal diffusion rate constant (mg/g/hr<sup>1/2</sup>)

$q_t$ : Amount of adsorbate removed by adsorbent at time, t (mg/g)

$c$ : Intercept of  $q_t$  vs.  $t^{1/2}$  curve (mg/g)

Note that  $q_t$ , is referred to as the adsorbent capacity or amount of adsorbate removed by adsorbent, and is given in equation (2). In addition, the subscript, 'e', refers to equilibrium time which is assumed as the final time in this particular study.

$$q_t = \frac{(C_o - C_t)V}{m} \quad (2)$$

Where:

$C_t$ : Concentration of adsorbate at time, t, and subscript 'o' denotes initial time (mg/L)

$V$ : Volume of adsorbate (L)

$m$ : Mass of adsorbent, i.e. adsorbent load (g)

The key to the internal diffusion model is to develop a plot of  $q_t$  versus  $t^{1/2}$ , which should produce a straight line. From this curve, the diffusion rate constant,  $k_i$ , can be calculated from the slope of the line. In the case that the curve passes through the origin, the constant,  $c$ , i.e. the intercept, is zero, and the rate limiting step is the pore transport stage alone (Nethaji et al. 2012). On the other hand, if the intercept of the plot is not zero and the constant,  $c$ , is given a value, then film diffusion is also important due to significant thickness of the boundary layer surrounding the adsorbent, and can be considered the rate limiting step as well (Nethaji et al. 2012). Therefore, the internal diffusion model provides insight into the significance of the diffusion phase, whether it is dominated solely by pore transport or a combination of the diffusion stages, in addition to noting the significance of the film surrounding the adsorbent (Nethaji et al. 2012).

#### *2.1.3.2 Adsorption Rate Models*

Furthermore, the adsorption step can be modelled by a range of kinetic models. It is worth nothing that for chemisorption, the rate mainly relies on bond formation during the final step of adsorption, thus the final step is considered rate-limiting (Metcalf and Eddy 2014).

##### *(1) Pseudo-First-Order (PFO) Model*

The most widespread adsorption kinetics model is Lagergren's pseudo-first-order (PFO) model (Lagergren 1898). In general, the Lagergren PFO model is most commonly used to model the removal of many pollutants from a variety of wastewaters by adsorption (Qui 2009). Lagergren's PFO model was developed based on a set of assumptions; first and foremost, that the adsorbate uptake on the adsorbent surface follows a first-order rate equation (Largitte and Pasquier 2016). Secondly, that the concentration of the adsorbent is assumed constant (Largitte and Pasquier 2016). Lagergren's PFO model assumes that upon encountering the surface of the adsorbent, the sorbed adsorbate molecules do not interact with each other and are only adsorbed at localized sites (Largitte and Pasquier 2016). In addition, at saturation, the adsorbates form a monolayer on the adsorbent's surface (Largitte and Pasquier 2016). Finally, the energy of adsorption is only a function of the forces that bring about adsorption, and is independent of the surface coverage (Largitte and Pasquier 2016). It is worth mentioning that the PFO model only considers the forward reaction, i.e. the adsorption process, and disregards the reversible, desorption component of the process (Largitte and Pasquier 2016). Also, Lagergren's model was assigned the term 'pseudo' to distinguish the PFO model from the conventional first-order rate law; in which the former is based

on adsorption capacity whereas the latter is fixed on the solution concentration (Qui 2009; Ho and McKay 1998). The PFO model is demonstrated in equation (3):

$$\frac{dq}{dt} = k_I(q_e - q_t) \quad (3)$$

Where:

$k_I$ : PFO rate constant ( $\text{hr}^{-1}$ )

$q_e$ : Amount of adsorbate removed by adsorbent at equilibrium (mg/g)

$q_t$ : Amount of adsorbate removed by adsorbent at time, t (mg/g)

By integration with boundary conditions: at time  $t = 0 \text{ min}$ ,  $q = 0 \text{ mg/g}$  and at time  $t = t \text{ min}$ ,  $q = q_t$ , the linear form of the PFO is given in equation (4) and the nonlinear form in equation (5).

$$\ln\left(1 - \frac{q_t}{q_e}\right) = -k_I t \quad (4)$$

$$q_t = q_e(1 - e^{-k_I t}) \quad (5)$$

## (2) Pseudo-Second-Order (PSO) Model

Furthermore, the pseudo-second-order (PSO) equation was developed for chemical bonding, hence for chemisorption specifically (Ho and McKay 1998). The main assumption of the PSO follows that the sharing and exchange of electrons that form valent forces constitute to chemical adsorption and is considered the rate limiting step, as mentioned earlier (Qui 2009). Moreover, the PSO equation is based on the same assumptions as the PFO model, with exception that the adsorbate uptake follows the second order rate equation (Largitte and Pasquier 2016). Similarly, the PSO model is assigned the term pseudo for the same reason as mentioned for PFO (Qui 2009). Equation (6) shows the PSO kinetics model as:

$$\frac{dq}{dt} = k_{II}(q_e - q_t)^2 \quad (6)$$

Where:

$k_{II}$ : PSO rate constant (g/mg/hr)

$q_e$ : Amount of adsorbate removed by adsorbent at equilibrium (mg/g)

$q_t$ : Amount of adsorbate removed by adsorbent at time,  $t$  (mg/g)

By integration with boundary conditions: at time  $t = 0 \text{ min}$ ,  $q = 0 \text{ mg/g}$  and at time  $t = t \text{ min}$ ,  $q = q_t$ , the integrated form of the PSO is given in equation (7) which can be rearranged to the nonlinear form in equation (8) and the linear form in equation (9).

$$\frac{1}{q_e - q_t} = \frac{1}{q_e} + k_{II}t \quad (7)$$

$$q_t = \frac{t}{\frac{1}{k_{II}q_e^2} + \frac{t}{q_e}} \quad (8)$$

$$\frac{t}{q_t} = \frac{1}{k_{II}q_e^2} + \frac{t}{q_e} \quad (9)$$

Identification of the adsorption rate constants is imperative for adsorption kinetics as it gives an insight to how fast adsorbates are transferred onto the surface of an adsorbent and consequently determines the efficiency of an adsorbate removal process using adsorbents of interest.

#### 2.1.4 Forces of Adsorption

During adsorption, interactions take place at three defined interfaces; adsorbate-water, adsorbate-adsorbent, and water-adsorbent (Crittenden, J. 2012). Depending on the type of adsorption taking place, a range of adsorption interactions of varying strengths occur at each interface.

##### *(1) Chemisorption Interactions*

To begin with, chemisorption interactions are primarily related to the type of chemical reaction that occurs between the adsorbate and the adsorbent at the adsorbent's surface (Crittenden, J. 2012). As mentioned earlier, the rate or strength of chemisorption depends on the extent of reaction that takes place; therefore, the forces that promote chemisorption occur primarily at the adsorbate-adsorbent interface. Chemisorption interactions are chiefly defined by strong intramolecular forces. Upon reaction of the adsorbate at the surface, a covalent or ionic bond forms depending on the electronegativities of both the adsorbate and adsorbent (Crittenden, J. 2012). The attraction between the adsorbent and adsorbate, based on electrostatic chemical bonds, form according to Coulomb's law; in which charged surface groups on the adsorbent will attract

opposite charges and repel like charges of the adsorbate (Crittenden, J. 2012). Ionic bonds developed through Coulomb's law result in complete transfer of electrons between the adsorbate and adsorbent. On the other hand, when electronegativities between the adsorbate and adsorbent do not vary, attractive and repulsive forces are balanced and electrons are shared to attract the adsorbate and adsorbent through a covalent bond. Given that chemisorption bonds hold atoms together within molecules, the length of these bonds are considered shorter and require higher bond energy, approximately greater than 42 kJ/mol (Crittenden, J. 2012). As described in section 2.1.1, chemisorption bonding of the adsorbate is specific to certain pores of the adsorbent in which bonding only occurs at particular sites or functional groups on the surface (Crittenden, J. 2012). For this reason, adsorption of this type cannot form more than one molecular layer (Crittenden, J. 2012).

## *(2) Physisorption Interactions*

In contrast, physisorption forces of attraction take place at all three interfaces aforementioned (Crittenden, J. 2012). The strength of the adsorbate-adsorbent interaction which chiefly depends on the adsorbent characteristics, to be discussed later, determines the extent of the overall adsorption process (Crittenden, J. 2012). Furthermore, solubility of the adsorbate and its ability to be removed from water determines the adsorbate-water interactions, and similarly adsorbent properties that determine its affinity to water, hydrophobic or hydrophilic, govern water-adsorbent interactions (Crittenden, J. 2012). In general, the weak intermolecular physical forces that govern physisorption are related to a balance of the attraction and repulsion of the adsorbate-adsorbent molecules at the long and short range respectively (Thomas and Crittenden, B. 1998). Weaker, intermolecular forces, responsible for physisorption, are electrostatic forces of attraction, collectively known as van der Waals forces (Solomons et al. 2011). Factors that control physical forces of attraction include the charges, dipole moments, ionization potential, and polarizability of both the adsorbate and adsorbent molecules (Maitland et al. 1981).

Van der Waals forces are generally categorized into two types; dipole-dipole, and London dispersion. Dipole-dipole forces occur between polar, non-charged groups as a result of permanent dipole moments on the molecules interacting (Solomons et al. 2011). A much stronger form of dipole-dipole bonding that requires up to 42 kJ/mol of energy is hydrogen bonding, in which a hydrogen atom bonds with a highly electronegative atom, specifically nitrogen, oxygen, or fluorine

(Crittenden, J. 2012; Solomons et al. 2011). In contrast, the major attractive force responsible for adsorption onto AC are London dispersion forces (Crittenden, J. 2012). London dispersion forces are weaker interactions between nonpolar molecules to form temporary or weak dipoles in any combination of the following with themselves or one another; permanent dipoles, induced dipoles, and quadrupole electrostatic effects (Thomas and Crittenden, B. 1998).

With regards to adsorbate removal and interactions at the various interfaces, it is crucial to understand the principle of van der Waals attractions since it is the most predominant force of attraction in physisorption. In general, a less polar adsorbate will exhibit lower solubility and therefore result in weaker adsorbate-water interactions and will ease the removal of the adsorbate (Crittenden, J. 2012). Furthermore, a larger adsorbate that is more polarizable, i.e. has a high ability to form dipoles, will become attracted to the adsorbent through van der Waals interactions (Crittenden, J. 2012). Most popularly, this form of interaction to nonpolar adsorbents is called hydrophobic bonding (Crittenden, J. 2012).

#### 2.1.5 Factors that Affect Adsorption Performance

The performance of an adsorption process depends on a variety of factors. To clearly understand the impact of each aspect on the overall process, the factors are classified according to characteristics of each components of the process. The factors affecting adsorption are listed as follows:

##### (1) *Adsorbent Characteristics*

The properties of the adsorbent used play a significant role in the performance of an adsorption process, mainly because the respective properties are responsible for effective removal of the adsorbate of concern from the solution of interest. Textural characteristics of the adsorbent play a vital role in the ability of an adsorbent to withdraw and embrace an adsorbate molecule within the surface. The two interrelated textural characteristics dominating the adsorbent capacity are the internal surface area and pore size distribution (Villacanas et al. 2005). These two factors directly affect the availability of adsorption sites in which a larger surface area provides for a greater amount of sites available (Crittenden, J. 2012). The pore size distribution indicates the range of pore sizes available on the site; whether micro, meso, or macropores (Crittenden, J. 2012). Based on the respective sizes of pores, adsorbate molecules can access the pores available on the

surface of the adsorbent. Accordingly, the porosity of the adsorbent is responsible for accessibility to the adsorption sites (Crittenden, J. 2012). It should be noted that while the adsorbent internal surface area and pore size affect the accessibility and availability of adsorption sites simultaneously they are inversely interrelated (Crittenden, J. 2012). For instance, a larger surface area is typically the result of smaller pore sizes for a given pore volume. In an essence, the smaller the adsorption sites, the more sites available on the surface for adsorption.

In addition to textural properties, the surface chemistry of the adsorbent also plays a predominant role in enhancing the performance of an adsorbent (Villacanas et al. 2005). Functional groups and chemical elements present on the surface determine the means by which adsorption takes place and forces responsible for adsorption. As described extensively in section 2.2.3, the presence of surface functional groups such as N-H primary amines, C-H benzene groups, and O-H groups identified on the surface of petroleum coke (PC) result in hydrogen bonding with hydroxyl groups of NAs (Pourrezaei et al. 2014a). Likewise, the detection of chemical elements on the surface an adsorbent identifies mechanisms for adsorption such as the identification of a low amount of nitrogen on PC which reveals that N-H hydrogen bonding is not the major means of adsorption (Pourrezaei et al. 2014a).

## (2) *Adsorbate Characteristics*

Various properties of the adsorbate of interest majorly contribute to the success of adsorbate removal. The overall feature that is desired in an adsorbate is hydrophobicity, in which all aspects of the adsorbate should contribute to the hostility of the adsorbate to water so that it may be easily removed. In most cases, the octanol-water coefficient,  $K_{OW}$ , defines the ability of a compound to partition out of water, in which a higher  $K_{OW}$  value indicates that a compound is more hydrophobic. This trend is generally applicable; yet, with regards to NAs, particularly those present in OSPW, there is no well-defined trend that expresses the hydrophobicity of NAs, mainly due to their complexity. However, some correlations have been determined through earlier studies. For example, both Zubot et al. (2012) and Pourrezaei et al. (2014a) identified that more complex NAs arising from higher carbon numbers, number of rings, and higher molecular weights are removed at higher rates. More specifically, Pourrezaei et al. (2014a) noted that as the carbon number increased for a particular  $-Z$  value (degree of unsaturation or hydrogen deficiency), this meant that the molecular weight of the NA compound increased, which caused the compound to

become less soluble, consequently raising its log  $K_{OW}$  value, hence becoming more hydrophobic. Furthermore, Zhang et al. (2015) estimated the  $K_{OW}$ s of NAs to identify that NAs, in general organic compounds, with higher carbon numbers and lower double bond equivalents are more hydrophobic.

With regards to adsorbates in general, many factors contribute to its ability to be removed. To begin with, similar to the adsorbent, the functional groups that make up the adsorbate contribute to its attractiveness to an adsorbent (Villacanas et al. 2005). Like adsorbents, the presence of specific functional groups in an adsorbate aids in facilitating specific forces of attraction. For instance, continuing with the example of PC, the presence of carboxylic acid groups in NAs improves the hydrophobic removal of NAs from OSPW (Pourrezaei et al. 2014a).

The functional groups an adsorbate contains relate to other properties that impact the removability of the adsorbate. For example, adsorbates with ionic functional groups are considered polar and highly hydrophilic and thus not easily adsorbed. The pKa of the adsorbate is a property that coincides with polarity, in which maximum removal of the polar species can be achieved at a pH where the species is undissociated and less soluble (Faust and Aly 1987). Furthermore, acid-base reactions at ionic functional groups may be promoted between inorganic adsorbents and adsorbates upon chemical bonding during chemisorption (Crittenden, J. 2012). Ionic adsorbates of this form are removed at optimum pH and ionic strength by means of electrostatic attraction (Crittenden, J. 2012).

On the other hand, neutral adsorbates such as neutral organics, rely on properties such as size and solubility for their adsorptive abilities (Crittenden, J. 2012). In general, an adsorbate with greater molecular size is considered less soluble and more easily removed from the solution by an adsorbent (Crittenden, J. 2012). The greater size of the adsorbate molecule enables it to form instantaneous dipoles and can be attracted due to dipole-neutral interactions (Crittenden, J. 2012). Therefore, the polarizability of neutral species is also considered an important aspect for the removal of neutral adsorbates (Crittenden, J. 2012).

In addition to the removal of neutral adsorbates in particular, the molecular size of any adsorbate in general plays an important role in the adsorption of adsorbate molecules into the pores of the adsorbent (Villacanas et al. 2005). This is explained by the steric effect in which the pore

size of the adsorbent determines the size of the species that may be adsorbed (Crittenden, J. 2012). As mentioned earlier, the surface of an adsorbent is characterized by pores of various sizes depending on whether the surface contains solely micro, meso, or macropores, or a combination of two or more pore sizes. Clearly, the size and structure of the adsorbate molecules of interest should be within the limits of the pore sizes present on the surface of the adsorbent. In a similar manner, molecular weight of adsorbate compounds affects the removal of an adsorbate from the solution and its adsorption into the pores of the adsorbent. In general, the heavier the adsorbate compound, the less soluble it is, and consequently easier to remove (Crittenden, J. 2012). Furthermore, the weight of the molecule controls the size and once again determines its ability to access the pores of the surface. Notably, the size also affects the rate of adsorption since a larger and heavier molecule would observe slower kinetics (Faust and Aly 1987). In general, molecular weight and molecular structure are usually correlated. There is no defined trend for the relation of molecular structure to hydrophobicity, however few observations have been determined. Typically, a high molecular weight is associated with a longer chain which is not only slower, but in some cases also more hydrophilic (Faust and Aly 1987).

### (3) *Solution Conditions*

Without doubt the most important components of an adsorption process are the adsorbate of interest and the adsorbent used to remove it. However, it should be noted that the overall objective of adsorption is to remove an adsorbate from a particular solution, in most cases water. In general, the challenge of adsorption is to overcome conditions that control the adsorbates' suspension in the solution. Therefore, certain solution conditions are considered factors that determine whether an adsorbate can be easily removed or sustained in suspension. A chief promoter to the attraction of an adsorbate to an adsorbent is the solution pH (Villacanas et al. 2005). The pH of the solution determines the electric state of the adsorbent, and as mentioned in the previous section, the dissociation of functional groups, particularly polar species dissolved in the solution and present on the surface of the adsorbent (Faust and Aly 1987). Therefore, controlling the pH of the solution governs the electrostatic interactions between the adsorbate and adsorbent (Faust and Aly 1987). For example, NAs exhibit a negative charge due to the carboxylic acid they contain (Barrow et al. 2010; Quinlan et al. 2015). To promote electrostatic attractions between NAs and the adsorbate used to remove it, for instance PC, the pH of the NA solution must

be below the pH of point zero charge ( $\text{pH}_{\text{PZC}}$ ) of PC so that the PC surface may exhibit an overall positive charge and attraction may be induced (Pourrezaei et al. 2014a). Conversely, if the pH is above the  $\text{pH}_{\text{PZC}}$ , the PC surface will exhibit a negative charge and repulsion will occur between the NAs and PC, hindering adsorption (Pourrezaei et al. 2014a).

In addition, a solution condition that affects adsorbate uptake is solution temperature (Faust and Aly 1987). The operating temperature directly affects the kinetics of adsorption through the Arrhenius equation, equation (10) (Faust and Aly 1987):

$$k = Ae^{-E_a/RT} \quad (10)$$

Where:

$k$ : Rate constant (units depend on reaction order)

$A$ : Activations energy (usually kJ/mol)

$E_a$ : Amount of adsorbate removed by adsorbent at time,  $t$  (mg/g)

$R$ : Universal gas constant (units depend on constant value chosen)

$T$ : Temperature (Kelvin)

Notably, diffusion-controlled process, i.e. physisorption mechanisms, generally observe an increase in the rate of adsorption as the temperature increases, given that the process is exothermic (Faust and Aly 1987).

Furthermore, the composition of the solution also affects the removal of an adsorbate. Firstly, the initial concentration of adsorbate present demonstrates the solubility state of the adsorbent (Villacanas et al. 2005). No exact trend between the initial concentration and adsorption has been defined, other than the models provided in equations (1) and (3) through (9), all of which are a function of the adsorbent capacity,  $q$ , which is dependent of the initial concentration. Faust and Aly (1987) noted that studies of the removal of alkylbenzenesulfonates by carbon showed that a more dilute solution, hence smaller initial concentration, resulted in more rapid adsorption. On the other hand, a study of the adsorption of 2,4-DCP and cyanonitrile demonstrated that as the

initial concentration increased, more adsorbate was removed per time, yet equilibrium time remained the same (Faust and Aly 1987). Moreover, not only is the reduction of adsorbates limited by the pores' availability, but also the presence of other potential adsorbents in the solution that may promote a form of competition (Villacanas et al. 2005). Solutions that contain multiple species initiate adsorbate competition if more than one type of molecule is attracted to the adsorbate. Depending on the various characteristics of adsorbates mentioned in the previous section, some adsorbates are more susceptible to adsorption than others mainly because they exhibit properties that advance their interactions with the adsorbent. Given that some adsorbate molecules can be at advantage over others, the number of sites vacant on the adsorbent for the adsorbate of interest becomes limited and thus competitive adsorption becomes a major concern.

#### (4) *Adsorbate-Adsorbent Interactions*

With regards to adsorption performance, the removal of an adsorbate by an adsorbent is clearly dependent of the affinity of the adsorbate to the adsorbent and the forces that attract them to one another. Forces responsible for adsorption, whether they may be weak intermolecular forces of physisorption or chemical bonds that dominate chemisorption, determine the effectiveness of adsorption. Simply, the stronger the force of attraction, the more removal achieved. The affinity and strength of interaction between the adsorbate and adsorbent are dependent of several factors all of which control the adsorption performance. To summarize, the textural properties and surface chemistry determine whether an adsorbent is eligible to undertake and house adsorbate molecules. In a similar manner, the functional groups that make up an adsorbate and the physical structure and size it exhibits determines whether an adsorbate has less affinity to the solution it is suspended in, i.e. hydrophobic, and is easily removed. Although hydrophobicity majorly contributes to the removal of an adsorbate from a solution, forces of attraction between the adsorbate and adsorbent must take place to ensure that the adsorbate is not only removed but adsorbed onto the surface of the adsorbent. Finally, the solution that contains the adsorbate and the adsorbent is introduced to must provide an environment that promotes the attraction of the adsorbate to the adsorbent to ensure effective removal.

## 2.2 Literature Review: A Review of Oil Sands Process-Affected Water Treatment

As mentioned in section 1.1, the oil and gas industry continues to process exceptionally large amounts of fresh water while simultaneously promoting a higher risk for water pollution. As

unconventional reserves become economically viable through emerging technologies, the stress on fresh water resources becomes more severe with a growing concern of contamination due to a substantial rise in wastewater production. For instance, the revolutionary shale oil and gas extraction process can use up to 4 million liters of water during the drilling stage followed by 7 to 18 million liters of water for hydraulic fracturing (fracking), with up to 40% of fracking water discharging out of the well as flowback wastewater (Gregory et al. 2011). Flowback wastewater has become an increasing problem due to its significant concentration of salts, metals such as iron, oils, greases, soluble organic compounds, and high concentration of dissolved organic matter including surfactants and acetic acids (Lester et al. 2015; Gregory et al. 2011). Likewise, conventional petroleum refineries worldwide are burdened with oilfield wastewaters that require treatment due to the alarming amounts of hazardous pollutants (Wang et al. 2015). Among these hazardous pollutants, NAs have become a contaminant of emerging concern for petroleum and petrochemical refineries due to their persistence and notable toxicity (Wang et al. 2015). Locally, NAs continue to be a major factor with regards to reclamation of the Alberta OSPW.

### 2.2.1 Naphthenic Acids

Dissolved organic compounds present in OSPW include; polycyclic aromatic hydrocarbons (PAHs), phenols, cresols, benzene, toluene, thiophenols, and NAs, the chief contributor of toxicity in OSPW (Allen 2008). NAs are a family of carboxylic acids, usually with one or more saturated ring structure (Barrow et al. 2010). Being lipophilic and hydrophilic, i.e. amphiphilic, NAs are classified as negatively charged carboxylate salts that are highly soluble in water and can act surface-active under certain conditions (Quinlan et al. 2015). NAs have the general chemical formula  $C_nH_{2n+Z}O_x$ ; n being the number of carbon atoms, Z is the number of hydrogen atoms lost due to the ring formation or the double bond, and x is the number of oxygen atoms (Barrow et al. 2010). It should be noted that NAs with an x value of 2 are known as classical NAs, and those with x values greater than 2 (usually 3 to 5) are referred to as oxygenated NAs (Barrow et al. 2010).

#### 2.2.1.1 Naphthenic Acids in OSPW

NAs are originally present in petroleum deposits as a result of two natural phenomena. Firstly, they are formed during partial aerobic biodegradation when bitumen is exposed to natural geographic events such as erosion or earthquakes (Watson et al. 2002). Second, NAs are formed during incomplete catagenesis of bituminous compounds in petroleum deposits that are at high

temperatures and pressures (Clemente et al. 2005). NAs become soluble and present at significant concentrations in slightly alkaline OSPW, pH 8.5, upon the extraction and mining of bitumen from oil sands ore (Schramm et al. 2000). The concentration of NAs in OSPW indicates the extraction efficiency, in which the solubilization of NA droplets in OSPW is essential for bitumen droplets to separate from sand particles (Sanford 1983). The surface-active properties of NAs play a fundamental role in bitumen recovery. NAs emerge in OSPW to assist bitumen-sand extraction by electrostatically repelling the two phases (Schramm et al. 2000). Afterwards, NAs remain in OSPW in order to not interfere with the bitumen-air adhesion process. NAs can be present in OSPW in concentrations up to 120 mg/L as mentioned previously (Allen 2008). Natural biodegradation reduces this concentration to approximately 40 to 70 mg/L in mature tailing ponds (Allen 2008). However, the NAs concentration will remain at a minimum of 19 mg/L in mature tailing ponds due to the resistance of some NAs fractions to biodegradation (Leung et al. 2001).

#### *2.2.1.2 Toxicity of NAs*

High concentrations of NAs in OSPW have resulted in significant acute and chronic toxic concerns on aquatic and mammalian species in addition to corrosive effects toward process equipment used in the bitumen extraction unit operations (Quinlan et al. 2015). Studies have shown that the surface-active properties of NAs make them the most toxic compound in OSPW (Rogers et al. 2002). The primary mode of NAs toxicity is by disrupting the cell membranes resulting in non-specific narcosis (Frank et al. 2009). Early studies have demonstrated that the acute lethality of NAs towards rainbow trout and water fleas is appreciably reduced upon removing NAs from OSPW (MacKinnon et al. 1986). Furthermore, recent studies have revealed that fathead minnows exposed to low concentrations of NAs (10 mg/L) had low reproductive abilities (Kavanagh et al. 2012). Moreover, bioassays demonstrated that untreated OSPW was acutely toxic to *Vibrio fischeri* and rainbow trout (Zubot et al. 2012). In addition, at high temperatures (200 to 400°C), NA multimers in OSPW dissociate into monomers and induce corrosion in the process equipment used in the bitumen process (Fan et al. 1991; Schramm et al. 2000). Metal ions near the metallic surface of the process equipment form metal carboxylates with NAs and have the potential to diffuse into the bulk fluid and degrade the metal surface (Chakravarti et al. 2013).

#### *2.2.2 Comprehensive Analysis of OSPW*

With emphasis on water pollution concerns from the extraction of unconventional reserves, investigation of the Alberta OSPW is conducted due to its effect on water resources in Alberta and

the surrounding environment. NAs and other constituents of OSPW must be thoroughly characterized prior to treatment to understand which treatment approach would provide plausible results.

To understand what are the constituents of OSPW and in an essence, what it contains, several techniques under a variety of conditions have been employed to analyze OSPW. A comprehensive study conducted by Barrow et al. (2010), used atmospheric pressure photoionization (APPI) and electrospray ionization (ESI) fourier transform ion cyclotron resonance (FTICR) mass spectrometry (MS) in both positive and negative ion modes. Positive mode was used to reveal the basic components of OSPW that require protonation in order to appear, whereas negative ion mode showed the acidic components, in which deprotonated NAs appear. This combination of technologies was used to overcome the complexity that petroleum related compounds exhibit. The results of Barrow's studies demonstrated that the predominant species of OSPW are oxygenated species, mainly NAs. The APPI in both ion modes revealed the presence of carbon, hydrogen, nitrogen, and sulfuric components. For example, sulfur present in the form of  $C_nH_{2n+Z}S$  appeared with carbon numbers 26 and 28, and Z at -12. Nitrogen, on the other hand appeared as  $C_nH_{2n+Z}N$  with carbon numbers ranging from 24 to 27 and Z numbers between -13 and -17. The structures of the nitrogen-containing compounds were identified as pyrrolic and pyridinic compounds. In addition, APPI in positive mode exhibited compounds such as; hydrocarbons,  $O_3S$ ,  $NO$ , and  $NO_2$  with Z numbers in the aliphatic to aromatic range. The most intense species observed in Barrow's studies were NAs that appeared in APPI with negative ESI mode. The NAs observed were those of high carbon number (10 to 25) and Z numbers ranging from 0 to -24, in which high Z numbers identified the presence of naphthenoaromatics.

Similar to Barrow's primary identification of NAs in OSPW, ultra-high resolution ESI-FTICR-MS studies by Grewer et al. (2010) noted that OSPW contained acid extractable organics (AEOs) of which NAs, both classical and oxy-, are components of. Grewer identified that NAs contained in OSPW mainly exhibited carbon numbers ranging from 8 to 30, Z numbers ranging from 0 to -12, and oxygen numbers ranging from 2 to 5. The mass spectroscopy studies showed that less than 50% of peaks were due to NAs, of which less than 20% of the total were due to classical NAs, and the remaining 50% were not categorized as NAs.

Given that Barrow and Grewer's studies established the presence of NAs in OSPW, Rowland et al. (2011) was among the first to establish the presence of tricyclic diamondoid acids as NAs. Rowland's investigations used two-dimensional comprehensive gas chromatography-mass spectrometry which demonstrated that OSPW contained classical NAs and their corresponding methyl esters in the form of bi- to pentacyclic acids, with carbon numbers ranging from 11 to 19, in addition to few minor hydrocarbons. An electrospray mass spectrometry of the OSPW revealed the major components of NAs were tri- and bicyclic acids. Moreover, the results of Rowland's studies revealed a broad sequence of diamondoid tricyclic acids in the form of adamantane-1-carboxylic acid and the corresponding adamantane-2-carboxylic acid. Likewise, pentacyclic NAs appeared in the form of diamantane-1-carboxylic acid. Moreover, the mass spectrometry identified a variety of methyl, dimethyl, and ethyl-adamantane carboxylic acids in addition to adamantane ethanoic acid isomers. Nonetheless, Rowland's studies demonstrated that oil in the oil sands has been highly biodegraded which result in the biotransformation of methyl, dimethyl, ethyl, and ethyl-methyladamantane hydrocarbons, which consequently bring about diamondoid acids.

To further understand the makeup of the NAs previously identified, the elemental composition of the NA species was revealed by Pereira et al. (2013) by employing liquid chromatography orbitrap mass spectrometry at both positive and negative ESI modes to disclose approximately 300 elemental compositions. Dominant heteroatom-containing homologue classes identified included;  $O_x$  species (x ranging from 1 to 6),  $NO_x$  species (x ranging from 1 to 4),  $SO_x$  species (x ranging from 1 to 4),  $NO_2S$  species, and nitrogen and sulfur species. It was noted that oxygenated species that appeared in both positive and negative ion ESI modes were chemically distinct from each other, in which  $O_2$  species appeared in both modes, however  $O_2^-$ , as classical NAs, only appeared in negative ESI ion mode. In comparison,  $O_2$  species detected in the positive ESI mode were detected as non-acidic compounds with dihydroxy, diketo, and ketohydroxy functionality, yet still deserve attention due to their potential toxicity.

With initial characterization and identification of NAs, later investigations by Bowman et al. (2014) classified NAs into five different classes based on the type of carboxylic acid and the alkyl substituted. Using comprehensive two-dimensional gas chromatography/ time of flight mass

spectrometry, Bowman identified that NA carboxylic acids contained a thiophene, indane, tetralin, cyclohexane, or adamantane moiety.

Characterization of NAs to identify their physical properties were conducted in earlier studies by Rogers et al. (2002). Rogers extracted 81 mg/L of NAs from 515.5 liters of tailing ponds water and using ESI-MS to analyze the NAs extracted. Rogers recognized that NAs mixtures were highly heterogeneous with identical proportions of monocyclic, polycyclic, and acyclic acids, and exhibited molecular weights between 220 to 360. The most notable impurities Rogers detected were biphenyls, naphthalenes, and phenanthrene/anthracene.

Further studies identified important properties such as investigations by Huang et al. (2014) which estimated the dissociation constant, pKa, of NAs in OSPW. Using liquid-liquid extraction and the aqueous layer acid-base equilibrium method, in addition to ultra-performance liquid chromatography time of flight mass spectroscopy the pKas were approximated. Around 33.6% of total extracted organic matter contained O<sub>2</sub>-, O<sub>3</sub>-, O<sub>4</sub>-NAs with pKa values of 3.5, 4.8, and 6.8 respectively. Overall, the results demonstrated that the addition of an oxygen atom to an NA increases the pKa since the oxygen atoms exist as a hydroxyl group. In addition, Huang recognized that double bonds and aromatic groups act as molecular electron withdrawing groups which consequently lower the pKa values.

With dissociation coefficients identified, the hydrophobicity of dissolved organic species in OSPW were quantified by Zhang et al. (2015) by estimating the octanol-water partitions (D<sub>ow</sub>). Zhang's results recognized that organic compounds with higher carbon numbers and lower double bond equivalents were more hydrophobic. Zhang's studies showed that classical NAs (O<sub>2</sub>-species) exhibited D<sub>ows</sub> ranging up to 100, whereas the higher coefficients were demonstrated for mono-oxygenated species, NO<sup>+</sup>, and SO<sup>+</sup> species, with D<sub>ows</sub> up to 1000, 127,000, and 203,000 respectively.

Recent studies by Bauer et al. (2015) further analyzed the relation between the molecular weights of AEO fractions and other properties of the species. Using ESI-high-resolution mass spectroscopy and synchronous fluorescence spectroscopy (SFS) Bauer characterized fractions derived from the distillation of an AEO mixture extracted from OSPW. Bauer identified that the mean molecular weights of AEO fractions ranged from 237 to 335 Daltons. Bauer's analysis

concluded that as the molecular weight increases, the relative abundance of ions (particularly nitrogen, sulfur, or oxygen-containing) also increases, in addition to an increase in the double bond equivalents, and degree of aromaticity. Furthermore, the SFS studies suggested that the structures of the higher fractions of AEOs could contain heteroatoms, dicarboxyl and dihydroxy groups, and organic acid compounds.

### 2.2.3 Removal of NAs from OSPW

The treatment of OSPW from NAs is essential for many reasons, primarily to improve the potential of OSPW as being recyclable to reduce fresh water intake (Islam et al. 2015a). Also, the toxicity of OSPW must be reduced prior to discharging OSPW to receiving environments (Islam et al. 2015a). Several remediation techniques have been reported for the reduction of NAs to an acceptable level in OSPW (Iranmanesh et al. 2014). Likewise, remediation of OSPW can be applied further to the treatment of petroleum refinery wastewaters and similar methods may be considered for the remediation of fracking water. Methods that have been investigated for the comprehensive removal of NAs from OSPW include, but are not limited to; advanced oxidation, biodegradation, coagulation/flocculation, membrane filtration, catalytic reactions, microbial reaction, and notably adsorption (Quinlan et al. 2015). The removal of NAs from OSPW using adsorption continues to be a widely explored research area.

#### 2.2.3.1 Adsorption Process used for the Treatment of OSPW

Activated carbon is known to be the most common adsorbent studied for the removal of NAs from OSPW. Adsorbents derived from activated carbon such as petroleum coke and sawdust have also been studied. In addition, other adsorbent materials include; spent fluid catalytic cracking catalyst, clays and synthetic resins, bio-film coated adsorbents for combined adsorption and bioremediation, and synthetic supramolecular polyurethane. Most recently, studies on the adsorption behavior of graphite to remove NAs from OSPW has also been examined, in addition to current studies on using zeolites, carbon xerogels, and chitosan polymers as feasible adsorbents. (Quinlan et al. 2015)

#### *(1) Activated Carbon*

Activated carbon (AC) is the most common adsorbent used for NA removal from OSPW (Quinlan et al. 2015). Iranmanesh et al. (2014) studied the adsorption of NAs on AC with high

surface area by preparing physically AC using sawdust from pinewood and comparing its performance to both chemically AC and commercial AC. Elemental analysis was performed to identify that the highest carbon content, 85%, was found in physically AC, 64% in commercial AC, and the lowest, 54%, in chemically AC. The highest BET surface area was found to be 895.23 m<sup>2</sup>/g for chemically AC, 739 m<sup>2</sup>/g for physically AC, and 489 m<sup>2</sup>/g for commercial AC. In terms of pore size distribution, physically AC showed similar trends for all macro, meso, and micropores, yet was most prominently microporous. Most of the pore volume for chemically AC was present in the micro range; however, more volume in mesopores were observed for chemically AC than physically AC. The higher mesoporous structure of chemically AC is the most probable reason for its higher surface area. Commercial AC on the other hand was shown to exhibit mesopores mainly. The adsorption capacity of all three AC types were compared in terms of isotherm plots of adsorption uptake of NA,  $q$  (mg-NAs/g-AC), versus initial concentration. Enhanced performance was observed for chemically AC, then physically AC, and lastly, the poorest performance was observed for commercial AC. The highest NAs removal was observed for chemically produced AC at 50 to 80% removal as a result of the higher surface area and mesoporous structure. Commercial AC NAs removal ranged from 50 to 70% and physically AC removed NAs in a range of 60 to a maximum of 77%.

Given that the performance of commercial AC individually is insufficient for optimal NAs removal, AC has been combined with other processes to utilize synergistic mechanisms to enhance adsorption behavior. For example, Islam et al. (2014) studied the effect of pre-treating OSPW through ozonation to improve the adsorption capacity of granular activated carbon (GAC) in a fluidized bed biofilm reactor. Significantly, GAC contains irregularly shaped particles which enable it to both absorb microorganisms into its biofilm and adsorb many chemicals. The porous structure of GAC allows for biodegradation of microbial colonization, which enhances its organic removal rate. Moreover, GAC has a large specific surface area (1,050 m<sup>2</sup>/g for this particular study) enhancing its adsorption capacity. Utilizing this method allowed for approximately 99.5% removal of NAs. It was noted by Islam that this advanced removal was due to two main principles. First, the application of ozonation to the OSPW prior to adsorption broke large NAs molecules into smaller sizes, allowing them to migrate into previously inaccessible GAC pores during adsorption. Secondly, the formation of a biofilm on the GAC surface allowed for bacterial metabolism on the adsorbent surface.

Likewise, Islam et al. (2015) extended the study on the simultaneous adsorption and biodegradation of GAC. Raw and ozonated OSPW that were treated with biodegradation, adsorption, and both treatments combined were compared to further understand the predominant mechanism in the synergistic effect of NAs removal. The results of combining both biodegradation and adsorption was larger than the sum of each mechanism individually, which establishes that the use of these two processes simultaneously provide enhanced results, with a greater impact due to adsorption. Similar to results found in previous studies, biodegradation removes some compounds from OSPW prior to adsorption, thus previously occupied sites become vacant for more compounds with less competition (Islam et al. 2014).

Additionally, recent studies by Islam et al. (2015b) looked into making use of the in-situ regenerative capacity of GAC biofilm to degrade adsorbed NAs and regenerate the adsorption capacity of the GAC. When OSPW is in contact with GAC for an extended period, the sites become occupied and the adsorbent must be replaced or regenerated. However, the surface of GAC is considered ideal for bacterial biofilm growth as a result of its porous, rough, and irregular surface. Therefore, combined removal of NAs is utilized by breaking down complex NAs structures into simpler molecules through ozonation, which are then adsorbed onto the GAC surface, and bacterial growth on the GAC surface biodegrades the organics and regenerates the GAC surface.

## *(2) Petroleum Coke*

One of the byproducts formed during the refinery of crude oil in the oil sand industry is petroleum coke (PC). Approximately 20 kg of PC is generated for every barrel of synthetic crude produced and this PC is mixed with OSPW at a concentration of 22% before the OSPW is transported to the tailing pond (Pourrezaei et al. 2014a). Consequently, upon transporting OSPW in pipelines, PC has shown to act as an adsorbent reducing the chemical oxygen demand (COD), acid extractable fractions (AEF), and NAs in OSPW, allowing the pipeline to act as a plug-flow carbon adsorption reactor (Pourrezaei et al. 2014a).

The elemental composition of PC was analyzed using X-ray photoelectron spectroscopy (XPS) exhibiting a carbon concentration of 89%, 6.6% oxygen, and notably a high amount of sulfur (4 to 6%) (Pourrezaei et al. 2014a; Zubot et al. 2012). The surface of PC was analyzed using scanning electron microscopy (SEM) and Brunauer-Emmet-Teller (BET) to illustrate the

spherical, non-porous structure of PC (Pourrezaei et al. 2014a). Due to the reduced porosity of PC, the BET surface area of PC ranges from 5.7 to 7.7 m<sup>2</sup>/g (Pourrezaei et al. 2014a; Zubot et al. 2012). Moreover, SEM images demonstrated that the pore size distribution of PC can be classified as mesoporous (Pourrezaei et al. 2014a). The adsorption of AEFs to PC predominantly fit the Langmuir isotherm, demonstrating that the surface of PC is homogeneous with unimolecular layers and no transmigration occurs on PC (Pourrezaei et al. 2014a). The adsorption capacity,  $q_{\max}$ , of PC quantified by the Langmuir isotherm was determined to be 1 mg of AEFs per gram of PC. In comparison, Zubot et al. (2012), determined that adsorption of total acid organics (TAO) fit the Langmuir, Freundlich, and Langmuir-Freundlich isotherm. At a concentration of 60 mg/L of TAO, the adsorption capacity ranged between 0.1 and 0.46 mg/g, with an average of 0.26 mg TAO per gram of PC. The affinity coefficient,  $K$ , for the Langmuir isotherm has proven to be small (approximately 0.030 L/mg), implying that large doses of PC are required to remove TAOs from OSPW in reasonable amounts (Zubot et al. 2012).

Pourrezaei et al. (2014a) analyzed the removal of NAs by PC by studying the distribution of NAs compounds as a function of the carbon number ( $n$ ) and the number of rings ( $-Z/2$ ) after treating OSPW with 200 g/L of PC for 16 hours. The NAs present in the OSPW of this study ranged in carbon numbers of 8 to 12 and number of rings ranged from 1 to 6, with no acyclic NAs present. Overall, the total NAs removal summed up to approximately 75%. For ring numbers,  $-Z$ , of 4, 6, 8, 10, and 12, NAs removed were in the carbon range of 17, 15-20, 15-19, 15-21, and 17-22 respectively. This observation indicated that an increase in the number of rings, and more dominantly the carbon number increased the removal of NAs by PC. Initially, Zubot et al. (2012) performed similar studies to analyze NA removal by PC in OSPW. Similarly, the OSPW contained mainly two and three ringed NAs with carbon numbers ranging from 12 to 16 and molecular weights between 190 and 260 g/mol. In contrast, Zubot studied the NAs removal at different doses of PC to observe higher removal rate at higher doses. In focus, NAs with high molecular weights, ( $n$  greater than 20) and ring structures were 99% removed with PC dose of 19.9 weight %, indicating that heavier and more complex NAs were removed more effectively.

Therefore, the results of Zubot et al. (2012) and Pourrezaei et al. (2014a) both confirm that as the carbon number and number of rings in the NAs increases, their molecular weights and complexity also increase which results in higher removal rates. In addition, Pourrezaei et al. (2014)

noted that the octanol-water coefficient,  $\log K_{ow}$ , increased as the  $n$  in each  $-Z$  group increased. Therefore, an increase in the molecular weight of the NAs compound, consequently increases the octanol-water coefficient making the compound more hydrophobic and less soluble, hence a higher affinity of large NAs molecules to PC surface and a higher tendency for adsorption. Since PC is classified as mesoporous, it is capable of adsorbing a wide range of NAs with molecular weights between 160 to 500 g/mol (Pourrezaei et al. 2014a). Thus, NAs present in the water ranging in molecular weight of 190 to 260 g/mol can easily diffuse into the mesopores with no size limitations (Zubot et al. 2012). Furthermore, NAs with aromatic rings or double bonds have an affinity towards the PC surface as a result of  $\pi$ - $\pi$  bonds with the graphite-like surface of the adsorbent (Pourrezaei et al. 2014a). The operating pH of OSPW is approximately 8.4, while the pKa of NAs range from 5 to 6. Thus, NAs in OSPW exist in dissociated form. In addition, the pH of point of zero charge ( $pH_{pzc}$ ) for PC is  $6.5 \pm 0.3$ , which means that at a pH higher than 6.5, the PC contains an overall negative charge. Therefore, at the pH of OSPW, electrostatic repulsion between PC and NAs reduce the adsorption capacity. However, this repulsion can be reduced by metal ions present in the OSPW that can neutralize the negative charge on the OSPW. Surface functional groups on PC were identified using Fourier transform infrared spectroscopy (FT-IR) absorption spectra in which carbonyl stretching vibrations, N-H bending vibration of primary amines, C-H bending vibration of benzene, and O-H groups were identified (Pourrezaei et al. 2014a). The N-H functional group in particular facilitates the formation of hydrogen bonds between PC and hydroxyl groups on NA. However, the composition analysis of PC did not indicate a high amount of nitrogen, which means that this form of hydrogen bonding is not the predominant mechanism in the adsorption of NAs to PC. Moreover, the mean free energy of AEF adsorption to PC was found to be less than 8 kJ/mol, which implies that the adsorption of NAs to PC is chiefly physisorption (Pourrezaei et al. 2014a). However, the physisorption is mainly dependent of the porosity of PC rather than the hydrogen bonding of the functional groups. Therefore, the dominant adsorption mechanism of NAs onto PC is a result of the hydrophobic character of NAs.

To further understand adsorption onto PCs, Zubot et al. (2012) studied the kinetics of TAOs onto PC to determine that the sorption followed pseudo-second order kinetic model ( $k_2=39.4$  g/mg-h and  $q_e=0.16$  mg/g). Zubot tested intraparticle diffusion (referred in this study as the internal diffusion model) by using the Weber and Morris model to deduce that the sorption process of TAOs onto PC was biphasic. Thus, the overall rate of adsorption onto PC was limited by two

processes or phases. Initially, the diffusion of TAOs from the liquid OSPW film onto the external macro structure of the PC surface was fast as the hydrophobic macro sites were easily accessible. Afterwards, the sorption rate decreases as the TAOs diffuse into the meso and micropores, thus making this phase the rate limiting step as it dominated the overall rate of removal.

To improve NAs removal from OSPW using PC, Gamal El Din et al. (2011) proposed the combination of PC adsorption with oxidation to provide a multibarrier treatment. PC adsorption was used as a pretreatment operation before the ozonation treatment of OSPW and has shown to remove dissolved organics from OSPW in addition to reducing the amount of ozone required for the ozonation step. The removal of the heavier, more complex NAs degrades or in fact removes organic compounds that are difficult to biodegrade, subsequently reducing ozone requirements. The combination of PC adsorption with ozonation has resulted in approximately 85% removal of NAs from OSPW and consequently increases the biodegradability of organic pollutants after this treatment OSPW, which previously exhibited lower removal rates.

Moreover, Pourrezaei et al. (2014b) studied the addition of PC to zero valent iron (ZVI) to enhance the removal of NAs, AEFs, fluorophore organic compounds, and trace metals from OSPW. PC is used for its electron conducting characteristics and serves as an electron mediator while simultaneously allowing for adsorption and oxidation of organic compounds. Alone, PC adsorbs hydrophobic and less soluble compounds, however in combination with ZVI it adsorbs soluble compounds that could not be removed previously. In terms of the synergistic effects that the combination of PC and ZVI provides, PC is more responsible for removal of NAs and AEFs whereas the ZVI contributes towards metal removal and eliminating vanadium leaching that occurs when PC is used alone. It should also be noted that the dissolved iron of ZVI forms complexes with the carboxylic functional groups of NAs, which consequently increases the hydrophobicity of NAs allowing them to be adsorbed more easily onto the PC surface.

### *(3) Graphite*

Recent studies by Moustafa et al. (2014) have investigated the potential of using graphite to remove NAs from OSPW. SEM techniques have demonstrated that exfoliated graphite (EG) is composed of 96% carbon and 4% oxygen, implying a mainly hydrophobic surface due to the low oxygen content. In addition, phenolic and carboxyl groups that induce hydrogen bonding and electrostatic effects were identified, making the surface charge of EG negative. The BET surface area of EG was determined to be approximately 76.9 m<sup>2</sup>/g and the pore size distribution was shown to be completely mesoporous, allowing all sizes of NAs to be adsorbed easily through molecular diffusion and promote faster kinetics, disregarding size exclusion. During the study, five NAs were of focus, and the adsorption of monocompounds was analyzed, and were represented by the Freundlich isotherm ( $q_{\max}= 6.26$  mg/g) to represent the heterogeneity of adsorption site affinities. Moustafa proposed that some compounds were adsorbed to the EG surface due to negatively charged assisted hydrogen bonding (-CAHB) that occurs between the negatively charged carboxyl or phenolic groups present on the EG surface and the negatively charge carboxyl groups on the NAs itself.

For comparison, the adsorption of multicompounds was also studied and fitted to the Langmuir Isotherm (Moustafa et al. 2014). However, the adsorption capacity of the multicompounds ( $q_{\max}= 4.84$  mg/g) was less than the capacity of monocompound due to competition between compounds to the adsorbent surface. To further understand this competitive adsorption, the adsorption of the multicompounds was observed for an extended period of time (24 hours) and was categorized into two stages. During the first 6 hours of the study, the removal of certain compounds was the highest demonstrating that formation of a self-assembled layer (SAL) due to the -CAHB and hydrophobic CH<sub>3</sub> groups and other compounds present to bond with the hydrophobic ends of the SAL, forming multilayers. For the remaining 18 hours, the adsorption equilibrium was achieved however removal rates decreased due to desorption from EG sites, breaking the SAL, inhibiting the adsorption of less hydrophobic compounds.

To further understand the significance of the formation of the SAL in EG adsorption, Moustafa et al. (2015) used amplitude modulation – frequency modulation atomic force microscopy (AM-FM AFM) to investigate the adsorption behavior of Decanoic acid (DA) onto highly ordered pyrolytic graphite (HOPG). Moustafa expanded on the adsorption mechanism of DAs by clarifying that proton exchange between negatively charged DAs and water increased the

hydrophobicity of DAs which resulted in the –CAHB that drives the adsorption onto HOPG. The AM-FM AFM technique was used to visualize the formation of the SAL developed by the adsorption of DAs onto HOPG. Resulting images showed that the –CAHB allows for the initial adsorption of DAs to form the SAL and multilayers formed onto the SAL appearing as aggregates. Moustafa observed the formation of SAL aggregates by testing both HOPG and functionalized-HOPG (FHOPG) to notice that aggregates formed onto the HOPG surface in the form of steps due to limited function groups. Whereas aggregates formed a uniform layer on the FHOPG as a result of more functional groups being present on FHOPG surface.

#### *(4) Other Adsorbents*

Moreover, Janfada et al. (2007) investigated the sorption of OSPW NAs onto organic rich soils to determine that soils with higher organic carbon fractions promote higher adsorption coefficients. Janfada explained that dissolved organic compounds adsorb onto soil by means of the hydrophobic effect. Likewise, the hydrophobicity of compounds depends on the solubility of the compound in water, which is a function of polarity. Molecular topology studies indicated that the molecular structure of NAs was also responsible for their sorption onto soil. This was shown by NAs with carbon numbers between 13 to 17 (at Z between 0 to -12) showing preferential sorption due to their increasing molecular size. In addition, mixtures of NAs sorb strongly to soil surfaces. It should be noted that OSPW containing inorganic salts promote higher adsorption capacity of organic compounds due to increased ionic strength.

On the other hand, Mohamed et al. (2015) evaluated a variety of sorbent materials for the fractionation of NA fraction components. The different adsorbents used included; activated carbon, cellulose, iron oxides (magnetite and goethite), polyaniline (PANI). In addition, biochar extracted from biomass were analyzed; BC-1 (rice husks), BC-2 (acacia low temperature), BC-3 (acacia high temperature). During this study, NAs were removed from OSPW onto the sorbent materials by means of the solid phase extraction method for fractionation. Using this method, different amounts of removal were observed for each adsorbent based on the surface chemistry and textual properties of the materials. For example, the high surface area of AC allowed for AC to observe the highest removal. In addition, a higher concentration of surface polar groups in biochar resulted in high removals. Overall, AC observed the highest removal of 92%, BC-1 24%, BC-2, BC-3, and goethite approximately 15%, and negligible removal for cellulose and magnetite.

During this study, Mohamed discovered that the desorption of NAs from AC using methanol allowed for the regeneration and recycling of AC effectively with less than 5% decrease in adsorption efficiency after the fourth cycle.

As discussed in section 2.2.2, various methods were used to characterize OSPW. Likewise, Headley et al. (2013) used adsorption with cyclodextrin-based copolymers to characterize OSPW. Specifically,  $\beta$ -CD-cross-linked with; 4, 4'-dicyclohexylmethane diisocyanate, 4,4'-diphenylmethane diisocyanate, and 1,4'-phenylene diisocyanate were used. Using this method, new compound classes were observed in OSPW such as; HC, N<sub>1</sub>O<sub>1</sub>, N<sub>1</sub>O<sub>2</sub>, N<sub>1</sub>O<sub>3</sub>, N<sub>1</sub>O<sub>4</sub>, N<sub>1</sub>O<sub>5</sub>, N<sub>2</sub>O<sub>1</sub>, N<sub>2</sub>O<sub>2</sub>, and N<sub>2</sub>O<sub>3</sub>. Headley's study showed that the structure of copolymer materials and the accessibility to inclusion sites resulted in selective sorption. In addition, the stability of the adsorbate-sorbent complex is based on; the chemical structure of NAs, their relative concentration in OSPW, the carbon number of specific NAs, their type of compound class, and cross-linking nature of copolymers. These factors also play a predominant role in selective sorption as they affect the hydrophile-lipophile properties of the adsorbate molecules.

#### 2.2.4 An Evaluation of Current Adsorption Treatments

As seen in section 2.2.2, the OSPW matrix predominantly consists of NAs which are complex in terms of composition and structure with regards to aromaticity and double bond equivalents. Likewise, NA compound properties such as molecular weight, pKa, and octanol-water coefficient range as the compounds are immersed within OSPW. Therefore, the removal of NAs from OSPW by employing adsorption must be designed while taking into account the complexity of NAs as mixtures in OSPW with varying structures, compositions, and properties. The phenomena of removal based on adsorption is founded on the interaction between the NA compounds being removed and the surface of the adsorbent used at the interfacial region. For this reason, upon assessing the viability of an adsorbent to remove NAs, factors that must be accounted for include; the concentration of NAs and their solubility in OSPW, the chemical structure of the NAs, the elemental composition of NAs including their carbon numbers and functional groups associated, and the type of NAs present with regards to the type of compound class (Headley et al. 2013). By taking these aspects into consideration, assessing the interaction between the adsorbent and the NA compounds being removed can be investigated with a better understanding of which adsorbent is more viable for the removal of NAs from OSPW.

Section 2.2.3.1 explored the various adsorbents studied for their potential of remediating OSPW from NAs. Three main adsorbents have been reviewed for their potential use to remove NAs from OSPW. Extensive research has been conducted on PC since it is already present in OSPW as a byproduct and can be used as an adsorbent rather than being discharged to waste. The carbon content of PC in comparison to other adsorbents reviewed in section 2.4 is reasonable, 89%, however its surface area is extremely low ( $7.7 \text{ m}^2/\text{g}$ ) compared to other adsorbents. Similar to other adsorbents, the pore size distribution of PC is mainly mesoporous allowing for the adsorption of a wide range of NAs. The removal of NAs through PC occurs mainly due to hydrophobic interactions and physisorption, yet is demonstrated by the Langmuir isotherm due to its homogenous surface. The adsorption capacity of PC ( $1.0 \text{ mg/g}$ ) is relatively low compared to other adsorbents, yet the use of PC has proven to remove all toxicity from OSPW with exception to *C. dubia* toxicity. The toxicity of *C. dubia* is due to the vanadium leaching from PC, which can be prevented by increasing the adsorption contact time, or by combining PC with ZVI as initially mentioned. Overall, adsorption of NAs by PC has provided for approximately 75% removal of NAs from OSPW, with NA compounds of specific structures being removed at a rate of 99%. Enhanced removal of NAs can be achieved by utilizing synergistic effects by combining PC adsorption treatments with ozonation. (Gamal El-Din et al. 2011; Pourrezaei et al. 2014a; Pourrezaei et al. 2014b; Zubot et al. 2012)

AC is most commonly used for adsorption of NAs, yet the physical and chemical activation of carbon has proven to provide better adsorption than commercial carbon. Carbon content of ACs were low compared to PC and EG, ranging from 54 to 85%. However, their surface areas have proven to be much higher ranging from 489 to  $895 \text{ m}^2/\text{g}$ . Commercial AC is characterized by its mesoporous structure, similar to PC. However, the activation of carbon enhances the porosity of the adsorbent providing for a microporous structure, allowing for enhanced adsorption. NAs removal using commercial or physically or chemically AC has demonstrated NAs removal rates ranging from 50 to 80%. Like PC, AC has been combined with other treatment methods such as ozonation to advance the NAs removal rate up to 99.5%. (Iranmanesh et al. 2014)

Recent studies on using graphite as an adsorbent has shown the potential of promising results if graphite is to be used to remove NAs from OSPW. Exfoliated graphite has shown to have the highest carbon content (96%) relative to the other adsorbents. The surface area of EG ( $76.9$

m<sup>2</sup>/g) has shown to be higher than that of PC but still low compared to AC. Similar to PC, and commercial AC, the surface of graphite is mainly characterized as mesoporous. The adsorption of NAs onto graphite was represented by the Freundlich isotherm due to the heterogeneity of the graphite sites and was represented by adsorption capacities (4.84 and 6.26 mg/g) higher than PC. Most notably, the adsorption of NAs onto graphite occurred due to the formation of the negatively charged assisted hydrogen bonding which helped develop a self-assembled layer on the adsorption surface promoting multilayer adsorption. (Moustafa et al. 2014; Moustafa et al. 2015; Pourrezaei et al. 2014a)

In addition to these three main adsorbents, other studies have been conducted on evaluating organic rich soils as adsorbents as well as current studies on carbon xerogel materials, zeolites, and chitosan polymers. Adsorbents are explored for optimal properties including carbon content, surface area, pore size distribution, and the relation between the adsorbent and NA compound of interest is described through isotherms. Upon evaluating the viability of an adsorbent for NAs removal, these properties should be taken into account in addition to focusing on determining the structure-activity relationship between the NA being removed and the adsorbent by considering the aforementioned factors such as chemical structure, composition, and concentration of NAs present. Accordingly, ideal adsorbent treatments can be designed with the most suitable adsorbent employed with enhanced NAs removal.

Overall, the use of adsorption to remove NAs from OSPW is a feasible treatment since a variety of adsorbents can be used to improve the quality of OSPW and promote its return to the environment or reuse applications. The utilization of petroleum coke as an adsorbent is considered satisfactory since it has the potential to remove NAs from OSPW at a reasonable rate and reduces the discharge of PC byproduct to the environment, however concerns of metal leaching hinders PC's ability to becoming a promising adsorbent for NAs removal. Moreover, the preparation of chemically activated carbon is recommended since chemically AC showed enhanced behavior compared to commercial AC and is considered more applicable in terms of NAs removal, particularly in combination with other treatment methods. Furthermore, the potential use of graphite as an adsorbent has shown to be a promising adsorbent due to its capability of forming multilayers allowing for advanced NAs removal. Finally, the use of adsorption with other processes to treat OSPW can provide superior removal of NAs and improve OSPW quality. It

should be noted that further adsorption studies should account more for the properties of NAs and their relation with the adsorbent at the interfacial level to enhance adsorption treatment methods.

### 2.3 Use of Carbon Xerogel Material as an Adsorbent

Seeing that most adsorbent material examined for the removal of NAs from OSPW are carbonaceous materials, it should be noted that carbon materials are considered universal adsorbents given that they have high adsorption capacity with low costs and are easily disposed of (Carabineiro et al. 2011). However, the performance of the adsorbent materials currently in use all exhibit limitations with no optimum adsorbent in place. Given that these adsorbents are derived from raw materials, their textural properties are dependent and hence limited by the raw materials they are originate from. For example, the texture of activated carbon is usually microporous and characteristics of the texture are dependent of the raw material the carbon is derived from (Job et al. 2005). Since the performance of an adsorbent is a function of the material's texture and its surface chemistry, the fixed texture of activated carbon limits its ability to perform under a variety of conditions (Carabineiro et al. 2011). As a result, relatively novel approaches have explored the potential of using synthesized carbonaceous materials, such as CX material that exhibit notable mesoporous character.

#### 2.3.1 Carbon Xerogel as an Adsorbent

Accordingly, studies have examined the use of materials that can be modified or tailored to meet application requirements. Early investigations by R.W. Pekala (1989) introduced the synthesis of carbonaceous gels which were formed by the polycondensation of resorcinol with formaldehyde under alkaline conditions. The synthesis of these gels is considered a sol-gel approach since the resulting surface appears as functionalized polymer clusters which are covalently cross-linked. Pekala's experiments demonstrated that the sol-gel process can form aerogels and xerogels, one through supercritical drying and the latter through evaporation of the liquid.

CXs in particular, are mesoporous materials used for applications such as reactions in the liquid phase where the xerogel acts as a catalyst support (Pekala 1989; Samant et al. 2005). The mesoporous character of the xerogel is a result of carbonization which is followed by the polycondensation step of the sol-gel process (Pekala 1989; Samant et al. 2005). In addition, oxygen functional groups are introduced to the surface of the xerogels if an activation step is applied which

enhances the ability of CX to be interactive (Pekala 1989; Samant et al. 2005). In comparison to conventional AC which is known to be mostly microporous, CX is considered more favorable not only because of its highly mesoporous character, but since its porous texture and surface chemical structure can be tailored by modifying the synthesis conditions (Carabineiro et al. 2011). In addition, CX is preferred over AC since it is polymer-based and can be prepared, whereas AC is not easily produced (Mahata et al. 2007). Other appealing factors of CX include; its high surface area which is comparable to that of AC, high density, high and controllable porosity, open pore network, and electric conductivity (Mahata et al. 2007).

Moreover, the desirable porosity of CX material depends on the pH operating conditions during synthesis of the material. The sol-gel process takes place under alkaline conditions; however, the pH of the precursor solutions determines the pore texture of the material. Job et al. (2004) demonstrated that micro-mesoporous CX were formed when synthesis took place at pH values between 5.50 and 6.25. As the pH decreases within this range, the pore volume and maximum pore size will increase. However, once the pH decreases below 5.50 the material becomes micro and macroporous and mechanical properties are seized. Conversely, Job observed that a completely non-porous material is formed if the pH exceeds 6.25.

Previous studies have investigated the use of CX not only as catalyst supports but also as adsorbents. For instance, Figueiredo et al. (2010) compared the performance of CX to AC in terms of the adsorption of textile dyes at different solution pHs. Figueiredo's experiments demonstrated that adsorption is maximized when the pH of the solution is below that of the  $pH_{PZC}$  and the performance of CX is less, if not similar, to that of AC. Similarly, Carabineiro et al. (2011), validated the comparable performance of CX during the adsorption of ciprofloxacin antibiotic which showed reasonable performance of CX compared to AC. Both Figueiredo and Carabineiro's studies confirmed that CX can act as a suitable substitute for AC due to its comparable performance. Notably, CX's performance relative to AC may be considered limited due to its reduced surface area, however its mesoporosity overcomes this drawback. Consequently, the mesoporous structure of CX promotes the adsorption of compounds with varying and generally larger molecular size, which appeals to adsorption treatment methods. For this reason, the employment of CX as an adsorbent for the treatment of OSPW is considered for the removal of NAs which constitute to a range of molecular weights and are generally considered "bulky".

Additionally, the many advantages of CX in terms of being designed to appeal to the conditions of OSPW and NAs, being easily generated at a low cost and easily disposed of, has advocated the consideration of CX to be employed as an adsorbent for the remediation of OSPW.

Upon investigating the removal of caffeine and diclofenac by CX, Álvarez et al. (2015) examined the textural properties of CX. N<sub>2</sub> adsorption isotherm studies at – 196°C were employed to conduct textural characterization, while the morphology of the CX surface was examined using SEM. Elemental microanalysis in addition to FT-IR were employed to identify chemical surface groups present on the CX surface. SEM micrographs illustrated a smooth, nonhomogeneous particle size distribution confirming the mesoporous property of CX. The elemental microanalysis demonstrated that CX is mainly carbonaceous as a result of approximately 91.26% carbon composition. Given that the general sol-gel preparation of CX does not involve an activation step, oxygen is only present on the CX surface in a small amount of 7.65%. Hydrogen, nitrogen, and sulfur were present on the CX surface in minimum amounts of 1.00, 0.08, and 0.01% respectively. Moreover, the FT-IR spectra demonstrated O-H stretching vibrations as a result of surface hydroxylic groups attributed to strong hydrogen bonds. In addition, the FT-IR recognized alkane or alkene groups present on the surface of the carbons from C-H vibrations. More specifically, stretching vibrations of C=O moieties identified the presence of; (i) carboxylic, ester, and lactones, (ii) quinone and or ion-radical structures, and (iii) diketone, ketoester, and keto-enol structures.

In addition, while examining the effect of synthesis pH on the structure of CX through transmission electron microscopy (TEM) and X-ray diffraction (XRD), Lin and Ritter (1997) recognized that CX prepared at pH 6 displays a highly porous nanostructure. In comparison to AC and graphite the TEM and XRD analysis illustrated that although CX is not completely amorphous, its crystalline character was more than AC but less than graphite respectively. Furthermore, the nanocrystalline structure of CX results in a highly porous structure comparable to the surface of graphite and more mesoporous than mostly microporous AC. Therefore, the partially nanocrystalline structure of CX exhibits textural properties intermediate of both AC and graphite.

## Chapter 3 Experimental Setup

To investigate the adsorption mechanisms of NAs onto CX, three model compounds were explored based on their structures. The compounds chosen include; heptanoic acid (HPA), 5-cyclohexanepentanoic acid (CHPA), and 5-Phenylvaleric acid (PVA). These NA model compounds vary by structure as shown in Table 3.2, in which all three contain a carboxylic acid group and a long chain. CHPA contains an additional cyclic ring (cyclohexane) and the cyclohexane in PVA is aromatic. The variation in structure between the three model compounds allow for the understanding of the effect of structure on the adsorption of NAs onto the surface of CX. Therefore, batch adsorption experiments are conducted for each of the model compounds individually onto CX. Furthermore, the adsorption experiments were conducted at different solution pHs to determine the role of electrostatic forces involved in the adsorption of the model NAs. All investigations are compared to GAC to evaluate the viability of CX as a promising adsorbent.

### 3.1 Materials

#### 3.1.1 Adsorbent Preparation

The established sol-gel technique was employed to prepare CX by the polycondensation of resorcinol and formaldehyde (Carabineiro et al. 2011; Mahata et al. 2007). Approximately 25 g of resorcinol was dissolved in 40 mL of Millipore® Milli-Q water (Synergy® UV, France) and 2M of NaOH was used to adjust the pH to 5.5 (Mahata et al. 2007). Afterwards, 34 mL of formaldehyde was added to the resorcinol solution and likewise the pH was adjusted to 5.5 by 2M NaOH (Mahata et al. 2007). Note that in general, for the preparation of CX, the exact amounts of resorcinol and formaldehyde are not fixed, yet it is necessary to mix them at a ratio of 1 to 2 (Job et al. 2005). Afterwards, the solution was then stirred for approximately 90 minutes to ensure complete dissolution and left in an isothermperature oven (Fisher Scientific, USA) at 60°C for 3 days to allow for gelation (Mahata et al. 2007). Curing of the gelled solution was done in the same isothermperature oven for a week at the following temperatures; first day 60°C, second day 80°C, third day 100°C, and 120°C for the fourth day, and finally maintained at 105°C for the last three days.

After curing, a red-brown opaque solid gel is obtained, which undergoes carbonization to obtain a mesoporous structure (Mahata et al. 2007). The dry gels went through pyrolysis in a Lindberg/Blue M™ furnace (Thermo Fisher Scientific, USA) in an inert atmosphere, under a nitrogen flow of 1 L/min. The CX gels were isothermally heated in the furnace by first being heated

from room temperature and held at 200°C for an hour, then heated up to 700°C and maintained for three hours before being cooled down to room temperature over the duration of an hour. Finally, the pyrolyzed gels were crushed and sieved to the desired size of 0.6 to 1.4 mm.

On the other hand, the GAC was purchased from CalgonCarbon® (Pennsylvania, USA) and was likewise sieved to 0.6 to 1.4 mm. Table 3.1 summarizes the textural properties of CX prepared at pH 5.5 and GAC. The textural characterization of the CX and GAC was based on the N<sub>2</sub> adsorption isotherms, determined at -196°C with an Autosorb Quantachrome 1MP instrument. Prior to the measurements, the samples were outgassed at 120°C for 5 hours under vacuum. The specific surface area of the mesopores ( $S_{\text{meso}}$ ) and the micropore volume ( $V_{\text{micro}}$ ) were calculated by the t-method. Moreover, the surface area ( $S_{\text{BET}}$ ) and the pore size of the samples were calculated by the Brunauer–Emmett–Teller (BET) method and Barrett-Joyner-Halenda (BJH) method, respectively.

**Table 3.1 Textural properties of GAC and CX**

<b>Sample</b>	<b><math>S_{\text{BET}}</math> (<math>\pm 10</math> <math>\text{m}^2 \text{g}^{-1}</math>)</b>	<b><math>S_{\text{meso}}</math> (<math>\pm 10</math> <math>\text{m}^2 \text{g}^{-1}</math>)</b>	<b><math>S_{\text{micro}}</math> (<math>\pm 10</math> <math>\text{m}^2</math> <math>\text{g}^{-1}</math>)</b>	<b><math>V_{\text{micro}}</math> (<math>\pm 0.01</math> <math>\text{cm}^3 \text{g}^{-1}</math>)</b>	<b><math>V_{\text{meso}}</math> (<math>\pm 0.01</math> <math>\text{cm}^3 \text{g}^{-1}</math>)</b>	<b>Total Pore Volume <math>V_{\text{total}}</math> (<math>\pm 0.01</math> <math>\text{cm}^3 \text{g}^{-1}</math>)</b>	<b>Average Pore Diameter Dp (nm)</b>
<b>CX-5.5</b>	573	135	438	0.205	1.340	1.545	11
<b>GAC</b>	976	137	839	0.386	0.017	0.599	2

### 3.1.2 NAs Stock Solution

To begin with, potassium phosphate buffer solution must be prepared for every model NA stock solution. Approximately 43.55 g of potassium dibasic monohydrogen phosphate, K<sub>2</sub>HPO<sub>4</sub>, (Fisher Chemical by Thermo Fisher Scientific™, New Jersey, USA) was dissolved in 250 mL of Milli-Q water to form 0.05M solution. Similarly, 34.02g of potassium monobasic dihydrogen phosphate, KH<sub>2</sub>PO<sub>4</sub>, (Fisher Chemical by Thermo Fisher Scientific™, New Jersey, USA) was dissolved in 250 mL of Milli-Q water to form 0.05 M solution. To have 0.05 M of buffer solution at pH 8, 235 mL of K<sub>2</sub>HPO<sub>4</sub> and 15 mL of KH<sub>2</sub>PO<sub>4</sub> were dissolved in 250 mL of Milli-Q water to result in 500 mL of pH 8 stock solution. In the same way 500 mL of 0.05M pH 6.5 stock solution was prepared with 82.38 mL of K<sub>2</sub>HPO<sub>4</sub>, 167.63 mL of KH<sub>2</sub>PO<sub>4</sub>, and 250 mL of Milli-Q water. Finally, to prepare 500 mL of 0.05 M pH 5 solution, 3.40 mL of K<sub>2</sub>HPO<sub>4</sub>, 246.60 mL of KH<sub>2</sub>PO<sub>4</sub>,

and 250 mL of Milli-Q water were dissolved. Three 500 mL buffer solutions were made at each pH for each model NA compound; HPA, CHPA, and PVA. (DeAngelis 2007).

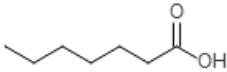
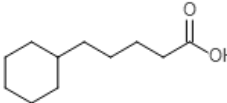
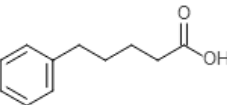
To prepare 50 mg/L of NA stock solution, 27  $\mu$ L of HPA (TCI Chemicals, Oregon, USA) was dissolved in each 500 mL phosphate buffer solution, 26  $\mu$ L of CHPA (Sigma-Aldrich®, Germany) was dissolved in each corresponding 500 mL solution, and 25 mg of PVA (Sigma-Aldrich®, Germany) similarly dissolved in each 500 mL solution. Therefore, 500 mL of 49.68 mg/L HPA were prepared at pH 8, 6.5, and 5, likewise 49.92 mg/L CHPA, and 50 mg/L of PVA.

Table 3.2 provides properties of the NAs model compounds that are imperative to this study. By recognizing the following properties, relations between the results of the experiments and these properties can be identified which can further verify the mechanisms responsible for the adsorption of NAs onto CX, in comparison to GAC. Note that the  $K_{OW}$  coefficients were obtained from ChemAxon logD predictor software (Appendix section A.1), the double bond equivalent (DBE) and hydrogen deficiency,  $-Z$ , were calculated using the following equations, and the polarizability coefficients and solubility were obtained from the ChemSpider chemical structure database. (Calisty 2017; Barrow et al. 2010; ChemSpider 2017).

$$DBE = C - \frac{H}{2} + \frac{N}{2} + 1 \quad (11)$$

$$-Z = H - 2C \quad (12)$$

Table 3.2 Properties of model NAs used in this study

Model Compound	Formula	Structure	Molecular Weight (g/mol)	Log K <sub>ow</sub> at pH 8	DBE	-Z	Polarizability (cm <sup>3</sup> )	Solubility at 25°C (mg/L)
<b>HPA (Heptanoic Acid)</b>	C <sub>7</sub> H <sub>14</sub> O <sub>2</sub>		130.2	-0.51	1	0	14.3±0.5 10 <sup>-24</sup>	1955
<b>CHPA (5-cyclohexanepentanoic acid)</b>	C <sub>11</sub> H <sub>20</sub> O <sub>2</sub>		184.3	0.60	2	2	20.8±0.5 10 <sup>-24</sup>	26.6
<b>PVA (5-Phenylvaleric acid)</b>	C <sub>11</sub> H <sub>14</sub> O <sub>2</sub>		178.0	0.01	5	8	20.3±0.5 10 <sup>-24</sup>	430.2

## 3.2 Methods

### 3.2.1 Batch Adsorption Experiments

Adsorption experiments were conducted at three operating pH conditions for all three model NA compounds. Provided that the  $pH_{PZC}$  of CX is approximately 6.8, the experiments ran at pH 8, 6.5, and 5 to deduce the effects of surface charge (Carabineiro et al. 2011). Precisely 50 mL of 50 mg/L NA stock solution were transferred into an Erlenmeyer flask that acted as the reactor. In addition, 25 mg of adsorbent (0.5 g/L) were transferred into the flask at the starting time and the flasks were placed in New Brunswick™ Innova® 2100 platform shaker (Eppendorf Inc., USA) that operated at 200 RPM. The experiment ran for 24 hours to allow for the attainment of equilibrium and samples were collected at times; 0, 0.5, 1, 2, 4, 6, 21, and 24 hours. Each experiment consisted of nine reactors which contained the following:

1. 25 mg CX and 50 mL CHPA
2. 25mg GAC and 50 mL CHPA
3. 25mg CX and 50 mL HPA
4. 25mg GAC and 50 mL HPA
5. 25mg CX and 50 mL PVA
6. 25mg GAC & 50 mL PVA
7. Control 1: 50mL CHPA (without adsorbent)
8. Control 2: 50 mL HPA (without adsorbent)
9. Control 3: 50 mL PVA (without adsorbent)

The samples collected were approximately 2 mL of solution and were collected by means of a BD Leur-Lok™ 5 mL syringe (New Jersey, USA) and were then transferred to vials for storage for further analysis. It is worth noting that as the samples were transferred to the vials, they first passed through Thermo Scientific™ Target2™ F-2500-2 30 mm nylon syringe 0.2  $\mu$ m filters (Tennessee, USA) to ensure that adsorbent particles that may have been removed while collecting the samples did not remain in the stored samples and act as a contaminant or possibly continue adsorption and remove some of the NAs from the samples. Each experiment was conducted in replicates, therefore with nine individual reactors, in replicates, at three different pH conditions, a total of 54 individual batch adsorption experiments were performed.

### 3.2.2 Liquid Chromatography – Mass Spectrometry (LC-MS) Analysis

To identify the concentration of the collected samples, a liquid chromatography – mass spectrometry (LC-MS) was used to analyze the samples. To prepare the samples for LC-MS analysis, the samples were transferred to Sigma-Aldrich® 29652-U Supelco Low adsorption 2 mL vials (Pennsylvania, USA) specifically designed for LC-MS with natural PTFE/silicone septa (with a slit). All HPA samples were transferred as is, while CHPA and PVA samples were first diluted 50 and 10 times respectively with Milli-Q water. Dilution was necessary to ensure that the sample concentrations remained below the LC-MS detection limit. LC-MS analysis also required samples of standard concentrations for each model compound. Thus, LCMS samples of 1, 5, 10, 20, 30, 40, and 50 mg/L from each stock NAs solution were prepared.

## Chapter 4 Results & Discussion

Batch adsorption kinetics experiments were performed at three pH conditions, pH 8, 6.5, and 5, for all three model compounds; HPA, CHPA, and PVA, as mentioned earlier. The concentration of the solutions at the different time intervals are presented in section A.2 of the appendix.

### 4.1 Data

Tables A.2 to A.4 present the concentrations, 'C', of all samples at the different operating pHs. Note that for all experiments, no significant change in temperature or pH were observed throughout the duration of the experiments. All pHs remained within  $\pm 0.1$  of the initial pH and temperatures remained within  $\pm 1^\circ\text{C}$  of the room temperature,  $19^\circ\text{C}$ , for all experiments. Please note that N/D in table A.4 indicates that no acid, specifically CHPA, was detected by the LC-MS for the respective samples.

### 4.2 Results

As seen in tables A.2 to A.4 in the appendix, slight variations are observed between values of the first and second run. It can be assumed that these variations are a result of the heterogeneity of the adsorbent surfaces. The GAC and CX surfaces are not homogenous in a sense that there is variation in properties such as; pore size, composition, and particle size given that the adsorbent particles range from 0.6 to 1.4 mm. Therefore, given the diversity of properties the adsorbents' surfaces exhibit and assuming that physisorption is the dominating mechanism in these experiments, the adsorption of the model NAs is not site specific and hence is adsorbed at sites of different sizes and containing different functional groups, all of which affects the amount of NAs adsorbed. For this reason, the average concentration of each run is used for further analysis.

In addition, the results of CHPA and PVA adsorption at pH 6.5 and 5 do not show reasonable results such as; inconsistency of the CHPA control solution which should remain within the proximity of 50 mg/L, given that no adsorbents are present in the solution, noticeable difference between the two runs, no or poor detection of CHPA at pH 5, and the concentrations of both CHPA and PVA in the initial samples being lower than 50 mg/L. It can be assumed that these observations were a result of the hydrophobicity of both CHPA and PVA compared to HPA. In spite of these observations, it is worth recalling that the pKa's of NAs can range from 5 to 6 (Pourrezaei et al. 2014) and more specifically are approximated as 3.5 for classical,  $\text{O}_2^-$ , NAs (Huang et al. 2014).

The exact pKa's of the NAs of this study have not been reported with exception to HPA which has been approximated to have a pKa that ranges from 4.4 to 4.89 (PubChem n.d.). Given that Huang (2014) noted that the presence of double bonds and rings lowers the pKa of a specific compound, it can be assumed that CHPA has a pKa lower than that of HPA, and the pKa of PVA is even much lower. Therefore, it can be assumed that at the experimental pHs of 5 and 6.5, all three model NA compounds are closely approaching their pKa values, yet due to the hydrophobic character of CHPA and PVA they become less soluble as they approach the pKa and as a result exhibit undissociation. For this reason, it is assumed that CHPA and PVA are essentially not present in the experimental solutions at the lower pHs and thus the data of those two compounds at the lower pHs are neglected.

Therefore, the three model NA compounds will be compared by analyzing the results of pH 8. In addition, given the consistent and reasonable results of HPA throughout all experiments, the removal of HPA, the most hydrophilic compound among the three, will be compared using the results at all three pH conditions.

#### 4.2.1 NAs Removal

To begin with, the removal of the model NAs by GAC or CX at pH 8 are demonstrated in Figures 4.1 and the removal of HPA at all three experimental pHs in figure 4.2. To account for the fact that the initial concentration was not 50 mg/L for all solutions, the removal is demonstrated as the residual concentration, also known as the fraction of the initial concentration remaining in the solution,  $C/C_0$ , throughout time. Moreover, to provide an understanding of the amount of NAs adsorbed or removed from the solution to results in the residuals remaining in Figures 4.1 and 4.2, Tables 4.1 and 4.2 list the percent of NAs removed with respect to the initial concentration of the NA at interest following equation (13).

$$\% \text{ Removed} = \frac{C_0 - C_t}{C_0} \times 100 \quad (13)$$

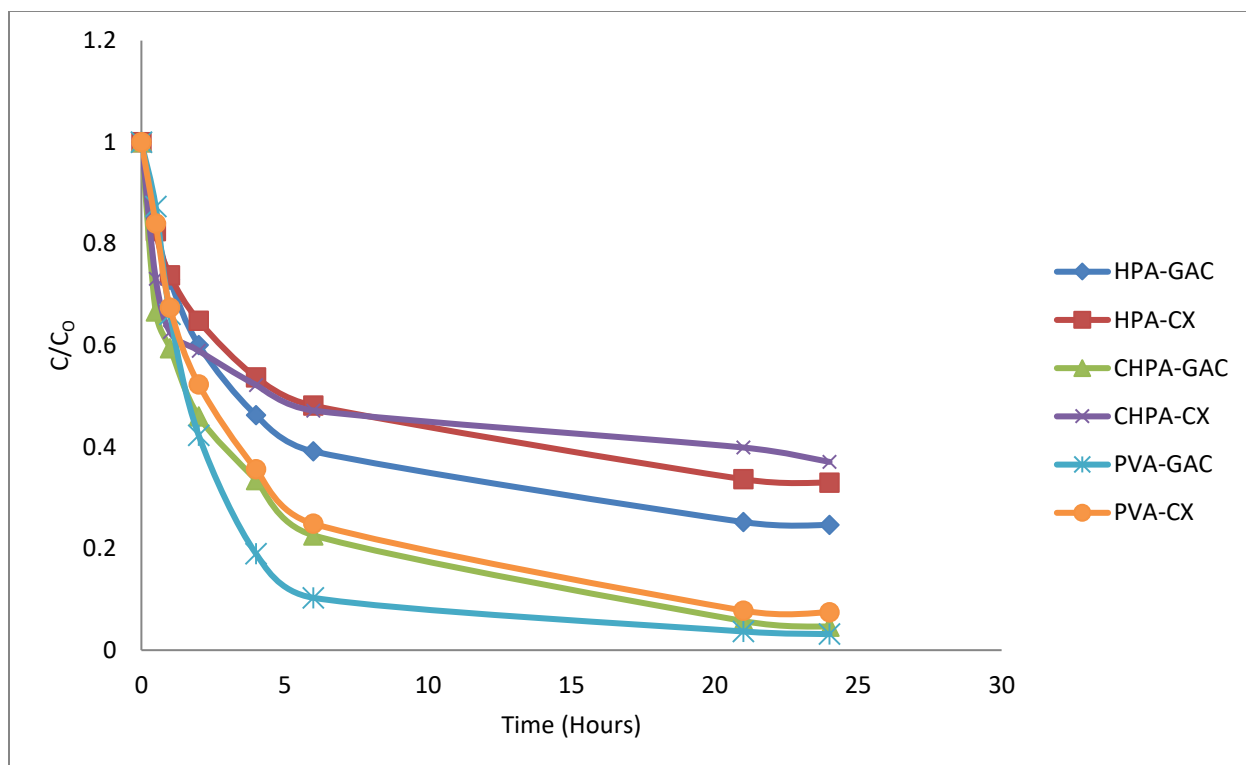


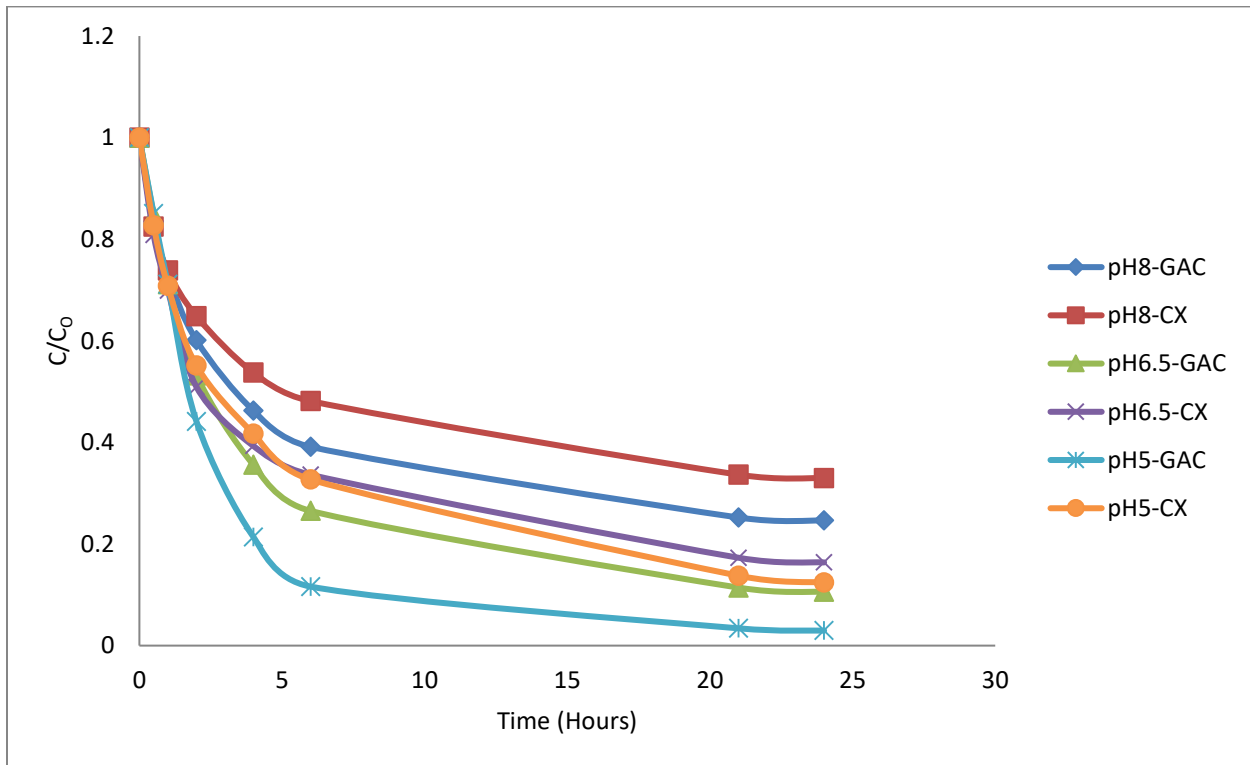
Figure 4.1 Residual concentration of HPA, CHPA, or PVA due to adsorption by GAC or CX at pH 8

Table 4.1 Percent removal of model NAs due to the adsorption by GAC or CX at pH 8

Percent Removal (%)						
Time (Hours)	HPA-GAC	HPA-CX	CHPA-GAC	CHPA-CX	PVA-GAC	PVA-CX
0	0.000	0.000	0.000	0.000	0.000	0.000
0.5	16.487	17.526	33.350	26.899	12.673	16.026
1	27.081	26.188	40.547	37.372	33.887	32.574
2	39.912	35.177	53.979	41.068	57.722	47.685
4	53.752	46.272	66.498	47.793	81.029	64.404
6	60.872	51.870	77.395	52.823	89.689	75.120
21	74.784	66.352	94.273	60.113	96.322	92.221
24	75.369	67.017	95.388	62.936	96.840	92.551

Firstly, the removal of each model NA from solution was illustrated in Figure 4.1 by observing the amount of each NA remaining in the solution after adsorption. Figure 4.1 illustrated that with regards to each model NA compound, GAC removed more NAs in comparison to CX given that it removed approximately; 96.84% PVA, 95.39% CHPA, and 75.37% HPA compared

to 92.55% PVA, 62.936% CHPA, and 67.02% HPA removed by CX. GAC adsorbed the model compounds in a clear trend of higher removal of PVA, then CHPA, followed by HPA, with relatively 96.84%, 95.39%, and 75.37% removed respectively. This trend directly correlates with an increase in the DBE or -Z value given that the DBE values of PVA, CHPA, and HPA are 5,2, and 1 respectively and the -Z values are 8,2, and 0. CX, on the other hand, did not remove model NAs with an established trend since PVA was adsorbed at a fairly high amount of 92.55% later followed by HPA at 67.02% removal and approximately 62.94% of CHPA removed. It can be noticed that approximately 25.53% PVA was removed more than HPA, whereas only 4.08% more HPA was removed than CHPA.



**Figure 4.2 Residual concentration of HPA due to adsorption by GAC or CX at different experimental pHs**

**Table 4.2 Percent removal of HPA due to the adsorption by GAC or CX at pH 8**

Percent Removal of HPA (%)						
Time (Hours)	pH8-GAC	pH8-CX	pH6.5-GAC	pH6.5-CX	pH5-GAC	pH5-CX
0	0.000	0.000	0.000	0.000	0.000	0.000
0.5	16.487	17.526	15.241	19.180	14.976	17.253
1	27.081	26.188	28.882	30.108	28.856	29.215
2	39.912	35.177	46.821	49.071	55.873	44.885
4	53.752	46.272	64.418	60.710	78.636	58.277
6	60.872	51.870	73.481	66.375	88.384	67.307
21	74.784	66.352	88.583	82.703	96.602	86.240
24	75.369	67.017	89.422	83.629	97.045	87.574

In general, Figure 4.2 indicates that overall, electrostatic forces were apparent since the amount of HPA remaining in the solution was least at pH 5, more at pH 6.5, and highest at pH 8. This was observed for both GAC and CX given that HPA was removed by 97.05% at pH 5, 89.42% at pH 6.5, and 75.37% at pH 8 by GAC. In comparison, CX resulted in lower removal fractions by removing HPA by 87.57% at pH 5, 83.63% at pH 6.5, and 67.02% at pH 8 .

#### 4.2.2 NA Adsorption onto CX or GAC

Given that the effectiveness of CX is evaluated based on its performance relative to GAC, the conventional adsorbent used for the removal of NAs, the performance of CX and GAC should be compared in a suitable manner. Thus, the amount of NAs adsorbed by GAC and CX were determined based on equation (2) and normalized by surface area using equation (14):

$$q_{t,N} = \frac{q_t}{S_{BET}} \quad (14)$$

Where  $S_{BET}$ , the BET surface area ( $m^2/g$ ), is 976 and 573  $m^2/g$  for GAC and CX respectively. Figures 4.3 illustrates the amount of HPA, CHPA, or PVA adsorbed onto the surface of GAC or CX with respect to the BET surface area of each adsorbent at pH 8. Furthermore, Figure 4.4 focusses only on the amount of HPA adsorbed onto the surface of GAC or CX throughout the different experimental pHs. The values corresponding to Figures 4.3 and 4.4 can be found in the appendix in tables A.5 and A.6. Unless otherwise stated, the normalized adsorption capacity,  $q_{t,N}$ , will be used for all further analysis to compare GAC and CX justly.

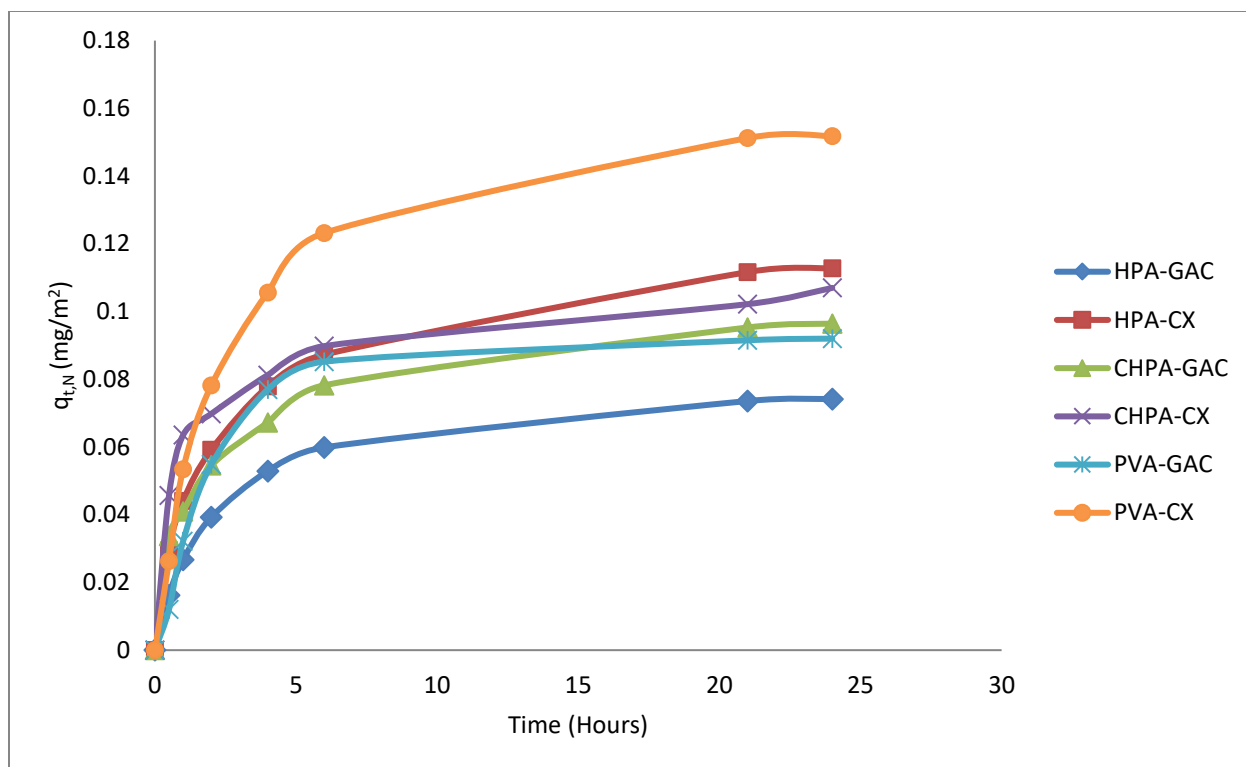


**Figure 4.3 Normalized adsorption capacity of GAC or CX at pH 8 for HPA, CHPA, or PVA**

The normalized adsorption of each model NA onto CX and GAC is illustrated in Figure 4.3 to demonstrate that CX adsorbs more NA molecules relative to GAC with respect to surface area. The higher adsorption of NAs by CX compared to GAC can clearly be attributed to the mesoporosity of CX. It is noticed that GAC adsorbs the model NAs in terms of hydrophobicity, in which a total of  $0.0964 \text{ mg/m}^2$  of CHPA is adsorbed, then  $0.0920 \text{ mg/m}^2$  PVA, followed by  $0.0742 \text{ mg/m}^2$  HPA. Accordingly, this trend follows more removal at higher  $K_{ow}$ 's following  $K_{ow}$  coefficients of 0.60, 0.01, and -0.51 for CHPA, PVA, and HPA respectively. CX, in comparison, adsorbed a total of  $0.1070 \text{ mg/m}^2$  of CHPA,  $0.1518 \text{ mg/m}^2$  PVA, and  $0.1128 \text{ mg/m}^2$  HPA confirming a higher capacity attributed to CX than GAC. However, the amount of NA adsorbed onto CX does not follow the same tendency as GAC, and once again follows the trend of high adsorption of PVA, followed by HPA, and CHPA, similar to the removal trend identified through Figure 4.2 and Table 4.2.

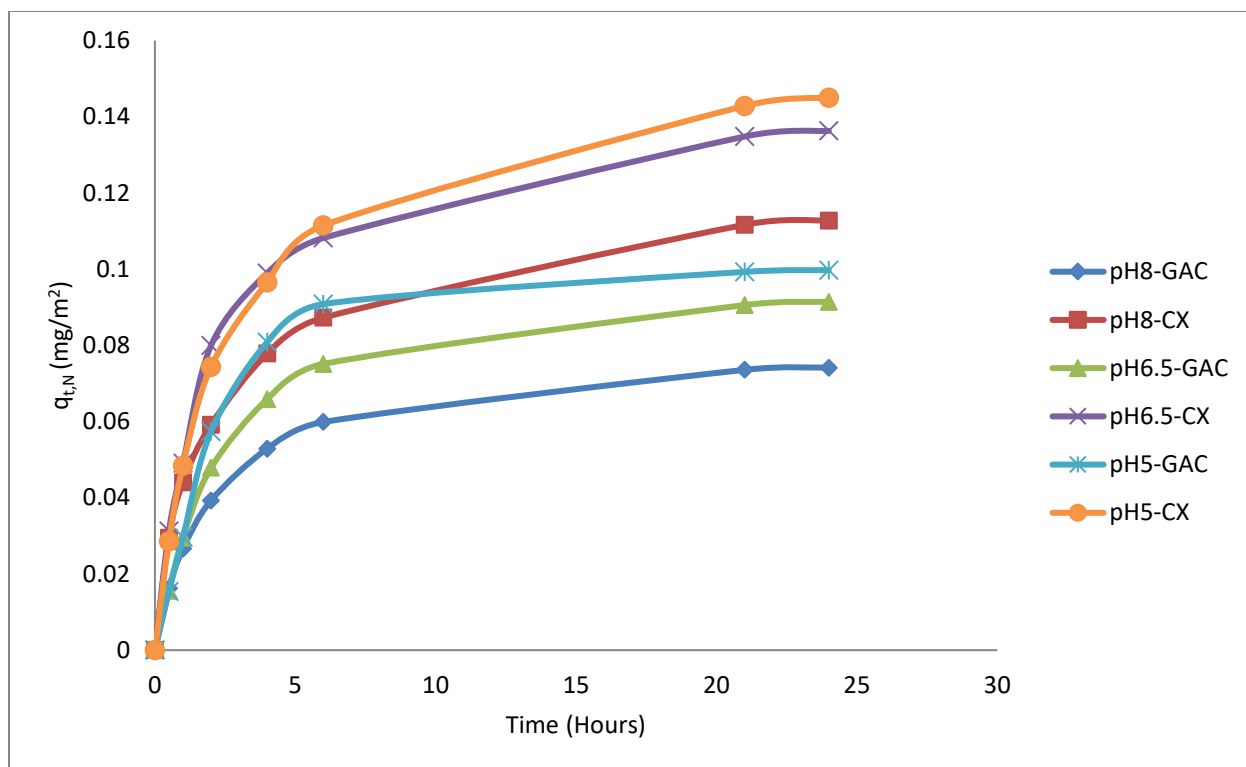


**Figure 4.4 Normalized adsorption capacity of GAC or CX at pH 8, 6.5, and 5 for HPA**

Figure 4.4 confirms the role of electrostatic forces in the adsorption of HPA onto CX and GAC at the different operating pH conditions with more attraction between the adsorbate and adsorbent at lower pHs. However, contrary to Figure 4.2 that indicates that GAC removes more HPA from the solution, CX adsorbs more HPA relative to its BET surface area which is lower than that of GAC. More specifically, at pHs 8, 6.5, and 5, CX adsorbed a total of 0.1128, 0.1363, and 0.1450 mg/m<sup>2</sup> HPA respectively. On the contrary, GAC only adsorbed a total of 0.00742, 0.00914, and 0.00997 mg/m<sup>2</sup> HPA in comparison. Therefore, at all pH conditions, the removal of HPA by CX is more effective than that of GAC. With more focus on electrostatic interactions, Figure 4.4 indicates that the electrostatic forces are consistent for both GAC and CX, in which the amount of HPA adsorbed by either GAC or CX at pH 6.5 is 23.20 and 20.83% higher than adsorption at pH 8. However, at pH 5 GAC and CX adsorb 9.08 and 6.38% more HPA respectively than at pH 6.5.

Furthermore, to understand the effect of pH on the ability of GAC and CX to adsorb HPA, Figure 4.5 demonstrates the normalized amount of HPA adsorbed at different pHs by both GAC and CX.

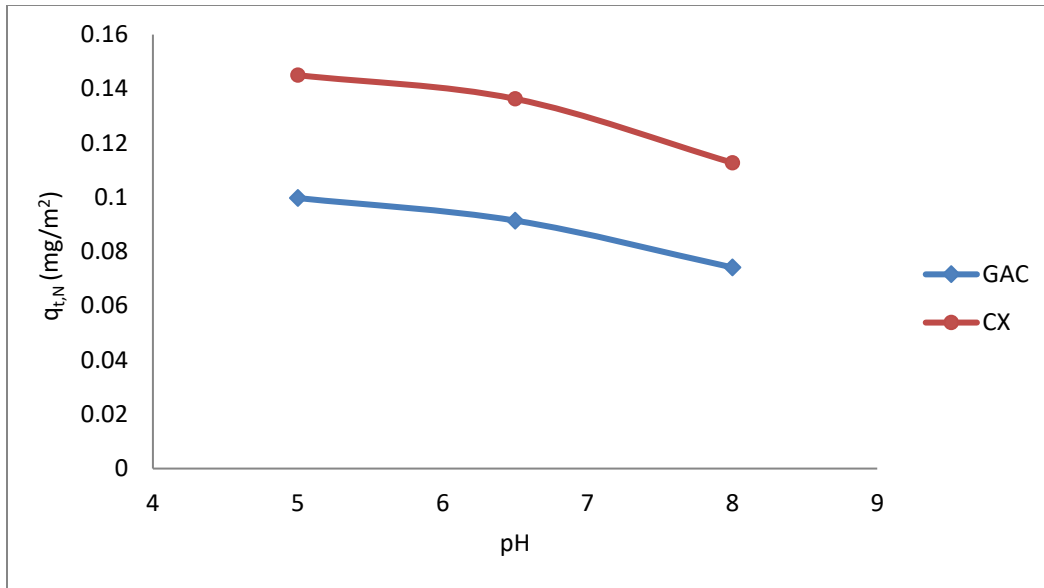


**Figure 4.5 Effect of pH on the normalized adsorption capacity of GAC or CX by HPA**

Figure 4.5 confirms the observations derived from Figure 4.4 as it clearly shows that while CX performs better compared to GAC, with an average of approximately 49% higher adsorption of HPA by CX at all pH conditions, both undertake higher attraction forces between the adsorbate and adsorbent at lower pHs. In general, both CX and GAC observe a steady trend in the electrostatic forces with GAC consisting of a slightly less steep trend. Most notably, the slope of the CX adsorption is sharper at pHs greater than 6.5. This observation, not only asserts the trend demonstrated in Figure 4.4, but also confirms that repulsion greatly hinders the adsorption of HPA onto CX at pHs above that of the  $pH_{PZC}$  and again at lower pHs as neutral and attractive electrostatic forces promote adsorption.

### 4.2.3 Adsorption Kinetics Modeling of Data

#### 4.2.3.1 Rate of Diffusion

The internal diffusion model, equation (1), was employed to identify the rate of diffusion,  $k_i$  (mg/m<sup>2</sup>/hr<sup>1/2</sup>), the significance of the boundary layer,  $c$  (mg/m<sup>2</sup>), the rate of film diffusion,  $k_{i-Film}$  (mg/m<sup>2</sup>/hr<sup>1/2</sup>), and the rate of pore diffusion,  $k_{i-Pore}$  (mg/m<sup>2</sup>/hr<sup>1/2</sup>). Note that the results of PFO and PSO models are presented in the appendix in section A.4. By obtaining these values, the rate limiting step of each adsorption mechanism can be identified.

Firstly, the rate of diffusion and boundary layer constant were obtained by developing a plot of normalized  $q_t$  versus  $t^{1/2}$  and determining the slope and intercept of the trendline.

(1) pH 8 Results

Figure 4.6 illustrates the internal diffusion model of the adsorption of all three model NAs on GAC or CX at pH 8.

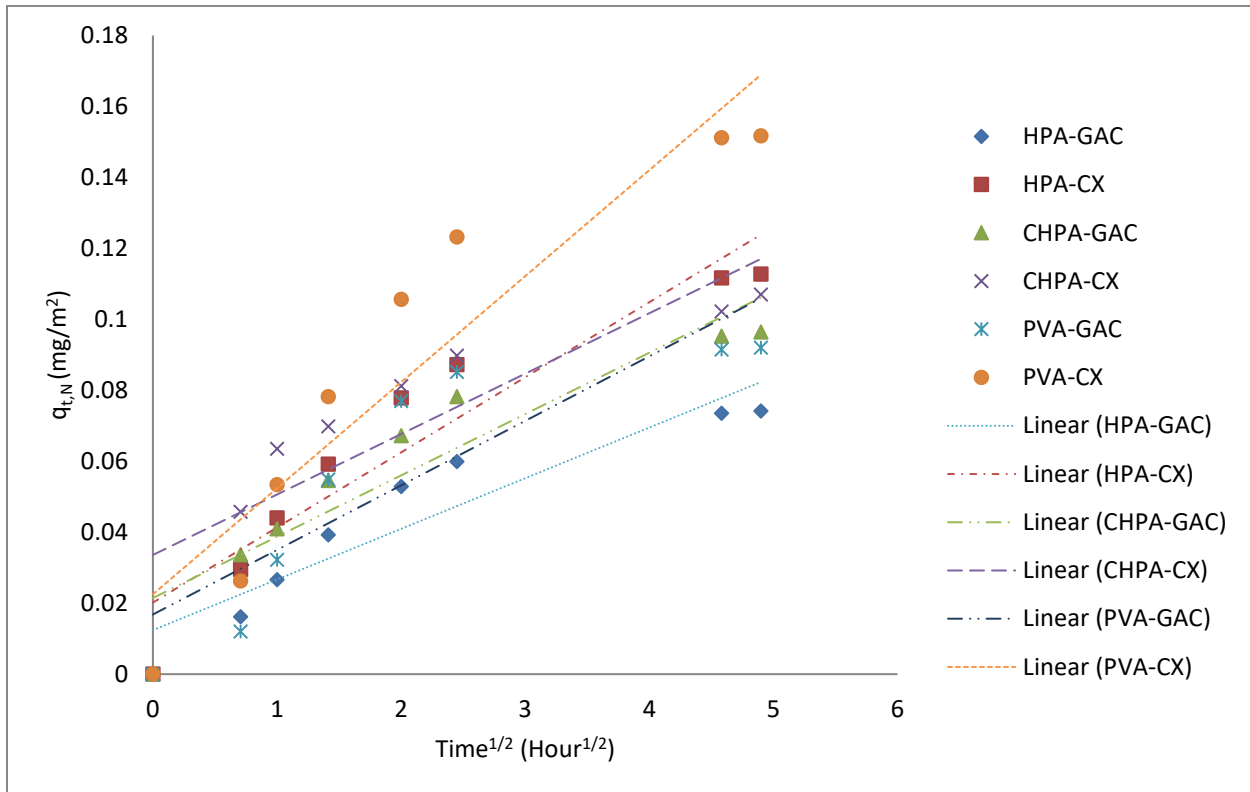


**Figure 4.6 Internal diffusion model of HPA, CHPA, or PVA onto GAC or CX at pH 8**

Using the linear best-fit lines of each curve in Figure 4.6, the slope and intercept were used to identify  $k_i$  and  $c$  as reported in table 4.3 along with the coefficient of determination,  $R^2$ , to indicate how close the trendline fits the data.

**Table 4.3 Internal diffusion parameters that model the diffusion of HPA, CHPA, or PVA onto GAC or CX at pH 8**

<b>Reaction</b>	<b><math>k_i</math> (mg/m<sup>2</sup>/hr<sup>1/2</sup>)</b>	<b><math>c</math> (mg/m<sup>2</sup>)</b>	<b>R<sup>2</sup></b>	<b>Rate Limiting Step</b>
<b>HPA-GAC</b>	0.0143	0.0124	0.8789	Film & Pore Diffusion
<b>HPA-CX</b>	0.0212	0.0202	0.8961	Film & Pore Diffusion
<b>CHPA-GAC</b>	0.0173	0.0215	0.8690	Film & Pore Diffusion
<b>CHPA-CX</b>	0.0170	0.0336	0.7602	Film & Pore Diffusion
<b>PVA-GAC</b>	0.0182	0.0168	0.7727	Film & Pore Diffusion
<b>PVA-CX</b>	0.0299	0.0225	0.8819	Film & Pore Diffusion

As presented in Table 4.3, the rate of diffusion of PVA and HPA into the CX surface were much higher than that for the diffusion of CHPA into CX, more specifically, 0.0299, 0.0212, and 0.0170 mg/m<sup>2</sup>/hr<sup>1/2</sup> respectively. Similar to earlier observations, the rates of diffusion followed the same trend of faster diffusion for PVA, HPA, and finally CHPA. The diffusion of the three model NAs into the surface of GAC, although generally slower than that of diffusion into CX, again follows the trend of faster diffusion rates for compounds with higher DBE or -Z values. In an essence, PVA, CHPA, and HPA are characterized by DBEs of 5,2, and 1 respectively and -Z values of 8,2, and 0. This coincides with the descending diffusion rates of 0.0182, 0.0173, and 0.0143 mg/m<sup>2</sup>/hr<sup>1/2</sup> for PVA, CHPA, and HPA respectively.

Note that Table 4.3 indicates that the constant of the internal diffusion model is not zero, thus the role of film diffusion due to the significance of the stagnant film surrounding the adsorbent surface must be taken into consideration. It is shown in Table 4.3 that in general, the constant values are higher for diffusion of the NAs into CX than GAC, however both observe the same trend in which an increase in K<sub>OW</sub> value, results in an increase in the constant value. Wherein, the

$K_{ow}$  coefficients for CHPA, PVA, and HPA are 0.60, 0.01, and -0.51 respectively. Likewise, the values of the constants for the diffusion of CHPA, PVA, and HPA into CX are 0.0336, 0.0225, 0.0202 mg/m<sup>2</sup> respectively. Similarly for the diffusion of CHPA, PVA, and HPA into GAC their constant values follow the same descending trend of 0.0215, 0.0168, 0.0124 mg/m<sup>2</sup> respectively. Therefore, the correlation between the  $K_{ow}$  coefficients and the constant values establishes the role of compound hydrophobicity on the significance of the boundary layer surrounding the adsorbent surface.

From the parameters identified in table 4.3, given that the constant,  $c$ , is not zero, it can be assumed that the boundary layer surrounding the surface of both GAC and CX in all adsorption experiments has a significant effect on the diffusion of the model NAs. Consequently, pore transport is not the dominating diffusion mechanism. For this reason, the data is fitted to two separate trendlines as recommended by Weber and Morris (1963) to identify the rate of film diffusion and pore diffusion and consequently the more dominant and rate limiting step is distinguished. Figure 4.7 shows the internal diffusion model of each model NA onto GAC or CX at pH 8. The data is fitted to two separate trendlines, the first indicating film diffusion and the second representing pore diffusion. The slope of the first best-fit line is identified as the rate of film diffusion,  $k_{i-Film}$ , and the slope of the second best-fit line corresponds to the rate of pore diffusion,  $k_{i-Pore}$ . The rates corresponding to each adsorption mechanism from Figure 4.7 are summarized in Table 4.4. Again, the coefficient of determination is provided to demonstrate how closely each data fits to its corresponding trendline.

**Table 4.4 Rates of film and pore diffusion of HPA, CHPA, or PVA onto GAC or CX at pH 8**

<b>Reaction</b>	<b><math>k_i\text{-Film}</math> (mg/m<sup>2</sup>/hr<sup>1/2</sup>)</b>	<b>R<sup>2</sup></b>	<b><math>k_i\text{-Pore}</math> (mg/m<sup>2</sup>/hr<sup>1/2</sup>)</b>	<b>R<sup>2</sup></b>
<b>HPA-GAC</b>	0.0254	0.9905	0.006	0.9931
<b>HPA-CX</b>	0.0360	0.985	0.0108	0.9936
<b>CHPA-GAC</b>	0.0308	0.9691	0.0076	0.9959
<b>CHPA-CX</b>	0.0637	0.9998	0.0102	0.94
<b>PVA-GAC</b>	0.0383	0.9665	0.0028	0.9971
<b>PVA-CX</b>	0.0526	0.987	0.0122	0.9895

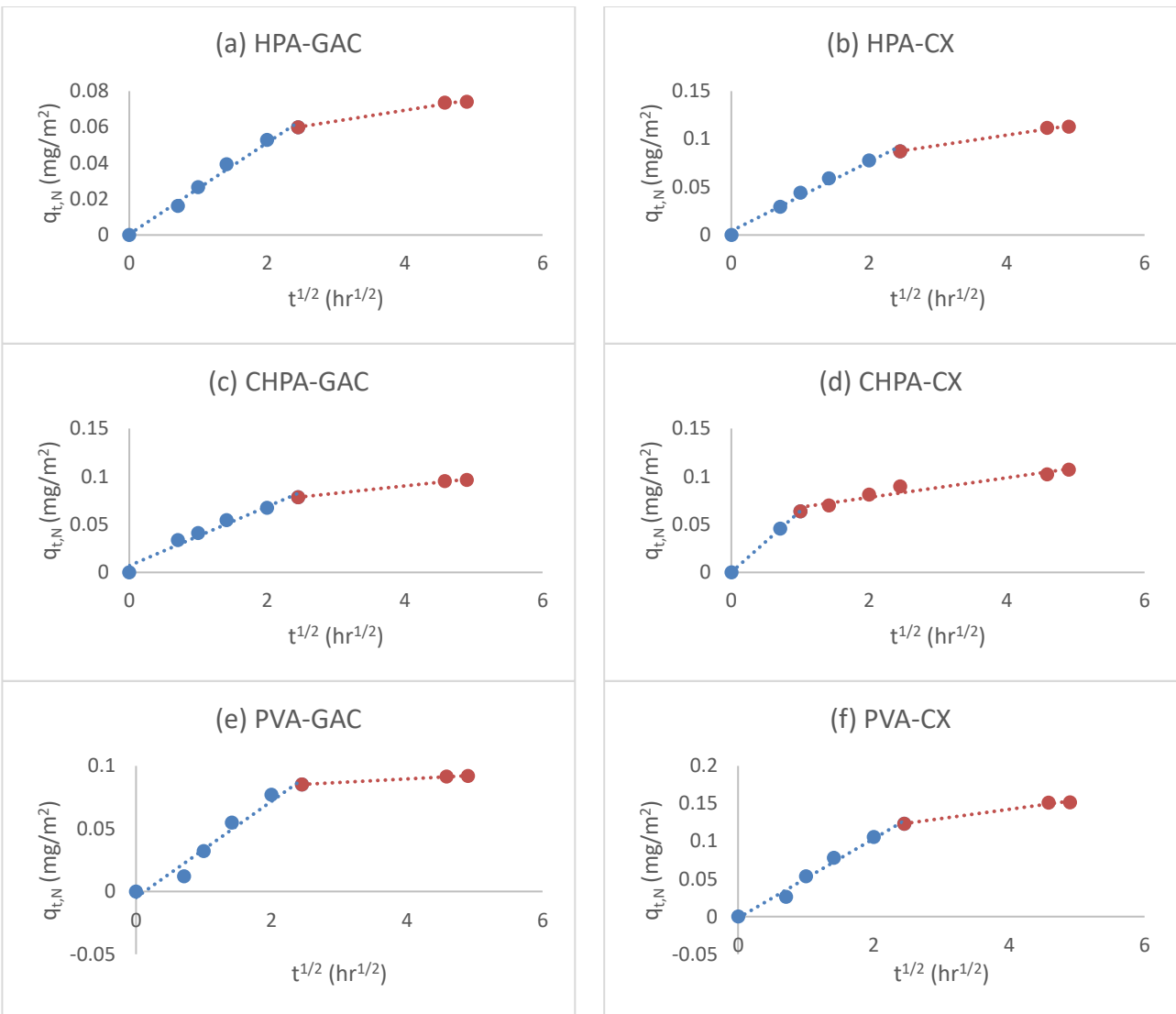


**Figure 4.7 Internal diffusion model of the adsorption of (a) HPA onto GAC, (b) HPA onto CX, (c) CHPA onto GAC, (d) CHPA onto CX, (e) PVA onto GAC, and (f) PVA onto CX at pH 8**

Overall, as seen in Table 4.4, the rate of film diffusion is higher than pore diffusion for the diffusion of each model compound on both adsorbents. Accordingly, this confirms that pore diffusion is the rate limiting step, yet film diffusion still maintains a significant role in the rate of diffusion. Film diffusion rate constants were estimated for all three model compounds to demonstrate higher film diffusion rate constants for CX compared to GAC; in which the rate of film diffusion of HPA, CHPA, and PVA were 0.0360, 0.0637, and 0.0526  $\text{mg/m}^2/\text{hr}^{1/2}$  onto CX and 0.0254, 0.0308, and 0.0383  $\text{mg/m}^2/\text{hr}^{1/2}$  onto GAC. More specifically, the diffusion of CHPA, PVA, and HPA into the film of CX followed the hydrophobic trend in which a higher  $K_{OW}$  results in a higher rate of diffusion into the film. Similar to earlier trends identified for adsorption of the

model NAs onto GAC, the rate of film diffusion is higher for compounds with greater DBE and - Z values.

It should be noted that in general the film diffusion is assumed for the first six points, first six hours of each experiment, while pore diffusion is assumed for the remaining three points, last 18 hours of each experiment. However, for the diffusion of CHPA onto CX, film diffusion occurs at a much higher rate, in which the rate of  $0.0637 \text{ mg/m}^2/\text{hr}^{1/2}$ , which is on average 42.5% higher than the other rate constants. In addition, the diffusion of CHPA into the film of CX approximately only occurs for the first three points, first hour, of the experiment, attributing to its higher hydrophobicity relative to the other model compounds.

Moreover, the diffusion of the model NAs into the pores was demonstrated by the pore diffusion rate constants in table 4.4 which indicates that the rate of diffusion into the pores of CX is greater than diffusion into the pores of GAC. Similar to earlier results, diffusion of NAs into the pores of CX follows the trend of highest rate for PVA diffusion, followed by HPA, then CHPA. The diffusion of the model NAs into the pores of GAC, on the other hand, followed the opposite trend of that into the CX pores.

## *(2) HPA Results*

Similarly, the diffusion of HPA onto GAC or CX at pH 8, 6.5, and 5 is modelled in Figure 4.8 and the slope,  $k_i$ , and intercept,  $c$ , of each best-fit line and the corresponding coefficients of determination are recorded in table 4.5.

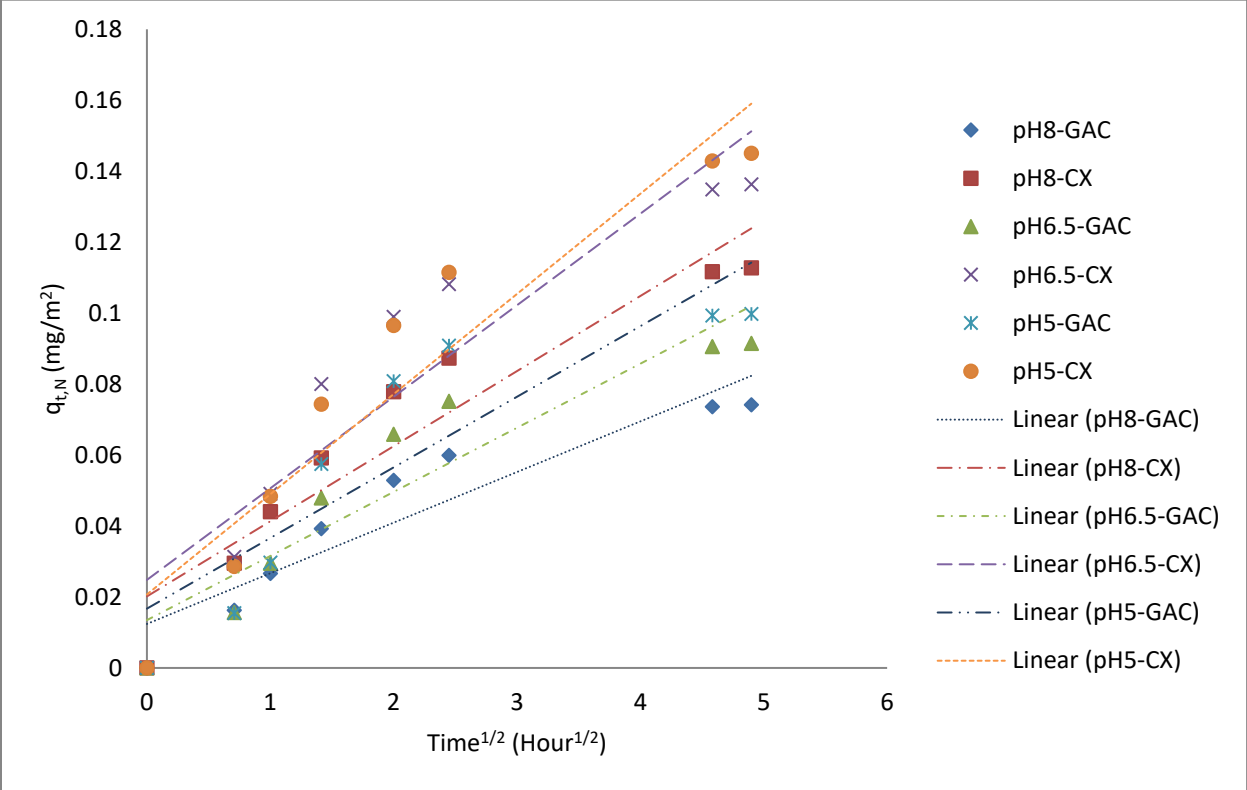


Figure 4.8 Internal diffusion model of HPA onto GAC or CX at pH 8, 6.5, and 5

**Table 4.5 Internal diffusion parameters that model the diffusion of HPA onto GAC or CX at pH 8, 6.5, and 5**

<b>Reaction (HPA)</b>	<b><math>k_i</math> (mg/m<sup>2</sup>/hr<sup>1/2</sup>)</b>	<b><math>c</math> (mg/m<sup>2</sup>)</b>	<b>R<sup>2</sup></b>	<b>Rate Limiting Step</b>
<b>pH8-GAC</b>	0.0143	0.0124	0.8789	Film & Pore Diffusion
<b>pH8-CX</b>	0.0212	0.0202	0.8961	Film & Pore Diffusion
<b>pH6.5-GAC</b>	0.0181	0.0135	0.8692	Film & Pore Diffusion
<b>pH6.5-CX</b>	0.0258	0.0248	0.8645	Film & Pore Diffusion
<b>pH5-GAC</b>	0.0199	0.0167	0.7966	Film & Pore Diffusion
<b>pH5-CX</b>	0.0282	0.0207	0.9051	Film & Pore Diffusion

The internal diffusion model was employed to identify the significance of diffusion in the adsorption of HPA onto CX and GAC and the role of electrostatic forces on these imperative steps. Overall, electrostatic interactions were apparent on the rate of diffusion, as shown in Figure 4.8 and table 4.5, in which at lower pHs, the rate of diffusion was higher and once again CX observed higher diffusion rates in comparison to that of GAC. This clearly indicates that diffusion into the pores of CX was faster than that of GAC and diffusion was enhanced at lower pHs due to attractive forces between the pores of CX and GAC and HPA molecules. However, the constants of the individual internal diffusion models were slightly deviant of the zero value, thus the role of film diffusion cannot be neglected due to significance of the stagnant film surrounding the surface of the adsorbents. From Table 4.5 it can be noted that the constant values were higher for CX relative to GAC. In terms of GAC, the role of electrostatic forces on the magnitude of the constant is clear, in which a higher constant was observed at lower pHs. Thus, attractive forces promote the

significance of the boundary layer surrounding the GAC surface. For CX on the other hand, the value of the constant was highest at pH 6.5 in which the CX surface observes a neutral charge. Afterwards, the magnitude of the constant is higher for pH 5 than pH 8 which notes the significance of attractive forces in comparison to repulsive forces.

Since, Figure 4.8 and table 4.5 indicate that pore diffusion is not the only rate limiting step since the intercept is not zero, the data was fit to two lines in Figure 4.9 to identify both the film and pore diffusion rates listed in Table 4.6.

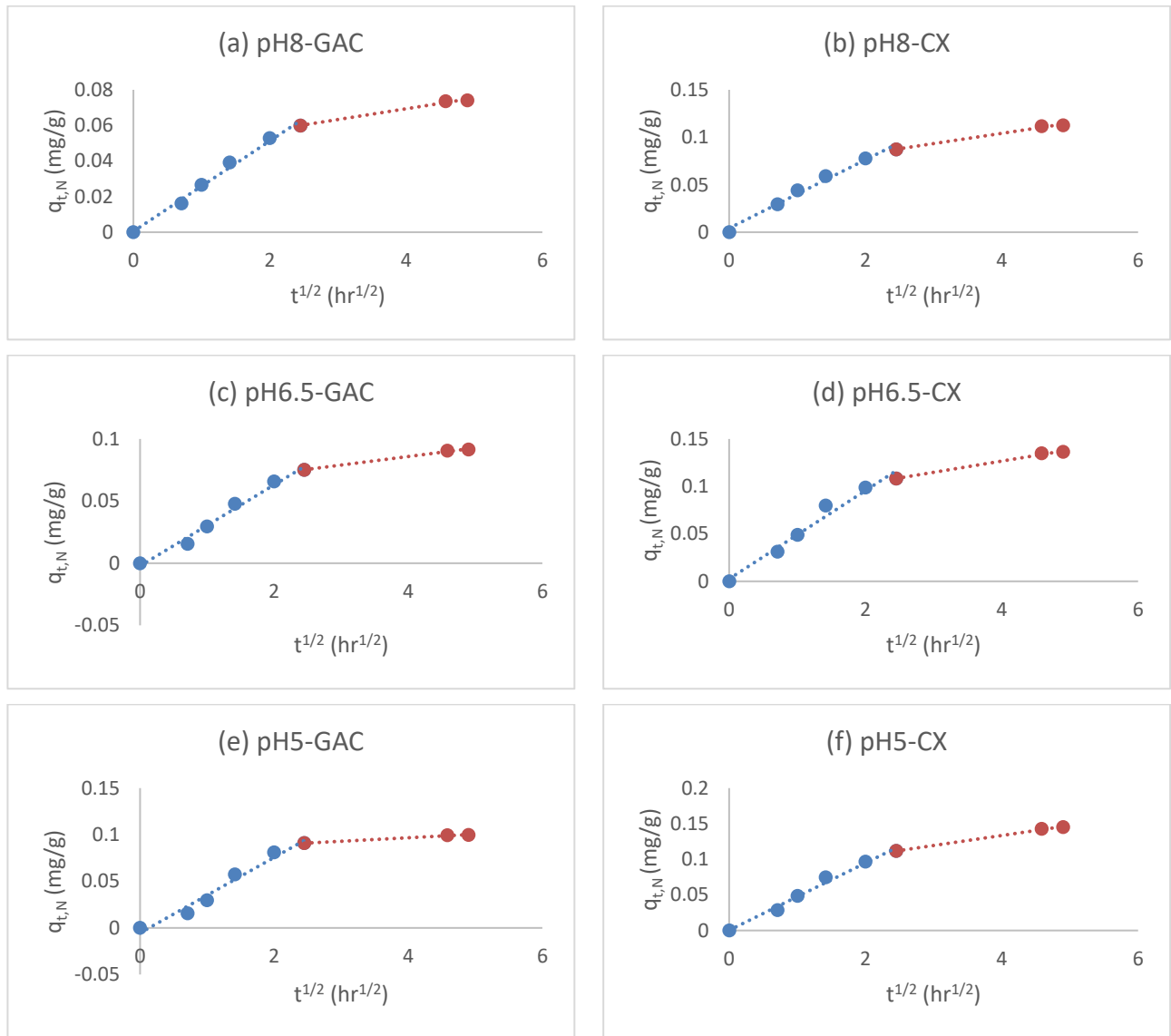


**Figure 4.9 Internal diffusion model of normalized adsorption of HPA (a) onto GAC at pH 8, (b) onto CX pH at 8, (c) onto GAC at pH 6.5, (d) onto CX at pH 6.5, (e) onto GAC at pH 5, and (f) onto CX at pH 5**

**Table 4.6 Rates of film and pore diffusion of HPA onto GAC or CX at pH 8, 6.5, and 5**

<b>Reaction (HPA)</b>	<b><math>k_{i-Film}</math> (mg/m<sup>2</sup>/hr<sup>1/2</sup>)</b>	<b>R<sup>2</sup></b>	<b><math>k_{i-Pore}</math> (mg/m<sup>2</sup>/hr<sup>1/2</sup>)</b>	<b>R<sup>2</sup></b>
<b>pH8-GAC</b>	0.0254	0.9905	0.006	0.9931
<b>pH8-CX</b>	0.0360	0.9850	0.0108	0.9936
<b>pH6.5-GAC</b>	0.0326	0.9851	0.0069	0.9948
<b>pH6.5-CX</b>	0.0465	0.9726	0.0118	0.9949
<b>pH5-GAC</b>	0.0405	0.9720	0.0038	0.9946
<b>pH5-CX</b>	0.0472	0.9884	0.0141	0.9964

In general, Table 4.6 indicates that the rates of film diffusion were higher than the rates of pore diffusion for the diffusion of HPA onto either GAC or CX at all experimental pHs. Consequently, slower rates of diffusion confirmed that pore diffusion is the rate limiting step in the adsorption of HPA onto CX and GAC at all pH conditions. However, since the constants in Table 4.5 are not zero, the stagnant films surrounding CX and GAC have a significant effect on the diffusion of HPA onto the adsorbents and the role of film diffusion, although not dominant, is still worth noting. In terms of film diffusion, CX observed higher rates relative to GAC with the rates at pH 5 and 6 much higher than that at pH 8, 0.0472, 0.0465, and 0.0360 mg/m<sup>2</sup>/hr<sup>1/2</sup> respectively. HPA film diffusion onto GAC on the other hand, while slower than that onto CX, observed a constant trend of higher rates at lower pHs noting the consistency of electrostatic forces. Moreover, pore diffusion rate constants followed the same trend as the overall diffusion rate constants, with faster rates for CX in comparison to GAC while the role of electrostatic interaction being consistent for both adsorbents, i.e. higher rates at lower pHs, due to attraction.

#### 4.2.3.2 Rate of Adsorption

Section 2.1.3.2 defines the two models used to model the rate of adsorption. The PFO model parameters are identified by using equation (4) and plotting  $\ln(q_e - q_t)$  versus time, and the slope of the linear best-fit line provides the PFO rate constant,  $k_1$ . Similarly, the PSO rate

constant,  $k_{II}$ , is obtained from the slope of the linear line developed through the plot of  $\frac{1}{(q_e - q_t)}$  and time, following equation (7).

(1) pH 8 Results

The linear PFO model is plotted in Figure 4.10 for the adsorption of HPA, CHPA, and PVA onto GAC and CX at pH 8.

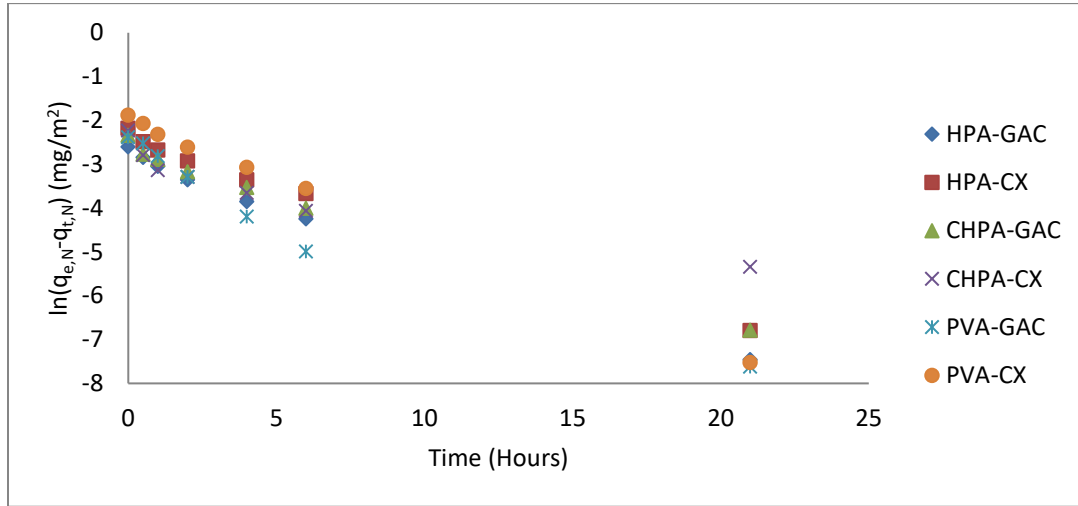


**Figure 4.10 Linear PFO model of the adsorption of HPA, CHPA, & PVA onto GAC or CX at pH 8**

To clearly identify PFO rate constant of each adsorption mechanism, each adsorption mechanism is plotted in Figure 4.11 and the rate constants are reported in Table 4.7. Note that the error calculated in Table 4.7 is based on comparing the actual equilibrium adsorption capacity,  $q_e$ , from the data to the equilibrium capacity identified from the intercept of the plot where:

$$q_{e-eqn} = e^{intercept} \quad (15)$$

And,

$$\% error = \frac{|q_{e-actual} - q_{e-eqn}|}{|q_{e-actual}|} \times 100 \quad (16)$$

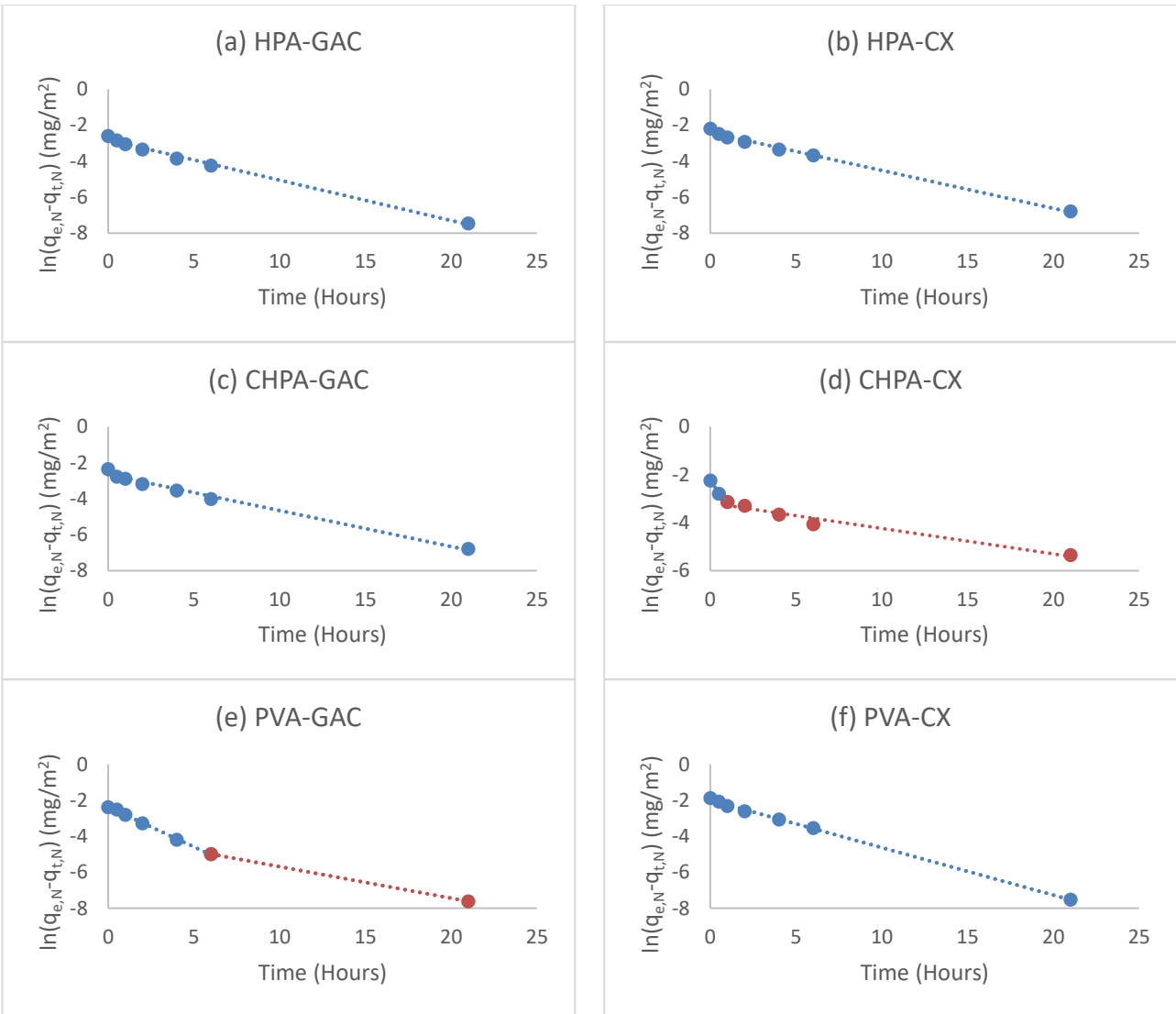


Figure 4.11 Linear PFO model of (a) HPA onto GAC, (b) HPA onto CX, (c) CHPA onto GAC, (d) CHPA onto CX, (e) PVA onto GAC, and (f) PVA onto CX at pH 8

Table 4.7 PFO rate constants of HPA, CHPA, and PVA onto GAC and CX at pH 8

Reaction	$k_f$ (hr <sup>-1</sup> )	R <sup>2</sup>	Intercept	$q_{e-eqn}$ (mg/m <sup>2</sup> )	$q_{e-actual}$ (mg/m <sup>2</sup> )	% Error
HPA-GAC	0.2243	0.9945	-2.8105	0.06017	0.07415	18.8489
HPA-CX	0.2108	0.9948	-2.4031	0.09043	0.1128	19.8030
CHPA-GAC	0.2000	0.9888	-2.6574	0.07013	0.09641	27.2612
CHPA-CX	0.9009    0.1062	0.9815    0.9675	-2.2708	0.1032	0.1070	3.5064
PVA-GAC	0.4440    0.1750	0.9981    1.000	-2.3695	0.09352	0.09200	1.6626
PVA-CX	0.2639	0.9988	-1.9912	0.1365	0.1518	10.0465

Note that for the (d) CHPA onto CX and (e) PVA onto GAC adsorption mechanisms, the overall PFO rate constants,  $k_t$ , are 0.1262 and 0.2444  $\text{hr}^{-1}$  respectively. However, these rate constants result in  $R^2$  values of 0.8709 and 0.9434, and 47.5642 and 31.9531% error. As a result, two separate PFO rate constants are estimated for each adsorption mechanism, in which for the CHPA-CX reaction the first three data points are fit to a best-fit line and the last four data points are fit to another best-fit line. Likewise, the first five data points of the PVA-GAC reaction are fit to one best-fit line and the last two points are fit to a separate best-fit line. As seen in Table 4.7, the two PFO rate constants for each reaction are tabulated resulting in higher  $R^2$  values and errors reduced to 3.5604 and 1.6626%.

Likewise, the PSO rate constants were evaluated from Figures 4.12 and 4.13 and the parameters are summarized in table 4.8 Note that for the PSO model, the estimated equilibrium adsorption capacity is calculated from the intercept as shown in equation (17).

$$q_{e-eqn} = \frac{1}{\text{intercept}} \quad (17)$$

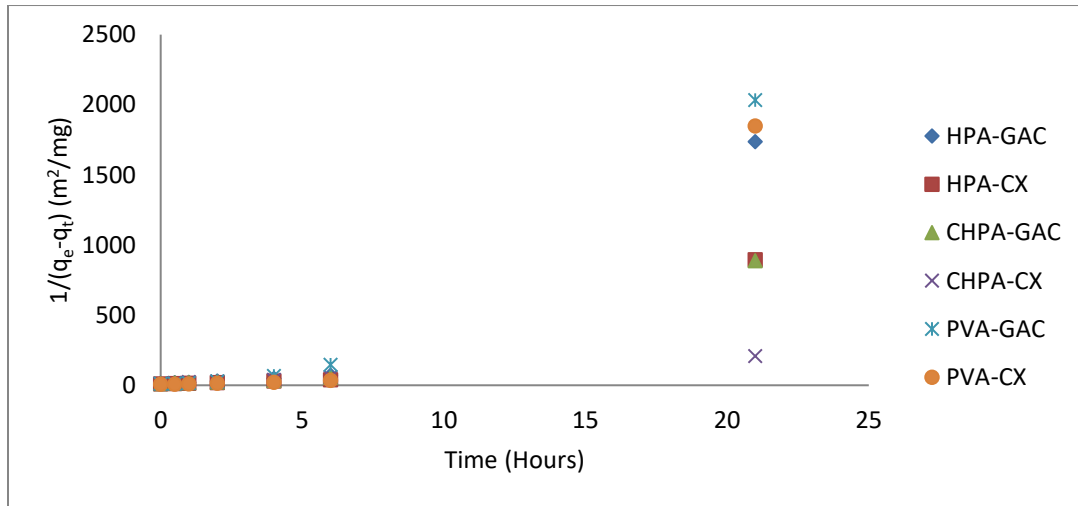


Figure 4.12 Linear PSO model of the adsorption of HPA, CHPA, and PVA onto GAC or CX at pH 8

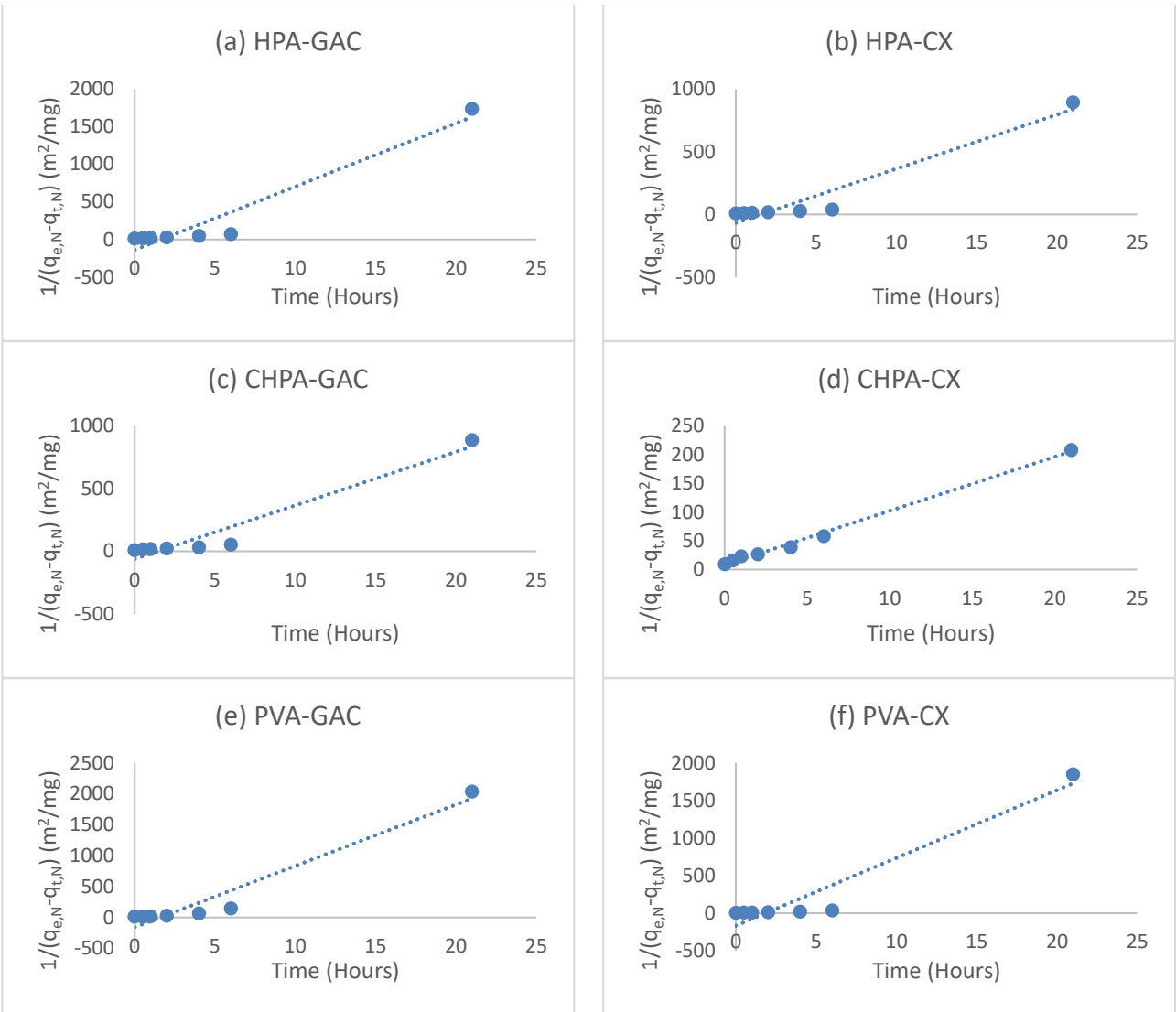


Figure 4.13 Linear PSO Model of (a) HPA onto GAC, (b) HPA onto CX, (c) CHPA onto GAC, (d) CHPA onto CX, (e) PVA onto GAC, and (f) PVA onto CX at pH 8

Table 4.8 PSO rate constants of HPA, CHPA, and PVA onto GAC and CX at pH 8

Reaction	$k_{II}$ ( $m^2/mg/hr$ )	$R^2$	Intercept	$q_{e-eqn}$ ( $mg/m^2$ )	$q_{e-actual}$ ( $mg/m^2$ )	% Error
HPA-GAC	84.190	0.9342	-138.62	-0.00721	0.074152	109.7287
HPA-CX	43.183	0.9347	-67.702	-0.01477	0.112769	113.0981
CHPA-GAC	42.729	0.9411	-61.342	-0.0163	0.096414	116.9084
CHPA-CX	9.4067	0.9952	8.0627	0.124028	0.106981	15.9348
PVA-GAC	99.085	0.9486	-157.76	-0.00634	0.091998	106.8901
PVA-CX	90.112	0.9257	-166.5	-0.00601	0.15178	103.9570

Lastly, the rate of adsorption of the model NAs onto CX and GAC were modeled by PFO in Figures 4.12 and 4.13. It is assumed that the PFO model is most suitable for these adsorption mechanisms given that physisorption is most likely the means of adsorption, given that no temperature change was observed during the experiments and no notable chemical reactions occurred. This is confirmed by high error (mainly above 100%) arising from estimation of the equilibrium adsorption capacity through the PSO model as seen in Table 4.8.

The PFO rate constants summarized in Table 4.7 do not indicate a clear dominance in terms of higher rates for GAC over CX or vice versa. However, in general the same trend follows for adsorption onto CX and GAC, in which the PFO rate of PVA adsorption, 0.2639 and 0.2444 hr<sup>-1</sup> for CX and GAC (following the overall PFO rate constant for GAC), was higher than the adsorption of HPA, 0.2243 and 0.2108 hr<sup>-1</sup> for GAC and CX, and finally the smallest rate for the adsorption of CHPA, 0.2000 and 0.1262 hr<sup>-1</sup> (following the overall PFO rate constant for CX). It should be noted that the highest adsorption rate was observed for PVA onto CX, while the smallest rate was noted for the adsorption of CHPA onto CX (with regards to the overall PFO rate constant for CX). Therefore, the PFO rates of the three model compounds are closer for the adsorption onto GAC, whereas the PFO rate constants of the adsorption of the model NAs onto CX are well spread apart. More specifically, the PFO rate onto GAC for PVA is 9% higher than the rate for HPA, and the rate of HPA is 12% higher than that of CHPA. In comparison, the PFO rate onto CX for PVA is 25% higher than the rate for HPA, and the rate of HPA is 67% higher than that of CHPA.

As mentioned earlier, the PFO rate for CHPA onto CX and PVA on GAC was divided to more suitably fit the data. It is worth mentioning that the rate of adsorption of CHPA onto CX is the slowest yet given that it is divided into two rates it correlates with the diffusion of CHPA into the pores of CX in which, the first PFO rate constant occurs during the same time as film diffusion and the second PFO rate constant is modelled during the same time period as pore diffusion.

## *(2) HPA Data*

Following the same methods as above, the PFO rate constants for the HPA adsorption onto GAC and CX at the different experimental pHs were identified by developing a plot of  $\ln(q_e - q_t)$  versus time in Figure 4.14 and the rate constant and error due to estimation from the slopes and intercepts of the best-fit lines of each adsorption mechanism are estimated from Figure 4.15. The

PFO rate constants, coefficient of determination, and error of each HPA- adsorption mechanism are summarized in table 4.9.

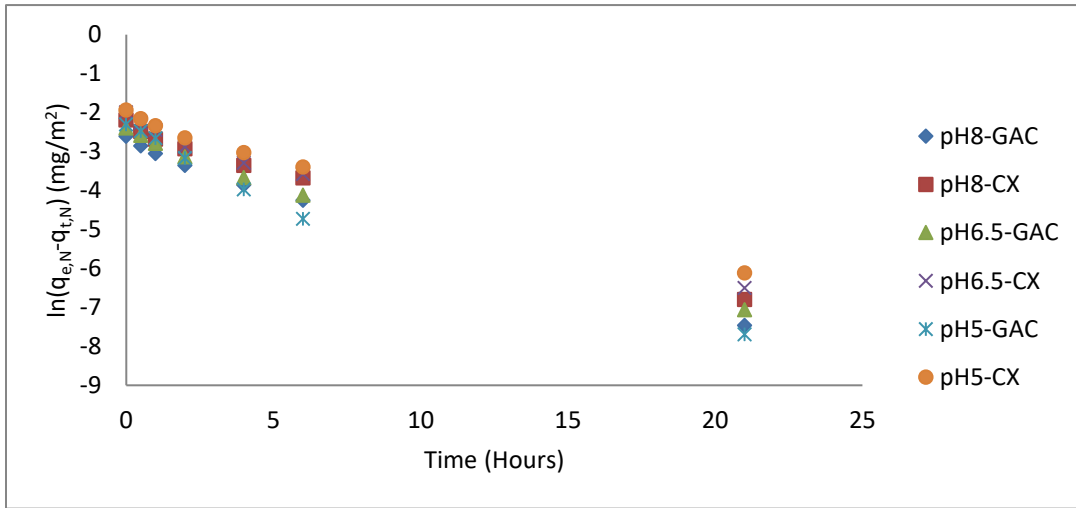


Figure 4.14 Linear PFO model of the adsorption of HPA onto GAC or CX at pH 8, 6.5, or 5

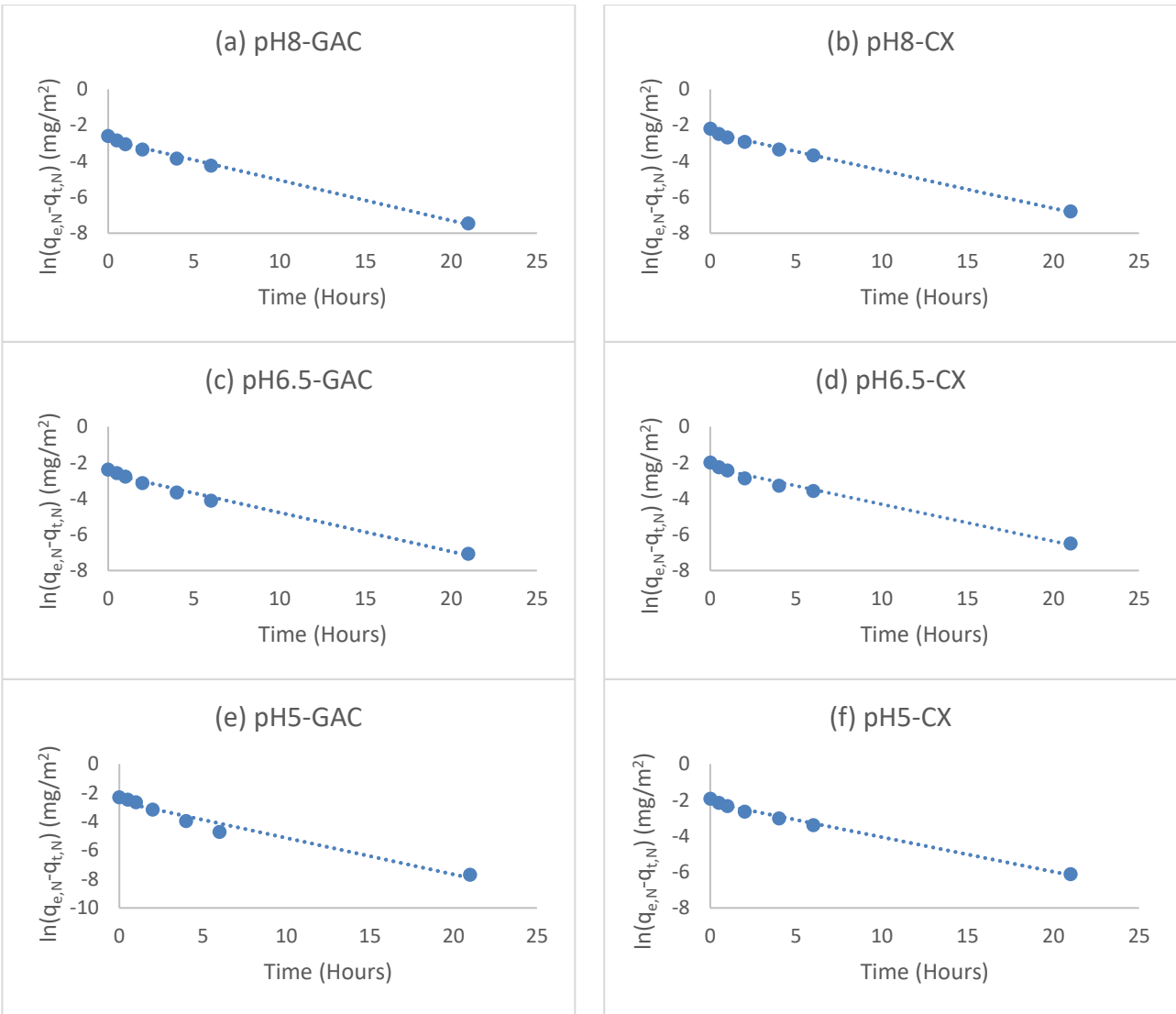


Figure 4.15 Linear PFO model of HPA (a) onto GAC at pH 8, (b) onto CX pH at 8, (c) onto GAC at pH 6.5, (d) onto CX at pH 6.5, (e) onto GAC at pH 5, and (f) onto CX at pH 5

Table 4.9 PFO rate constants of HPA onto GAC and CX at pH 8, 6.5, and 5

Reaction (HPA)	$k_i$ (hr <sup>-1</sup> )	R <sup>2</sup>	Intercept	q <sub>e</sub> -eqn (mg/m <sup>2</sup> )	q <sub>e</sub> -actual (mg/m <sup>2</sup> )	% Error
pH8-GAC	0.2243	0.9945	-2.8105	0.060175	0.074152	18.84886
pH8-CX	0.2108	0.9948	-2.4031	0.090437	0.112769	19.803
pH6.5-GAC	0.2168	0.9894	-2.6072	0.073741	0.091434	19.35124
pH6.5-CX	0.2052	0.9871	-2.261	0.104246	0.136318	23.52699
pH5-GAC	0.2529	0.9663	-2.6081	0.073674	0.099743	26.13565
pH5-CX	0.1923	0.9923	-2.138	0.11789	0.145045	18.72172

Likewise, the PSO rate constants, coefficients of determination, and error are summarized in table 3.13 and illustrated in Figure 4.16 and 4.17.

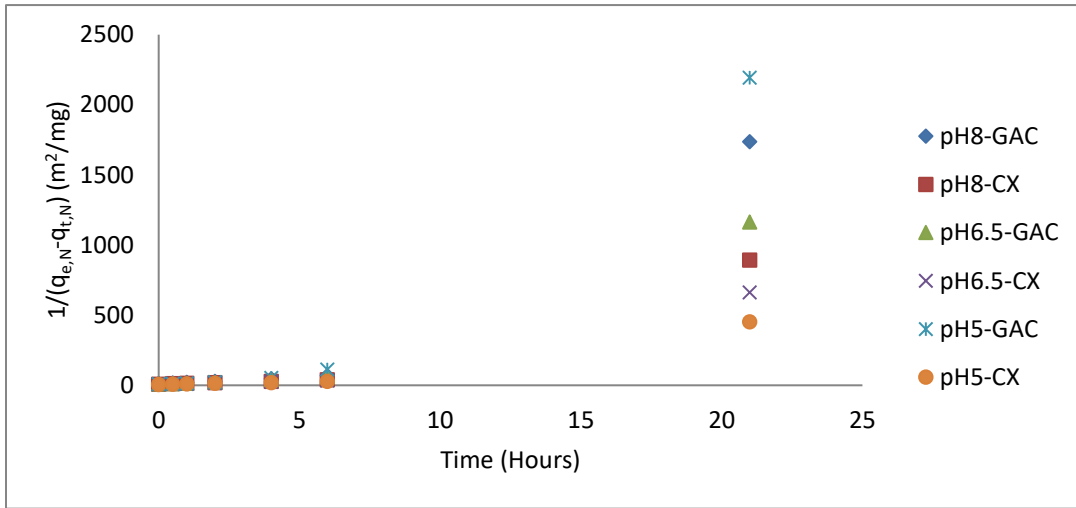


Figure 4.16 Linear PSO model of the adsorption of HPA onto GAC or CX at pH 8, 6.5, or 5

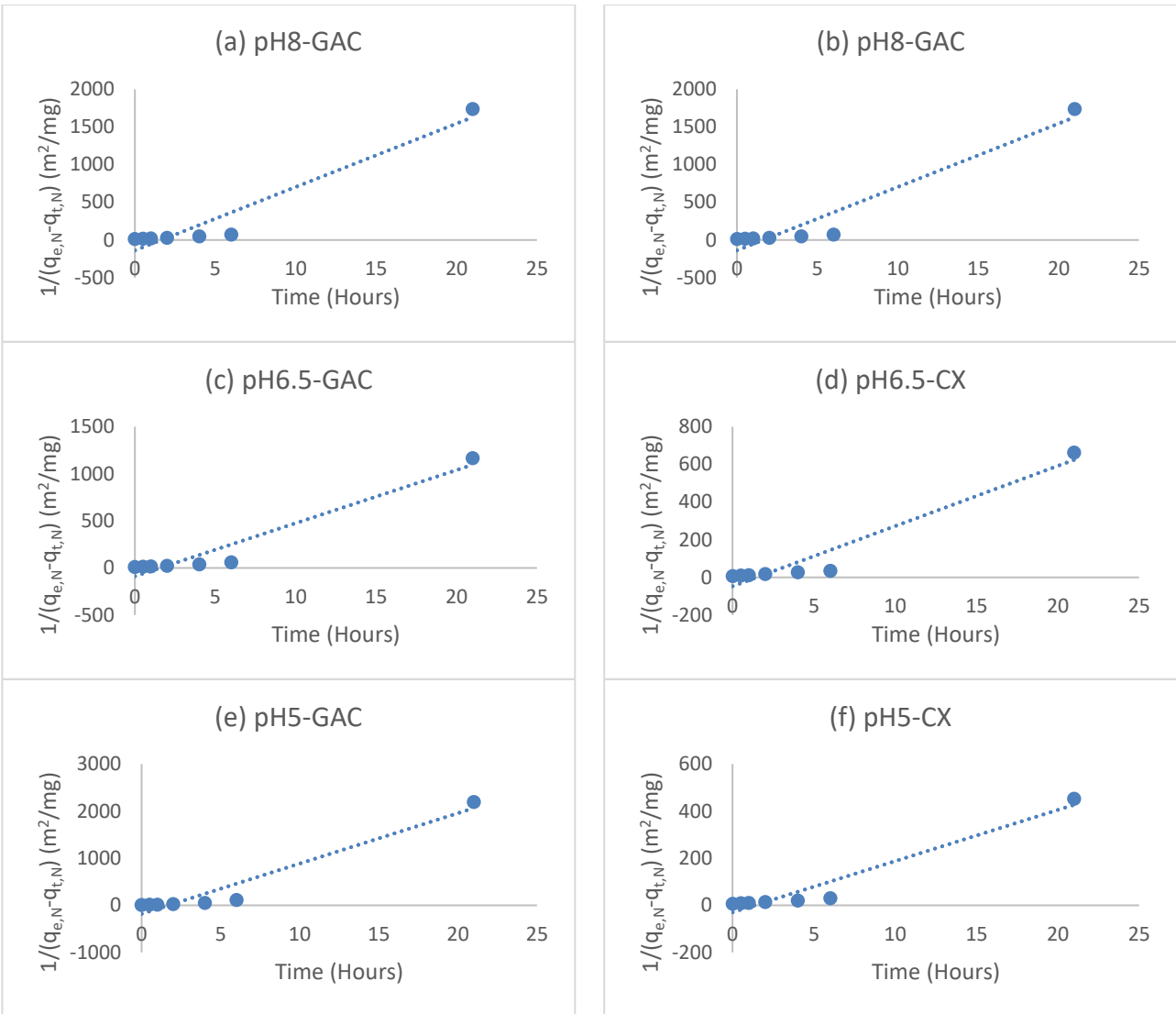


Figure 4.17 Linear PSO model of HPA (a) onto GAC at pH 8, (b) onto CX pH at 8, (c) onto GAC at pH 6.5, (d) onto CX at pH 6.5, (e) onto GAC at pH 5, and (f) onto CX at pH 5

Table 4.10 PSO rate constants of HPA onto GAC and CX at pH 8, 6.5, and 5

Reaction (HPA)	$k_{II}$ (m <sup>2</sup> /mg/hr)	R <sup>2</sup>	Intercept	q <sub>e-eqn</sub> (mg/m <sup>2</sup> )	q <sub>e-actual</sub> (mg/m <sup>2</sup> )	% Error
pH8-GAC	84.19	0.9342	-138.62	-0.00721	0.074152	109.7287
pH8-CX	43.183	0.9347	-67.702	-0.01477	0.112769	113.0981
pH6.5-GAC	56.379	0.9392	-88.102	-0.01135	0.091434	112.4138
pH6.5-CX	31.943	0.9394	-47.315	-0.02113	0.136318	115.5042
pH5-GAC	106.92	0.9401	-181.51	-0.00551	0.099743	105.5235
pH5-CX	21.732	0.9424	-29.54	-0.03385	0.145045	123.3392

Finally, the rates of HPA adsorption onto the surface of CX and GAC followed the PFO model most closely. This is apparent due to less error (average error of 21%) as a result of the estimation of the equilibrium amount of HPA adsorbed on the surface compared to higher error (all above 100%) present in the PSO model, also since HPA adsorption can be assumed to occur by physisorption and the PSO model is most suited for chemisorption.

In general, Figures 4.14 and 4.15 and Table 4.9 indicate that the PFO rates of HPA adsorption were higher onto GAC compared to adsorption onto CX, contrary to many of the earlier observations. Furthermore, the HPA PFO rate constants show a trend of faster adsorption onto GAC at pH 5, 8, and 6.5, with rate constants of 0.2529, 0.2243, and 0.2168  $\text{hr}^{-1}$  respectively. On the other hand, the PFO rate constants of HPA onto CX were faster for pH 8, 6.5, and 5, with constants of 0.2108, 0.2052, and 0.1923  $\text{hr}^{-1}$  respectively. These observations do not show a clear trend in the role of attractive forces on the rate of adsorption of HPA onto either adsorbent, however it can be noted that the charge of the surface has a greater impact on GAC than it does on CX, where higher adsorption rates were noted at pH 8 which exhibits repulsive forces and the slowest rate of adsorption onto CX was observed at pH 5 which promotes attraction.

### 4.3 Discussion of Results

#### 4.3.1 The Effect of NA Structure on its Adsorption by CX and GAC

To begin with, the structure-activity relationship between the NA model compounds and the CX surface along with the GAC surface are postulated to identify the probable mechanisms of adsorption. This is done by comparing that adsorption of HPA, CHPA, and PVA onto CX and GAC to clarify the role of a long chain, cyclic ring, and aromatic ring in promoting the adsorption of NAs, all of which contain a carboxylic acid. As mentioned in section 2.1.5, some correlations have been made between chemical structure and its ability to be removed from water based on factors such as; molecular weight, carbon number, double bond equivalency, hydrogen deficiency, and partition coefficients. The experiments conducted at pH 8 were conducted to pinpoint the effect of these factors on the removal of NAs by CX or GAC, which at this pH experience a negative charge, and thus the effect of electrostatic forces that may contribute to adsorption may be overlooked.

All in all, the role of compound structure on the adsorption of NAs generally follows that unsaturated compounds with pi bonds represented through DBE and hydrogen deficiency are

removed more easily from a solution and adsorbed effectively onto CX and GAC. This trend is clear for the performance of GAC in which GAC removes a greater amount of NA compounds with higher DBE and -Z as seen in Figure 4.1 and Table 4.1. Similarly, this trend is noticed during diffusion in which higher rates of diffusion appeared in the same trend as illustrated in Figure 4.6 and Table 4.3. From Figure 4.3, it has been demonstrated that the role of hydrophobicity is more apparent in terms of normalized adsorption capacity in which the GAC surface generally adsorbs a greater amount of the more hydrophobic (higher  $K_{OW}$ ) NA compound.

On the other hand, CX adsorption of the model NAs did not follow a clear trend in terms of structure. In general, PVA was removed more from the solution (Figure 4.1 and Table 4.1), adsorbed more onto the CX surface (Figure 4.3), diffused faster into the pores (Figure 4.6 and Table 4.3), and was finally adsorbed at a faster rate, followed by HPA, then CHPA (Figures 4.10 and 4.11, and Table 4.7). This identifies an apparent trend in which the aromatic ring present in PVA enables the compound to be easily removed from the solution and adsorbed more easily onto CX. Given that CX exhibits a graphite-like structure, the notably high removal of PVA by CX can be noted as a result of  $\pi$ - $\pi$  bonds between the CX surface and the aromatic ring of PVA. This is similar to earlier studies confirming that  $\pi$ - $\pi$  bonds are responsible for the adsorption of NAs with double bonds and aromatic rings onto PC (Pourrezaei et al. 2014a). Furthermore, the higher adsorption of HPA, which is contrary to its DBE, -Z, and  $K_{OW}$  ranking relative to the other model NAs, shows that the structure of HPA may be considered surfactant-like in which the long chain is hydrophobic while the carboxylic acid is hydrophilic (Solomons et al. 2011). The ability of HPA to act as a surfactant and the dipole-dipole forces that promote its interactions with CX, as discussed in the next section, allow for higher adsorption onto CX. Finally, the results show that the cyclic ring present in CHPA forces it to be more soluble than the others although this contrary to the defined hydrophobic parameter,  $K_{OW}$ . The hindered adsorption of CHPA onto CX can be attributed primarily to two assumptions. Firstly, given that the molecular weight of CHPA, 184.3 g/mol (Table 3.2), is the highest among the three model compounds, it can be assumed that CHPA was the heavier compound and thus adsorbed at a slower rate. This is verified by the PFO rate of adsorption of CHPA onto CX,  $0.1262 \text{ hr}^{-1}$ , which is the lowest among all PFO rate constants as seen in Figure 4.10 and confirmed by Faust and Aly (1987) whom recognized that heavier adsorbates are adsorbed at a slower rate (refer to section 2.1.5). Also, the polarizability of CHPA as seen in Table 3.2,  $20.8 \pm 0.5 \cdot 10^{-24} \text{ cm}^3$ , is also the highest among the three model compounds.

Although polarizability more directly correlates to the ability of a compound to form dipoles, since the polarity of the model NAs of interest have not been previously reported, it can be assumed that this high polarizability indicates that CHPA is highly polar among the three. Following Crittenden, J.'s (2012) proposition that more polar compounds are more hydrophilic and not easily removed, it can be assumed that the polarizability of CHPA contributed to its poor adsorption onto CX (refer to section 2.1.5).

With these correlations in mind, it should be noted that hydrophobic interactions play an apparent role in the diffusion of the model NAs into the film surrounding the surface of CX (Figure 4.6 and Table 4.4). This is due to a clear trend of faster film diffusion rates for model NAs with higher  $K_{OW}$  values and likewise the same trend observed for the constant value of the internal diffusion model which denotes the significance of the boundary layer surrounding the CX surface. This observation demonstrates that hydrophobic-hydrophobic interactions are present and significant between the model NA compound and the CX at the stagnant film surrounding the surface. Given that the CX surface is comparable to graphite, as mentioned earlier, the identification of hydrophobic interactions can be correlated to earlier studies by Moustafa et al. (2014) that recognized the adsorption of NAs onto graphite occurred by -CAHB. Moustafa confirmed hydrophobic interactions between NAs and graphite by recognizing that a small amount of oxygen groups on the surface of graphite resulted in a hydrophobic surface. Likewise, the surface of CX can be assumed to be highly hydrophobic given its low oxygen content, as mentioned in section 2.3.1, and given that it was not activated upon preparation (Álvarez et al. 2015). With hydrophobic-hydrophobic interactions recognized, Moustafa noted that deprotonation of C-OH and COOH groups on the graphite surface in aqueous alkaline solutions promotes hydrogen bonding with NAs. Similarly, the characterization studies of Álvarez identified the presence of C=O moieties on CX in addition to surface hydroxylic groups which both promote strong hydrogen bonds. Therefore, given that the experiments were conducted at pH 8, the hydrophobic-hydrophobic interactions resulted in hydrogen bonding of the NAs to the CX surface similar to hydrogen bonding noted for NA adsorption onto graphite. Moreover, Moustafa also noted that the negatively charged carboxylic groups of NAs and the negative charge on the graphite surface due to the presence of carboxyl and phenol groups contributed to the -CAHB. In a similar manner, the carboxylic groups and ion-radical structures on CX result in a negatively charged

surface at pH 8, confirmed by the  $pH_{PZC}$ , additionally resulting in -CAHB being the form of hydrophobic interactions between NAs and CX.

Overall, as mentioned in section 2.1.4, hydrophobic interactions are among the strongest forces of adsorption. Consequently, given that they are predominant during film diffusion which is considered one of the crucial steps of adsorption, it can be proposed that hydrophobic forces in the form of -CAHB along with the mesoporousity of the CX surface can be attributed to the exceptional performance of CX relative to GAC.

#### 4.3.2 The Effect of pH on HPA Adsorption by CX and GAC

Furthermore, the second set of results correlate to the adsorption of HPA onto CX and GAC at three different experimental pHs. HPA in particular was selected for investigation as it is assumed to be the most hydrophilic (based on  $K_{OW}$ ) among the three model NA compounds under investigation. Accordingly, the role of hydrophobic-hydrophobic interactions can be overlooked and electrostatic interactions can be examined in focus. To detect electrostatic interactions, experiments were performed at pH 8, 6.5, and 5. Given that the  $pH_{PZC}$  of CX is approximately 6.8, conducting experiments at the listed pHs result in a negative, neutral, and positive charge on the CX surface respectively. Since NAs are negatively charged, this would result in repulsion, neutral, and attraction forces between HPA and the CX surface during adsorption. Since the surface of CX was not activated during the preparation, the  $pH_{PZC}$  of CX is similar to that of GAC, approximately 6.2, given that they are both carbonaceous material (Dai 1994). Thus, the same electrostatic forces should be apparent during the various experiments with GAC as well. All in all, intermolecular forces in the form of van der Waals attractive forces are responsible for the adsorption of the NAs onto both CX and GAC (Crittenden, J. 2012).

Altogether, the results of HPA removal from the solution (Figure and Table 4.2), normalized amount of HPA adsorbed onto the surface (Figure 4.4), the role of diffusion (Figures 4.8), and rate of adsorption onto GAC (Figure 4.14) all show a consistent trend of higher or faster adsorption at lower pHs confirming the role of electrostatic forces in the adsorption of HPA onto GAC. Given that the charge of the GAC surface has an effect on the adsorption of HPA, it can be assumed that London dispersion interactions are the main type of forces responsible for HPA adsorption onto GAC (Crittenden, J. 2012).

In contrast, the effect of pH on the adsorption of HPA onto CX did not show a clear, consistent, trend in terms of electrostatic interactions. In general, the amount of HPA adsorbed onto CX did increase as the pH decreased, not overwhelmingly due to attractive forces, but mainly as a result of impeding the repulsive forces present at pH 8. This is demonstrated in the results of the normalized adsorption onto CX in Figure 4.4 and the relation between pH and amount adsorbed in Figure 4.5, all of which confirm that although the performance of CX at pH 5 is higher than that at pH 6.5 by approximately 6.4%, the performance is not significantly different compared to the difference between the performance at pH 8 relative to that of pH 6.5, 20.8%. These results indicate that electrostatic attractive forces do play an important role in the adsorption of HPA but is not as critical as other forces of attraction. This is further confirmed by the rates of diffusion quantified in Figures 4.8 and 4.9, in which both the overall and pore rate of diffusion do increase when attractive electrostatic forces are present. However, the film diffusion rates (Figure 4.9) in particular again demonstrated that while the rate of film diffusion at pH 5 and 6.5 are much higher than that of pH 8, they are relatively closer to each other. This observation can be related to the fact that constant value determined in Table 4.5 corresponding to the overall rate of diffusion is highest at pH 6.5, indicating that the boundary layer formed at this pH does have a significant impact compared to the films formed at pH 5 during attraction and at pH 8 when repulsion occurs. Similarly, the rate of adsorption of HPA onto CX demonstrated that adsorption was slower as the pH decreased, thus attractive forces delayed adsorption (Figures 4.14 and 4.15).

Given that adsorption is promoted at pH 6.5 where electrostatic attraction is not dominant due to an uncharged surface, it can be proposed that the adsorption of HPA onto CX mainly occurs through dipole-dipole interactions and these forces mainly occur at the stagnant film since their direct effect are apparent in the film diffusion rate constant. Furthermore, as identified in the previous section, the surfactant-like structure along with van der Waals forces of attraction, in the form of dipole-dipole bonds, the mesoporous structure of CX, and the -CAHB promote the adsorption of HPA onto CX. However, given that the adsorption of HPA onto GAC is attributed to its hydrogen deficiency and weaker dispersion forces, and taking into account the microporosity of GAC, it has been reasoned that the adsorption of HPA onto GAC is less than that of CX.

## Chapter 5 Conclusions & Recommendations

Nonetheless, with the pronounced demand in oil and gas production from unconventional resources, a substantial rise in processed wastewater continues to escalate, all of which containing contaminants of emerging concern. Of local focus, the Alberta oil sands production continues to contribute to, not only the stress on fresh water sources, but also the raising concern of contamination in the Athabasca river and an overall ecological imbalance in Northern Alberta. The removal of NAs, the main contributor to toxicity in OSPW, has been extensively studied by a wide variety of treatment technologies for the reclamation of OSPW. More specifically, adsorption processes have been examined by a range of adsorbents such as AC, PC, and graphite, all of which have been designed to treat NAs in their original forms, modified, or in combination with other treatment methods to employ synergistic effects. As seen, commonly used adsorbents for the removal of NAs are derived from carbonaceous materials that originate from raw materials. Given that these adsorbents tend to come from raw materials, their textural properties are assumed fixed which consequently limits their performance and ability to be optimum adsorbents. For this reason, novel approaches explored the use of synthesized carbonaceous materials, such as CX, which can be prepared under specific pH conditions to obtain a desired mesoporous structure. Accordingly, well-focussed studies that examine the ability of CX to adsorb NAs can contribute to designing the optimum adsorption process that can treat OSPW from NAs.

Given that CX is a relatively innovative material, rather than immediately examining the performance of CX in OSPW, introductory studies exploring the mechanisms responsible for the adsorption of NAs onto CX were conducted. The presented study has examined the performance of CX in terms of the adsorption of specific model NAs individually. More precisely, the model NAs investigated; HPA, CHPA, and PVA, were similar in structure yet varied in terms of whether a cyclic ring existed and if the ring contained additional double bonds. As a result, this difference in structure provided insight on the effect of structure on adsorption onto CX. In comparison to the performance of GAC, under the same conditions, the performance of CX in terms of the removal of model NAs has demonstrated that CX has a promising potential to become a feasible adsorbent for the removal of NAs from OSPW through adsorption. CX has shown to accomplish more removal of NAs compared to GAC at faster rates confirming its effectiveness and exceptional performance although its surface area is smaller, yet mainly due to its extended mesoporous surface, hydrophobic bonding, and stronger dipole-dipole forces. Moreover, the present study has

demonstrated that the NAs of interest have adsorbed onto CX based on structure in which more complex NAs are considered easier to adsorb, yet not in a consistent trend. In a clear manner, the most complex structure, PVA, which consisted of a carboxylic acid, long chain, and aromatic ring, was removed more easily by CX. Afterwards, HPA, the simpler among the three, was removed, most probably due to its ability to act as a surfactant more effectively. Furthermore, CHPA, the intermediate structure with a carboxylic acid, cyclic ring, and long chain, was adsorbed the least by CX. This was assumed due to its slower adsorption rate as a result of being the heaviest among the three. Of note, hydrophobic-hydrophobic interactions, which may be attributed to -CAHB, between the model NAs of interest and CX were shown to be present at the stagnant film surrounding the surface of CX which are confirmed by faster diffusion into the film of CX of the more hydrophobic compounds. More specifically, HPA which exhibits the simplest structure among the three and considered more hydrophilic based on its low  $K_{OW}$  value has demonstrated that it is adsorbed onto CX through electrostatic forces, mainly dipole-dipole attractions. In comparison to CX, GAC has shown to adsorb a smaller amount of the model NAs relative to its surface area given its microporous structure.

To further confirm the viability of CX, additional research should be conducted to characterize the surface of CX to visualize the interactions between NAs and CX and elucidate the mechanisms by which NAs in OSPW can be adsorbed onto CX. Furthermore, the performance of CX in OSPW should be examined to understand the ability of CX to remove actual NAs, which may differ from model NAs, while accounting for competitive adsorption and the complexity of OSPW's NAs. By doing so, a comprehensive study on CX can assist in developing the ideal synthesis conditions that will prepare the optimum CX adsorbent for effective removal of NAs from OSPW. Likewise, these studies can be extended to adsorption processes used to treat other unconventional oil processed water such as flowback water from shale and gas oils. Accordingly, the results established can be applied to other conditions in which CX material can be synthesized and utilized to tailor the properties of contaminants in shale flowback water.

## References

- Ahad, J.M.E., and Pakdel, H. 2013. Direct evaluation of in situ biodegradation in Athabasca oil sands tailings ponds using natural abundance radiocarbon. *Environmental Science and Technology*, **47**: 10214-10222.
- Allen, E. 2008. Process water treatment in Canada's oil sands industry: I. Target pollutants and treatment objectives. *Journal of Environmental Engineering and Science*, **7**(2): 123–138.
- Álvar, S., Ribeiro, R. S. Gomes, H. T., Sotelo, J. L. and García, J. 2015. Synthesis of carbon xerogels and their application in adsorption studies of caffeine and diclofenac as emerging contaminants. *Chemical Engineering Research & Design: Transactions of the Institution of Chemical Engineers*, **95** (Part A): 229-238.
- Anderson, J.C., Wiseman, S.B., Wang, N., Moustafa, A., Perez-Estrada, L., Gamal El-Din, M., Martin, J.W., Liber, K., and Giesy, J.P., 2012. Effectiveness of ozonation treatment in eliminating toxicity of oil sands process-affected water to *Chironomus dilutus*. *Environmental Science and Technology*, **46** (1): 486-493.
- Barrow, M. P., Witt, M., Headley, J. V., and Peru, K. M. 2010. Athabasca oil sands process water: Characterization by atmospheric pressure photoionization and electrospray ionization fourier transform ion cyclotron resonance mass spectrometry. *Analytical Chemistry*, **82** (9): 3727-3735.
- Bauer, A. E., Frank, R. A., Headley, J. V., Peru, K. M., Hewitt, L. M., and Dixon, D. G. 2015. Enhanced characterization of oil sands acid-extractable organics fractions using electrospray ionization–high-resolution mass spectrometry and synchronous fluorescence spectroscopy. *Environmental Toxicology and Chemistry*, **34** (5): 1001-1008.
- Bowman, D. T., Slater, G. F., Warren, L. A., and McCarry, B. E. 2014. Identification of individual thiophene-, indane-, tetralin-, cyclohexane-, and adamantane-type carboxylic acids in composite tailings pore water from Alberta oil sands. *Rapid Communications in Mass Spectrometry*, **28** (19): 2075-2083.
- Calistry. 2017. Double Bond Equivalent (DBE)/ Level of Unsaturation Calculator [online]. Available from <http://calistry.org/calculate/DBEcalculator> [cited 13 October 2016].
- Carabineiro, S.A.C, Thavorn-amornsri, T., Pereira, M.F.R, Serp, P., and Figueiredo, J.L. 2011. Comparison between activated carbon, carbon xerogel and carbon nanotubes for the adsorption of the antibiotic ciprofloxacin. *Catalysis Today*, **186** (2012): 29-34.

- Chakravarti, R., Patrick, B.N., Barney, M., Kusinski, G., and Devine, T.M. 2013. Toward the mechanism of corrosion in crude oil: a study using vibrational spectroscopic techniques at elevated temperatures. *Energy Fuels*, **27**: 7905–7914.
- ChemAxon. 2017. LogD Predictor [online]. Available from <https://disco.chemaxon.com/apps/demos/logd/> [cited 21 December 2016].
- ChemSpider. 2017. 5-Cyclohexylpentanoic acid [online]. Available from <http://www.chemspider.com/Chemical-Structure.85505.html?rid=e1ec9fbf-1414-4b43-901b-3a475519b35a> [cited 16 March 2017].
- ChemSpider. 2017. 5-Phenylvaleric acid [online]. Available from <http://www.chemspider.com/Chemical-Structure.15886.html?rid=5d14f09f-2b6a-494f-9939-e3a59a915bdb> [cited 16 March 2017].
- ChemSpider. 2017. n-heptanoic acid [online]. Available from <http://www.chemspider.com/Chemical-Structure.7803.html?rid=2bbdb5ad-54a5-4734-ab53-7f59f60233b8> [cited 16 March 2017].
- Cheung, W., Szeto, Y., and McKay, G. 2007. Intraparticle diffusion processes during acid dye adsorption onto chitosan. *Bioresource Technology*, **98**(15): 2897-2904.
- Clemente, J.S., and Fedorak, P.M. 2005. A review of the occurrence, analyses, toxicity, and biodegradation of naphthenic acids. *Chemosphere*, **60**: 585–600.
- Crittenden, J.C. 2012. *MWH's Water Treatment: Principles and Design*. 3<sup>rd</sup> Edition. John Wiley and Sons, Hoboken, N.J.
- Dai, M. 1994. The Effect of Zeta Potential of Activated Carbon on the Adsorption of Dyes from Aqueous Solution. *Journal of Colloid and Interface Science*, **164**: 223-228.
- DeAngelis, K.M. 2007. Preparation of 0.1 m Potassium Phosphate Buffer at 25°C [online]. Available from [http://cshprotocols.cshlp.org/content/2006/1/pdb.rec8543.full?text\\_only=true](http://cshprotocols.cshlp.org/content/2006/1/pdb.rec8543.full?text_only=true) [cited 26 October 2016].
- Fan, T.P. 1991. Characterization of naphthenic acids in petroleum by fast atom bombardment mass spectrometry. *Energy Fuels*, **5**: 371–375.
- Faust, S. D., and Aly, O. M. 1987. *Adsorption processes for water treatment*. Elsevier, Boston: Butterworth.

- Figueiredo, J. L., Sousa, J. P. S., Orge, C. A., Pereira, M. F. R., and Órfão, J. J. M. 2010. Adsorption of dyes on carbon xerogels and templated carbons: influence of surface chemistry. *Adsorption*, **17**(3): 431-441.
- Frank, R.A., Fischer, K., Kavanagh, R., Burnison, B.K., Arsenault, G., Headley, J.V., Peru, K.M., Van Der Kraak, G., and Solomon, K.R. 2009. Effect of carboxylic acid content on the acute toxicity of oil sands naphthenic acids. *Environmental Science and Technology*, **43**: 266–271.
- Gamal El-Din, M., Fu, H., Wang, N., Chelme-Ayala, P., Perez-Estrada, L., Drzewicz, P., and Smith, D. W. 2011. Naphthenic acids speciation and removal during petroleum-coke adsorption and ozonation of oil sands process-affected water. *Science of the Total Environment*, **409**(23): 5119-5125.
- Gregory, K. B., Vidic, R. D., and Dzombak, D. A. 2011. Water management challenges associated with the production of shale gas by hydraulic fracturing. *Elements*, **7**(3): 181-186.
- Grever, D.M., Young, R.F., Whittal, R.M., and Fedorak, P.M. 2010. Naphthenic acids and other acid-extractables in water samples from Alberta: What is being measured. *Science of the Total Environment*, **408**: 5997-6010.
- Hagen, M.O., Katzenback, B.A., Islam, M.S., Gamal El-Din, M., and Belosevic, M. 2014. The analysis of Goldfish (*Carassius auratus* L.) innate immune responses after acute and subchronic exposures to oil sands process-affected water. *Toxicological Sciences*, **138** (1): 59-68.
- Headley, J. V., Peru, K. M., Mohamed, M. H., Wilson, L., McMartin, D. W., Mapolelo, M. M., Lobodin, V. V., Rodgers, R. P., and Marshall, A. G. 2013. Atmospheric pressure photoionization fourier transform ion cyclotron resonance mass spectrometry characterization of tunable carbohydrate-based materials for sorption of oil sands naphthenic acids. *Energy and Fuels*, **28** (3): 1611-1616.
- Headley, J.V., Peru, K. M., Fahlman, B., Colodey, A., and McMartin, D. W. 2013. Selective solvent extraction and characterization of the acid extractable fraction of Athabasca oils sands process waters by orbitrap mass spectrometry. *International Journal of Mass Spectrometry*, **345**: 104-108.
- Ho, Y. S., and McKay, G. 1998. A comparison of chemisorption kinetic models applied to pollutant removal on various sorbents. *Process Safety and Environmental Protection*, **76**(4):332-340.

- Huang, R., Changelov, M., Sun, N., Chelme-Ayala, P., McPhedran, K.N., and Gamal El-Din, M. 2015. Fractionation of Oil sands-process affected water using pH-dependent extractions: A study of dissociation constants for naphthenic acids species. *Chemosphere*, **127**: 291-296.
- Hughes, J. D. 2013. Energy: A reality check on the shale revolution. *Nature*, **494** (7437): 307-308.
- Iranmanesh, S., Harding, T., Abedi, J., Seyedeyn-Azad, F., and Layzell, D. B. 2014. Adsorption of naphthenic acids on high surface area activated carbons. *Journal of Environmental Science and Health, Part A: Toxic/Hazardous Substances and Environmental Engineering*, **49**(8): 913-922.
- Islam, M. S., Dong, T., McPhedran, K. N., Sheng, Z., Zhang, Y., Liu, Y., and Gamal El-Din, M. 2014. Impact of ozonation pre-treatment of oil sands process-affected water on the operational performance of a GAC-fluidized bed biofilm reactor. *Biodegradation*, **25**(6): 811-823.
- Islam, M., Zhang, Y., McPhedran, K. N., Liu, Y., and Gamal El-Din, M. 2015a. Granular activated carbon for simultaneous adsorption and biodegradation of toxic oil sands process-affected water organic compounds. *Journal of Environmental Management*, **152**: 49-57.
- Islam, M.S., Zhang Y., McPhedran, K.M., Liu, Y., and Gamal El-Din, M. 2015b. Mechanistic investigation of industrial wastewater naphthenic acids removal using granular activated carbon (GAC) biofilm based process. *Science of the Total Environment*, **541**: 238-246.
- Janfada, A., Headley, J.V., Peru, K.M., and Barbour, S.L. 2007. A laboratory evaluation of the sorption of oil sands naphthenic acids on organic rich soils. *Journal of Environmental Science and Health, Part A*, **41**(6): 985-997.
- Job, N., Heinrichs, B., Ferauche, F., Noville, F., Marien, J., and Pirard, J. P. 2005. Hydrodechlorination of 1, 2-dichloroethane on Pd–Ag catalysts supported on tailored texture carbon xerogels. *Catalysis Today*, **102**: 234-241.
- Job, N., Pirard, R., Marien, J., and Pirard, J. P. 2004. Porous carbon xerogels with texture tailored by pH control during sol–gel process. *Carbon*, **42**(3): 619-628.
- Kavanagh, R.J., Frank, R.A., Burnison, B.K., Young, R.F., Fedorak, P.M., Solomon, K.R., and Van Der Kraak, G. 2012. Fathead minnow (*Pimephales promelas*) reproduction is impaired when exposed to a naphthenic acid extract. *Aquatic Toxicology*, **116–117**: 34–42.
- Lagergren, S. 1898. About the Theory of So-Called Adsorption of Soluble Substances. *Kungliga Svenska Vetenskapsakademiens Handlingar*, **24**:1-39.

- Largitte, L., and Pasquier, R. 2016. A review of the kinetics adsorption models and their application to the adsorption of lead by an activated carbon. *Chemical Engineering Research and Design*, **109**: 495-504.
- Lester, Y., Ferrer, I., Thurman, E.M., Sitterley, K.A., Korak, J., A., Aiken, G., and Linden, K. G. 2015. Characterization of hydraulic fracturing flowback water in Colorado: Implication for water treatment. *Science of the Total Environment*, **512–513** (2015): 637–644.
- Leung, S.S., MacKinnon, M.D., and Smith, R.E.H. 2001. Aquatic reclamation in the Athabasca, Canada, oil sands: naphthenates and salt effects on phytoplankton communities. *Environmental Toxicology and Chemistry*, **20**: 1532–1543.
- Lin, C., and Ritter, J.A. 1997. Effect of synthesis pH on the structure of carbon xerogels. *Carbon*, **35**(9): 1271-1278.
- MacKinnon, M.D., and Boerger, H. 1986. Description of two treatment methods for detoxifying oil sands process water. *Water Pollution Research Journal of Canada*, **21**: 496–512.
- Mahata N., Silva, A.R., Pereira, M.F.R., Freire, C., Castro, B. de, and Figueiredo, J.L. 2007. Anchoring of a [Mn(*salen*)Cl] complex onto mesoporous carbon xerogels. *Journal of Colloid and Interface Science*, **311**(2007): 152-158.
- Maitland, G.C., Rigby, M., Smith, E.B., and Wakeham, W.A. 1981. *Intermolecular Forces- their origin and determination*. OxfordUniversity Press, Oxford.
- Metcalf and Eddy. 2014. *Wastewater Engineering: Treatment and Reuse*, 4th Edition. McGraw-Hill, New York, N.Y.
- Mohamed, M.H., Wilson, L.D., Shah, J.R., Bailey, J., Peru, K.M., and Headley, J.V. 2015. A novel solid-state fractionation of naphthenic acid fraction component from oil sands process-affected water. *Chemosphere*, **136**: 252-258.
- Moustafa, A. M. A., Huang, J., McPhedran, K. N., Zeng, H., and El-Din, M.G. 2015. Probing the adsorption of weak acids on graphite using amplitude modulation-frequency modulation atomic force microscopy. *Langmuir*, **31**(10): 3069–3075.
- Moustafa, A. M. A., McPhedran, K. N., Moreira, J., and El-Din, M.G. 2014. Investigation of mono/competitive adsorption of environmentally relevant ionized weak acids on graphite: Impact of molecular properties and thermodynamics. *Environmental Science and Technology*, **48**(24): 14472-14480.

- National Center for Biotechnology Information. n.d. PubChem Compound Database; CID=8094 [online]. Available from: <https://pubchem.ncbi.nlm.nih.gov/compound/8094> [cited 9 February 2017].
- Nethaji, S., Sivasamy, A., and Mandal, A. B. 2013. Adsorption isotherms, kinetics and mechanism for the adsorption of cationic and anionic dyes onto carbonaceous particles prepared from *Juglans regia* shell biomass. *International Journal of Environmental Science and Technology*, **10**(2):231-242.
- Pekala, R.W. 1989. Organic aerogels from the polycondensation of resorcinol with formaldehyde. *Journal of Material Science*, **24**: 3221-3227.
- Pereira, A.S., Bhattacharjee, S., and Martin, J.W. 2013. Characterization of oil sands process-affected waters by liquid chromatography orbitrap mass spectrometry. *Environmental Science and Technology*, **47**: 5504-5513.
- Pereira, A.S., Islam, M.S., Gamal El-Din, and M., Martin, J.W. 2013. Ozonation degrades all detectable organic compound classes in oil sands process-affected water; an application of high-performance liquid chromatography/orbitrap mass spectrometry. *Rapid Communications in Mass Spectrometry*, **27** (21): 2317-2326.
- Pourrezaei, P., Alpatova, A., Chelme-Ayala, P., Perez-Estrada, L. A., Jensen-Fontaine, M., Le, X. C., and El-Din, M. G. 2014a. Impact of petroleum coke characteristics on the adsorption of the organic fractions from oil sands process-affected water. *International Journal of Environmental Science and Technology*, **11**(7): 20-37.
- Pourrezaei, P., Alpatova, A., Khosravi, K., Drzewicz, P., Chen, Y., Chelme-Ayala, P., and Gamal El-Din, M. 2014b. Removal of organic compounds and trace metals from oil sands process-affected water Using zero valent iron enhanced by petroleum coke. *Journal of Environmental Management*, **139**: 50-58.
- Qiu, H., Lv, L., Pan, B. C., Zhang, Q. J., Zhang, W. M., and Zhang, Q. X. 2009. Critical review in adsorption kinetic models. *Journal of Zhejiang University-Science A*, **10**(5): 716-724.
- Quinlan, P. J., and Tam, K. C. 2015. Water treatment technologies for the remediation of naphthenic acids in oil sands process-affected water. *Chemical Engineering Journal*, **279**: 696-714.
- Rogers, V.V., Liber, K., and MacKinnon, M.D. 2002. Isolation and characterization of naphthenic acids from Athabasca oil sands tailings pond water. *Chemosphere*, **48**: 519-527.

- Rowland, S.J., Scarlett, A.G., Jones, D., West, C.E., and Frank, R.A. 2011. Diamonds in the rough: Identification of individual naphthenic acids in oil sands process water. *Environmental Science and Technology*, **45**: 3154-3159.
- Samant, P.V., Pereira, M.F.R., and Figueiredo, J.L. 2005. Mesoporous carbon supported Pt and Pt-Sn catalysts for hydrogenation of cinnamaldehyde. *Catalysis Today*, **102-103**:183-188.
- Sanford, E.C. 1983 Processability of Athabasca oil sand: interrelationship between oil sand fine solid, process aids, mechanical energy, and oil sand age after mining. *Canadian Journal of Chemical Engineering*, **61**: 554–567.
- Schindler, D.W., and Donahue, W.F. 2006. An impending water crisis in Canada's western prairie provinces. *Proceedings of the National Academy of Sciences*, **103**: 7210–7216.
- Schramm, L.L., Stasiuk, E.N., and MacKinnon, M.D. 2000. Surfactants in the Athabasca Oil Sands Slurry Conditioning, Flotation Recovery, and Tailings Processes, in: *Surfactants: Fundamentals and Applications in the Petroleum Industry*. Cambridge University Press, Cambridge.
- Scott, A.C., Zubot, W., Mackinnon, M. D., Smith, D.W, and Fedorak. P.M. 2008. *Ozonation of oil sands process water removes naphthenic acids and toxicity*. *Chemosphere*, **71**(1): 156-160.
- Solomons, T. W. G., Fryhle, C. B., and Snyder, S. A. 2011. *Organic Chemistry*, 10<sup>th</sup> Edition. John Wiley and Sons, Inc., Hoboken, N.J.
- Thomas, W.J., and Crittenden, B. 1998. *Adsorption Technology and Design*. Elsevier Science and Technology Books.
- Villacañas, F., Pereira, M. F. R., Órfão, J. J., and Figueiredo, J. L. 2006. Adsorption of simple aromatic compounds on activated carbons. *Journal of Colloid and Interface Science*, **293**(1):128-136.
- Wang, B., Wan, Y., Gao, Y., Guomao, Z., Yang, M., Wu, S., and Hu, J. 2015. Occurrences and Behaviors of Naphthenic Acids in a Petroleum Refinery Wastewater Treatment Plant. *Environmental Science and Technology*, **49**: 5796–5804.
- Watson, J.S., Jones, D.M., Swannell, R.P.J., and van Duin, A.C.T. 2002. Formation of carboxylic acids during aerobic biodegradation of crude oil and evidence of microbial oxidation of hopanes. *Organic Geochemistry*, **33**:1153-1169.

- Weber, W. J., and Morris, J. C. 1963. Kinetics of adsorption on carbon from solution. *Journal of the Sanitary Engineering Division*, **89**(2): 31-60.
- Zhang, K., Pereira, A. S., and Martin, J. W. 2015. Estimates of octanol-water partitioning for thousands of dissolved organic species in oil sands process-affected water. *Environmental Science and Technology*, **49** (14): 8907-8913.
- Zubot, W., MacKinnon, M. D., Chelme-Ayala, P., Smith, D. W., and Gamal El-Din, M. 2012. Petroleum coke adsorption as a water management option for oil sands process-affected water. *Science of the Total Environment*, **427-428**: 364-372.

## Appendices

### A.1 K<sub>OW</sub> Coefficients of Model NA Compounds

The K<sub>OW</sub> coefficients obtained from the ChemAxon log D predictor are listed in Table A.13 at different pHs. (ChemAxon 2017)

**Table A.1 K<sub>OW</sub> Coefficients of Model NAs at Different pHs**

Log K <sub>OW</sub>			
pH	HPA	CHPA	PVA
0	2.26	3.41	2.94
1	2.26	3.41	2.94
2	2.26	3.41	2.94
3	2.25	3.41	2.94
4	2.23	3.38	2.90
5	2.02	3.16	2.61
6	1.35	2.46	1.85
7	0.41	1.51	0.90
8	-0.51	0.60	0.01
9	-1.11	0.04	-0.47
10	-1.25	-0.10	-0.57
11	-1.27	-0.12	-0.58
12	-1.27	-0.12	-0.58
13	-1.27	-0.12	-0.58
14	-1.27	-0.12	-0.58

### A.2 Experimental Data

The results of the adsorption kinetics experiments are listed in Tables A.2, A.3, and A.4 for the experiments conducted at pH 8, 6.5, and 5 respectively.

**Table A.2 pH 8 Experiment Results: Concentration 'C' of the HPA, CHPA, & PVA solutions with I. Control, II. GAC, & III. CX**

<b>I. Control (No Adsorbent)</b>									
	<i>HPA</i>			<i>CHPA</i>			<i>PVA</i>		
	<b>1<sup>st</sup> Run</b>	<b>2<sup>nd</sup> Run</b>	<b>Average</b>	<b>1<sup>st</sup> Run</b>	<b>2<sup>nd</sup> Run</b>	<b>Average</b>	<b>1<sup>st</sup> Run</b>	<b>2<sup>nd</sup> Run</b>	<b>Average</b>
<b>Time (Hours)</b>	<b>C (mg/L)</b>	<b>C (mg/L)</b>	<b>C (mg/L)</b>	<b>C (mg/L)</b>	<b>C (mg/L)</b>	<b>C (mg/L)</b>	<b>C (mg/L)</b>	<b>C (mg/L)</b>	<b>C (mg/L)</b>
<b>0</b>	47.898	46.705	47.301	50.375	49.950	50.163	47.070	47.290	47.180
<b>0.5</b>	47.049	47.502	47.276	45.950	43.350	44.650	44.060	47.390	45.725
<b>1</b>	47.332	48.026	47.679	39.200	44.000	41.600	46.620	49.030	47.825
<b>2</b>	47.794	46.481	47.138	40.050	44.500	42.275	46.270	46.900	46.585
<b>4</b>	47.528	47.282	47.405	40.850	46.550	43.700	45.470	47.270	46.370
<b>6</b>	47.572	46.499	47.036	41.550	43.700	42.625	47.290	48.220	47.755
<b>21</b>	47.810	48.295	48.053	40.950	43.500	42.225	46.720	47.710	47.215
<b>24</b>	47.237	48.536	47.887	44.250	44.950	44.600	47.440	47.990	47.715
<b>II. GAC</b>									
	<i>HPA</i>			<i>CHPA</i>			<i>PVA</i>		
	<b>1<sup>st</sup> Run</b>	<b>2<sup>nd</sup> Run</b>	<b>Average</b>	<b>1<sup>st</sup> Run</b>	<b>2<sup>nd</sup> Run</b>	<b>Average</b>	<b>1<sup>st</sup> Run</b>	<b>2<sup>nd</sup> Run</b>	<b>Average</b>
<b>Time (Hours)</b>	<b>C (mg/L)</b>	<b>C (mg/L)</b>	<b>C (mg/L)</b>	<b>C (mg/L)</b>	<b>C (mg/L)</b>	<b>C (mg/L)</b>	<b>C (mg/L)</b>	<b>C (mg/L)</b>	<b>C (mg/L)</b>
<b>0</b>	48.740	47.284	48.012	49.350	49.300	49.325	46.370	46.350	46.360
<b>0.5</b>	40.751	39.441	40.096	32.450	33.300	32.875	37.940	43.030	40.485
<b>1</b>	36.349	33.670	35.010	27.900	30.750	29.325	28.980	32.320	30.650
<b>2</b>	30.388	27.310	28.849	22.100	23.300	22.700	19.700	19.500	19.600
<b>4</b>	23.247	21.162	22.205	17.400	15.650	16.525	9.710	7.880	8.795
<b>6</b>	19.593	17.979	18.786	11.500	10.800	11.150	5.770	3.790	4.780
<b>21</b>	12.061	12.152	12.107	3.000	2.650	2.825	1.890	1.520	1.705
<b>24</b>	11.751	11.900	11.826	2.200	2.350	2.275	1.730	1.200	1.465

III. CX									
	HPA			CHPA			PVA		
	1 <sup>st</sup> Run	2 <sup>nd</sup> Run	Average	1 <sup>st</sup> Run	2 <sup>nd</sup> Run	Average	1 <sup>st</sup> Run	2 <sup>nd</sup> Run	Average
Time (Hours)	C (mg/L)	C (mg/L)	C (mg/L)	C (mg/L)	C (mg/L)	C (mg/L)	C (mg/L)	C (mg/L)	C (mg/L)
0	48.380	48.039	48.209	48.925	48.475	48.700	46.700	47.270	46.985
0.5	39.627	39.893	39.760	35.350	35.850	35.600	37.390	41.520	39.455
1	34.959	36.209	35.584	31.150	29.850	30.500	29.900	33.460	31.680
2	30.512	31.989	31.251	27.950	29.450	28.700	23.690	25.470	24.580
4	25.359	26.445	25.902	25.050	25.800	25.425	17.660	15.790	16.725
6	22.538	23.868	23.203	22.150	23.800	22.975	11.670	11.710	11.690
21	16.175	16.268	16.222	18.850	20.000	19.425	3.570	3.740	3.655
24	15.956	15.846	15.901	15.900	20.200	18.050	3.550	3.450	3.500

Table A.3 pH 6.5 Experiment Results: Concentration of HPA, CHPA, & PVA solutions with I. Control, II. GAC, & III. CX

I. Control (No Adsorbent)									
	HPA			CHPA			PVA		
	1 <sup>st</sup> Run	2 <sup>nd</sup> Run	Average	1 <sup>st</sup> Run	2 <sup>nd</sup> Run	Average	1 <sup>st</sup> Run	2 <sup>nd</sup> Run	Average
Time (Hours)	C (mg/L)	C (mg/L)	C (mg/L)	C (mg/L)	C (mg/L)	C (mg/L)	C (mg/L)	C (mg/L)	C (mg/L)
0	47.802	47.420	47.611	33.100	28.700	30.900	46.200	42.290	44.245
0.5	47.493	49.536	48.515	33.950	43.400	38.675	47.260	35.260	41.260
1	46.52	48.211	47.3655	37.500	48.450	42.975	46.640	34.490	40.565
2	45.911	49.036	47.474	34.900	44.700	39.800	47.100	34.190	40.645
4	47.307	49.365	48.336	33.750	42.950	38.350	48.410	21.970	35.190
6	47.317	49.417	48.367	37.000	42.750	39.875	49.640	36.140	42.890
21	50.353	49.969	50.161	33.450	58.250	45.850	45.600	36.160	40.880
24	49.892	50.831	50.362	34.400	51.300	42.850	47.090	42.270	44.680

<b>II. GAC</b>									
	<i>HPA</i>			<i>CHPA</i>			<i>PVA</i>		
	<b>1<sup>st</sup> Run</b>	<b>2<sup>nd</sup> Run</b>	<b>Average</b>	<b>1<sup>st</sup> Run</b>	<b>2<sup>nd</sup> Run</b>	<b>Average</b>	<b>1<sup>st</sup> Run</b>	<b>2<sup>nd</sup> Run</b>	<b>Average</b>
<b>Time (Hours)</b>	<b>C (mg/L)</b>	<b>C (mg/L)</b>	<b>C (mg/L)</b>	<b>C (mg/L)</b>	<b>C (mg/L)</b>	<b>C (mg/L)</b>	<b>C (mg/L)</b>	<b>C (mg/L)</b>	<b>C (mg/L)</b>
<b>0</b>	52.807	46.989	49.898	31.650	30.500	31.075	46.360	33.040	39.700
<b>0.5</b>	44.781	39.805	42.293	25.950	38.350	32.150	40.870	32.780	36.825
<b>1</b>	36.721	34.252	35.487	18.050	30.850	24.450	28.930	18.180	23.555
<b>2</b>	26.990	26.081	26.536	10.450	21.500	15.975	17.100	9.180	13.140
<b>4</b>	17.374	18.135	17.755	3.800	6.800	5.300	6.330	4.700	5.515
<b>6</b>	12.691	13.774	13.233	2.350	4.700	3.525	2.970	1.370	2.170
<b>21</b>	5.922	5.472	5.697	0.350	1.450	0.900	0.720	0.000	0.360
<b>24</b>	5.734	4.822	5.278	0.400	0.900	0.650	0.380	0.000	0.190
<b>III. CX</b>									
	<i>HPA</i>			<i>CHPA</i>			<i>PVA</i>		
	<b>1<sup>st</sup> Run</b>	<b>2<sup>nd</sup> Run</b>	<b>Average</b>	<b>1<sup>st</sup> Run</b>	<b>2<sup>nd</sup> Run</b>	<b>Average</b>	<b>1<sup>st</sup> Run</b>	<b>2<sup>nd</sup> Run</b>	<b>Average</b>
<b>Time (Hours)</b>	<b>C (mg/L)</b>	<b>C (mg/L)</b>	<b>C (mg/L)</b>	<b>C (mg/L)</b>	<b>C (mg/L)</b>	<b>C (mg/L)</b>	<b>C (mg/L)</b>	<b>C (mg/L)</b>	<b>C (mg/L)</b>
<b>0</b>	46.878	46.523	46.701	38.300	37.550	37.925	45.550	48.200	46.875
<b>0.5</b>	36.437	39.050	37.744	29.150	35.000	32.075	37.470	38.120	37.795
<b>1</b>	31.671	33.609	32.640	42.000	28.550	35.275	30.670	29.320	29.995
<b>2</b>	26.036	21.532	23.784	17.500	21.400	19.450	21.970	18.050	20.010
<b>4</b>	20.769	15.928	18.349	9.900	14.650	12.275	13.000	11.060	12.030
<b>6</b>	17.791	13.615	15.703	8.100	11.550	9.825	8.330	6.960	7.645
<b>21</b>	9.766	6.390	8.078	2.350	3.950	3.150	1.430	1.030	1.230
<b>24</b>	9.492	5.799	7.646	2.100	2.800	2.450	1.260	0.500	0.880

**Table A.4 pH 5 Experiment Results: Concentration of the HPA, CHPA, & PVA solutions with I. Control, II. GAC, & III. CX**

<b>I. Control(No Adsorbent)</b>									
	<i>HPA</i>			<i>CHPA</i>			<i>PVA</i>		
	<b>1<sup>st</sup> Run</b>	<b>2<sup>nd</sup> Run</b>	<b>Average</b>	<b>1<sup>st</sup> Run</b>	<b>2<sup>nd</sup> Run</b>	<b>Average</b>	<b>1<sup>st</sup> Run</b>	<b>2<sup>nd</sup> Run</b>	<b>Average</b>
<b>Time (Hours)</b>	<b>C (mg/L)</b>	<b>C (mg/L)</b>	<b>C (mg/L)</b>	<b>C (mg/L)</b>	<b>C (mg/L)</b>	<b>C (mg/L)</b>	<b>C (mg/L)</b>	<b>C (mg/L)</b>	<b>C (mg/L)</b>
<b>0</b>	39.744	43.117	41.4305	0.000	2.250	1.125	31.630	29.470	30.550
<b>0.5</b>	47.403	44.921	46.162	7.650	0.000	3.825	46.540	24.830	35.685
<b>1</b>	47.181	48.088	47.6345	14.700	1.800	8.250	47.920	22.810	35.365
<b>2</b>	48.264	50.211	49.238	18.350	1.900	10.125	48.690	26.390	37.540
<b>4</b>	47.579	50.476	49.0275	24.250	1.200	12.725	50.250	26.300	38.275
<b>6</b>	47.28	55.165	51.223	27.250	3.250	15.250	49.750	28.060	38.905
<b>21</b>	48.380	54.09	51.235	5.600	2.500	4.050	40.840	24.140	32.490
<b>24</b>	48.829	51.071	49.950	28.950	1.150	15.050	42.080	28.320	35.200
<b>II. GAC</b>									
	<i>HPA</i>			<i>CHPA</i>			<i>PVA</i>		
	<b>1<sup>st</sup> Run</b>	<b>2<sup>nd</sup> Run</b>	<b>Average</b>	<b>1<sup>st</sup> Run</b>	<b>2<sup>nd</sup> Run</b>	<b>Average</b>	<b>1<sup>st</sup> Run</b>	<b>2<sup>nd</sup> Run</b>	<b>Average</b>
<b>Time (Hours)</b>	<b>C (mg/L)</b>	<b>C (mg/L)</b>	<b>C (mg/L)</b>	<b>C (mg/L)</b>	<b>C (mg/L)</b>	<b>C (mg/L)</b>	<b>C (mg/L)</b>	<b>C (mg/L)</b>	<b>C (mg/L)</b>
<b>0</b>	49.690	50.623	50.157	0.000	<i>N/D</i>	0.000	29.110	26.510	27.810
<b>0.5</b>	48.117	37.173	42.645	6.650	<i>N/D</i>	6.650	34.210	21.940	28.075
<b>1</b>	40.397	30.970	35.684	13.050	<i>N/D</i>	13.050	26.710	13.940	20.325
<b>2</b>	26.405	17.860	22.133	15.000	<i>N/D</i>	15.000	14.380	9.180	11.780
<b>4</b>	12.601	8.830	10.716	12.250	<i>N/D</i>	12.250	5.590	2.800	4.195
<b>6</b>	6.952	4.700	5.826	9.300	<i>N/D</i>	9.300	1.330	1.070	1.200
<b>21</b>	2.209	1.200	1.705	28.600	<i>N/D</i>	28.600	0.460	0.060	0.260
<b>24</b>	1.676	1.288	1.482	3.600	<i>N/D</i>	3.600	0.130	0.040	0.085

III. CX									
	HPA			CHPA			PVA		
	1 <sup>st</sup> Run	2 <sup>nd</sup> Run	Average	1 <sup>st</sup> Run	2 <sup>nd</sup> Run	Average	1 <sup>st</sup> Run	2 <sup>nd</sup> Run	Average
Time (Hours)	C (mg/L)	C (mg/L)	C (mg/L)	C (mg/L)	C (mg/L)	C (mg/L)	C (mg/L)	C (mg/L)	C (mg/L)
0	47.221	47.683	47.452	0.000	N/D	0.000	26.430	24.280	25.355
0.5	42.230	36.300	39.265	11.700	N/D	11.700	27.600	17.810	22.705
1	36.056	31.122	33.589	5.950	N/D	5.950	20.670	12.310	16.490
2	27.277	25.029	26.153	14.200	N/D	14.200	10.840	6.560	8.700
4	21.220	18.377	19.799	12.200	N/D	12.200	5.360	2.480	3.920
6	16.797	14.230	15.514	10.600	N/D	10.600	1.400	0.880	1.140
21	6.648	6.411	6.530	8.350	N/D	8.350	0.630	0.100	0.365
24	5.643	6.150	5.897	5.300	N/D	5.300	0.190	0.090	0.140

### A.3 Normalized Adsorption Capacity Results

#### A.3.1 pH 8 Data

**Table A.5 Normalized adsorption capacity of GAC or CX at pH 8 for HPA, CHPA, or PVA**

q <sub>t,N</sub> (mg/m <sup>2</sup> )					
Time (hours)	HPA-CX	CHPA-GAC	CHPA-CX	PVA-GAC	PVA-CX
0	0.0000	0.0000	0.0000	0.0000	0.0000
0.5	0.0295	0.0337	0.0457	0.0120	0.0263
1	0.0441	0.0410	0.0635	0.0322	0.0534
2	0.0592	0.0546	0.0698	0.0548	0.0782
4	0.0779	0.0672	0.0812	0.0770	0.1056
6	0.0873	0.0782	0.0898	0.0852	0.1232
21	0.1117	0.0953	0.1022	0.0915	0.1512
24	0.1128	0.0964	0.1070	0.0920	0.1518

A.3.2 HPA Data

**Table A.6 Normalized adsorption capacity of GAC or CX at pH 8, 6.5, or 5 for HPA**

<b><math>q_{t,N}</math> (mg/m<sup>2</sup>)</b>						
<b>Time (hours)</b>	<b>pH8-GAC</b>	<b>pH8-CX</b>	<b>pH6.5-GAC</b>	<b>pH6.5-CX</b>	<b>pH5-GAC</b>	<b>pH5-CX</b>
0	0.0000	0.0000	0.0000	0.0000	0.0000	0.0000
0.5	0.0162	0.0295	0.0156	0.0313	0.0154	0.0286
1	0.0266	0.0441	0.0295	0.0491	0.0297	0.0484
2	0.0393	0.0592	0.0479	0.0800	0.0574	0.0743
4	0.0529	0.0779	0.0659	0.0990	0.0808	0.0965
6	0.0599	0.0873	0.0751	0.1082	0.0908	0.1115
21	0.0736	0.1117	0.0906	0.1348	0.0993	0.1428
24	0.0742	0.1128	0.0914	0.1363	0.0997	0.1450

## A.4 Adsorption Kinetics Data

### A.4.1 pH 8 Data

**Table A.7 PFO and PSO model parameters for the adsorption of HPA, CHPA, and PVA onto GAC or CX at pH 8**

Time (hours)	PFO: $\ln(q_{e,N}-q_{t,N})$ (mg/m <sup>2</sup> )						PSO: $1/(q_{e,N}-q_{t,N})$ (m <sup>2</sup> /mg)					
	HPA-GAC	HPA-CX	CHPA-GAC	CHPA-CX	PVA-GAC	PVA-CX	HPA-GAC	HPA-CX	CHPA-GAC	CHPA-CX	PVA-GAC	PVA-CX
0	-2.602	-2.182	-2.340	-2.235	-2.386	-1.885	13.486	8.868	10.372	9.347	10.870	6.588
0.5	-2.849	-2.486	-2.770	-2.793	-2.526	-2.075	17.262	12.008	15.948	16.325	12.506	7.968
1	-3.047	-2.678	-2.893	-3.136	-2.817	-2.319	21.049	14.556	18.041	23.012	16.721	10.167
2	-3.356	-2.927	-3.174	-3.292	-3.292	-2.609	28.666	18.665	23.892	26.901	26.909	13.591
4	-3.851	-3.355	-3.534	-3.660	-4.198	-3.076	47.018	28.647	34.246	38.847	66.576	21.664
6	-4.250	-3.670	-4.007	-4.063	-4.992	-3.555	70.110	39.236	54.986	58.173	147.210	34.982
21	-7.460	-6.796	-6.788	-5.340	-7.617	-7.522	1736.655	893.916	887.273	208.364	2033.333	1848.387
24	--	--	--	--	--	--	--	--	--	--	--	--

### A.4.2 HPA Data

**Table A.8 PFO and PSO model parameters for the adsorption of HPA onto GAC or CX at pH 8, 6.5, or 5**

Time (hours)	PFO: $\ln(q_{e,N}-q_{t,N})$ (mg/m <sup>2</sup> )						PSO: $1/(q_{e,N}-q_{t,N})$ (m <sup>2</sup> /mg)					
	pH8-GAC	pH8-CX	pH6.5-GAC	pH6.5-CX	pH5-GAC	pH5-CX	pH8-GAC	pH8-CX	pH6.5-GAC	pH6.5-CX	pH5-GAC	pH5-CX
0	-2.602	-2.182	-2.392	-1.993	-2.305	-1.931	13.486	8.868	10.937	7.336	10.026	6.894
0.5	-2.848	-2.486	-2.579	-2.253	-2.473	-2.150	17.262	12.008	13.184	9.519	11.855	8.586
1	-3.047	-2.678	-2.782	-2.439	-2.658	-2.337	21.049	14.556	16.154	11.463	14.268	10.346
2	-3.356	-2.927	-3.134	-2.877	-3.163	-2.649	28.666	18.665	22.957	17.753	23.631	14.144
4	-3.851	-3.355	-3.666	-3.287	-3.967	-3.026	47.018	28.647	39.114	26.768	52.851	20.609
6	-4.250	-3.670	-4.117	-3.571	-4.722	-3.394	70.110	39.236	61.349	35.557	112.339	29.791
21	-7.460	-6.800	-7.060	-6.496	-7.693	-6.115	1736.655	893.916	1164.678	662.428	2193.258	452.607
24	--	--	--	--	--	--	--	--	--	--	--	--